Adesina, Adeyinka Olumide. Ph.D. Study of Delivery Systems Utilizing Functionalized Single Wall Carbon Nanotubes. (2022)
Directed by Dr. Tetyana Ignatova and Dr. Daniel Herr. 115 pp

Functionalized single wall carbon nanotubes (SWCNT) are a class of one-dimensional nanomaterials that has been used for various biological applications such as biosensing, bioimaging, drug delivery, tissue engineering, etc. This dissertation focuses on the design of a hybrid material made from SWCNT and single strand DNA (ssDNA) to serve as a delivery vector for two major tasks namely intracellular gene introduction and nongenetic modification of bacteria cells. Current biomedical research methods consider the use of oligomer-based nanoparticles for targeted cancer therapy and immunotherapy. However, crossing biological membranes for delivery at specific sites *in vivo* is a challenging task, hence it needs to be further studied.

We used Förster resonance energy transfer to monitor the unzipping and hybridization of oligomer-based nanoparticles. We observed an unexpected enhancement of the SWCNT photoluminescence. The atomic force microscopy measurements revealed changes in optical responses of SWCNT with the nano-tree and nano-brush assemblies' formations.

In a bid to manipulate the light-harvesting antenna properties of *S. elongatus* bacteria (SE), the non-bleaching peptide *nblA* was introduced into the bacteria using ssDNA-SWCNT delivery cargo. The degradation kinetics of SE photoactivity was studied over 126 hours. Phycobilisomes in SE with the nblA-ssDNA-SWCNT hybrid were found to degrade faster than in the control sample (SE). Concurrently, adenosine triphosphate production in the designed bacteria was reduced by half. We explain these changes with the interruption in the energy and electron transfer pathway by incorporation of *nblA*, forming a complex with the phycocyanin pigment.

This research will contribute to knowledge by establishing ssDNA-SWCNT hybrid as a veritable vehicle that can be used in the delivery of genetic and nongenetic materials. We established that the properties of the ssDNA-SWCNT can be manipulated *ex vivo* for a specific purpose, hence it is useful for delivery science applications in the pharmaceutical and agriculture industries.

STUDY OF DELIVERY SYSTEMS UTILIZING FUNCTIONALIZED SINGLE WALL CARBON NANOTUBES

by

Adeyinka Olumide Adesina

A Dissertation
Submitted to
the Faculty of The Graduate School at
The University of North Carolina at Greensboro
in Partial Fulfillment
of the Requirements for the Degree
Doctor of Philosophy

Greensboro

2022

Approved by

Dr. Tetyana Ignatova
Committee Co-Chair

Dr. Daniel Herr
Committee Co-Chair

APPROVAL PAGE

This dissertation written by Adeyinka Olumide Adesina, has been approved by the following committee of the Faculty of The Graduate School at The University of North Carolina at Greensboro.

Committee Co-Chair

Dr. Tetyana Ignatova

Committee Co-Chair

Dr. Daniel Herr

Committee Members

Dr. Dennis LaJeunesse

Dr. Eric Josephs

Dr. Hemali Rathnayake

June 24, 2022

Date of Acceptance by Committee

April 19, 2022

Date of Final Oral Examination

ACKNOWLEDGEMENTS

I wish to express my heartfelt gratitude to my advisors Dr. Tetyana Ignatova and Dr. Daniel Herr for the undiluted professional guidance that they have given me over the years. Their support and encouragement have been very massive. I would not have reached this stage without them.

Sincere appreciation to all my committee members: Dr. Josephs, Dr. Rathnayake and Dr LaJeunesse for the detailed corrections, guidance, and cooperation they offered to ensure the completion of this dissertation.

I would like to acknowledge the financial support I received during my stay at the Joint School of Nanoscience and Nanoengineering (JSNN), a collaboration between The University of North Carolina Greensboro and North Carolina A&T State University. The support, guidance, and sterling leadership of our amiable Dean Dr. Sherine Obare will not go unmentioned.

I am immensely grateful to the staff at JSNN for their advice, training, and equipment troubleshooting, especially Dr Kyle Nowlin, Dr Olubunmi Ayodele and Dr Akamu Ewenkum. I appreciate the support of the members of Ignatova laboratory namely Sajedeh Pourianejad, Md Arifur Rahman, Swapna Kalkar, Anthony Trofe, Jared Averitt, and Kirby Schmidt.

I thank my friends Olumide Oni, Bolaji Sadiku, Samuel Akinjare, Frank Tukur, Olubukola Ayanbajo and Adesewa Maselugbo for being my best supporters and cheerleaders.

Finally, I appreciate my parents and siblings for being my backbone. I immensely appreciate my precious wife (Oluwayemisi) for the endurance, unalloyed understanding and

support I received from her throughout my time in the laboratory and the PhD program, this degree is for us!

TABLE OF CONTENTS

LIST OF TABLES

LIST OF FIGURES

CHAPTER I: INTRODUCTION

1.1 Nanomaterials for Bioresearch

Nanomaterials (NM) can be defined as materials with dimensions (at least in one dimension out of x, y, z) close to the unit cell size (in a range of 1-100 nm). Examples include: (i) 2D materials, like graphene, layered structures with at least one atomic layer in thickness; (ii) 1D materials, like nanotubes or nanowires with extended length in one dimension, but below 100 nm in other two dimensions; and (iii) 0D materials, like nanoparticles and quantum dots, with all dimensions below 100 nm. The unique size-dependent electronic, magnetic, and optical properties allow to use nanomaterials for bio-medical and bio-electronic applications. For example, the dimercaptosuccinic acid (DMSA) modified ultra-small particles of iron oxide (USPIO) were synthesized for immunohistochemical detection. Here, the ultra-small nanoprobe was employed to detect epidermal growth factor receptor (EGFR) over-expressed on the membrane of esophageal cancer cells (Wu et al., 2011). In Zhang et al.'s study (2010), the authors investigated the PVP-coated ultra-small Fe_3O_4 nanoparticles as an MRI contrast agent.

The use of colloidal silver nanostructures in anticancer treatment of human breast cancer cells was reported by Franco-Molina et al. (2010). Similarly, TiO_2 nanoparticles were investigated to develop a novel pH responsive drug delivery system for daunorubicin (DNR) (Zhang et al., 2010), and reduce DNR side effects (Zhang et al., 2012). The use of the Fe–Pt nanoparticles in photothermal therapy was studied to treat breast cancer. The Fe–Pt nanoparticles were functionalized with folic acid and used to target an EMT-6 breast cancer cell line (Chen et al., 2013).

There are multiple reports on single walled carbon nanotubes (SWCNT) biomedical/

applications and discussions on their biocompatibility with living cells. The physical properties of SWCNTs, such as their ultra-small size, large surface-area-to-mass ratio, and high reactivity, which are different from bulk materials (in microscale) of the same composition, make the SWCNTs better nanomaterial with various biological applications. These properties enable the SWCNTs to adsorb or conjugate with a wide variety of therapeutic molecules (drugs, proteins, antibodies, DNA, enzymes), hence making SWCNTs useful in pharmacy and medicine for drug delivery systems in therapeutics (Kumar & Kumbhat, 2016). Two different systems of drug delivery which conjugate with SWCNT have been described either with or without internalization of the SWCNT-carrier. These therapeutic agents can enter the cells via the endocytosis pathway or through the insertion and diffusion pathway. Phagocytosis is another pathway where a therapeutic agent can enter cells. In phagocytosis, a large solid matter is taken into the cell, thereby forming a phagosome (He et al., 2013).

Other applications of nanomaterials include the use of nanomagnetic/carbon composite for MRI shielding, nano-emulsions in the manufacture of surface disinfectant, nanoporous ceramic materials for membrane filtration, hydroxyapatite nanoparticles for toothpaste manufacturing, and semiconductor quantum dots as luminescent biomarkers, among others.

Advances in medical nanotechnology, often referred to as nanomedicine, benefit patients directly by improving imaging systems and devices to carry drugs to a targeted location (Hirlekar et al., 2009, Schmidt & Storsberg, 2015). Currently, optical biosensors and vector carriers are under intense investigation. Antibody-modified SWCNTs have been used to develop biosensors for the detection of cardiac troponin, for myocardial infarction, HE4, for early detection of ovarian cancer, and urokinase plasminogen activator, for the detection of metastatic prostate cancer (Dresselhaus et al., 1996). Zhu et al., (2014) used the carbon nanotube non-woven fabrics

(CNTFs) to sense glucose from a glucose oxidase-impregnated polyvinyl alcohol solution. The DNA-encapsulated SWCNTs can be localized in the lumen of endosomes/lysosomes, where lipid accumulation in models of lysosomal storage disorders were measured (Jena et al., 2017a). You and coworkers used gold particles with a radius of approximately 2 nm that were functionalized with a hydrophobic core to ensure stability of the device, followed by a layer of poly- (ethylene glycol) designed to optimize biocompatibility and surface-charged residues to interact with target proteins (You et al., 2007).

SWCNTs have been used to detect and monitor several diseases, especially diabetes and bacterial infection. Punbusayakul et al., 2013 used electrochemical monitoring of immune-SWCNT complexes for salmonella detection, thus reducing the detection time and facilitating the sample preparation compared to existing methods. An immunosensor for adiponectin—an obesity biomarker—was obtained by grafting oriented antibodies on the double wall carbon nanotube (DWCNT) surface to immobilize them. A second antibody, conjugated with horse radish peroxidase (HRP)-streptavidin binds to adiponectin and reacts with the substrate during cyclic voltammetry monitoring, allowing fast detection and quantification (Ojeda et al., 2015). The combination of diagnostics and therapeutics, in the form of a nanomaterial-derived theragnostic, seems to be a promising avenue to precisely target malignancies at the cellular level and deliver tailored treatments to the appropriate recipient. This approach reduces patients' burden caused by high-dosage application of pharmaceutical remedies (Hirlekar et al., 2009). In general, nanomaterials are promising tools for the design and manufacture of diagnostic biosensors, biomedical imaging, and drug/gene delivery.

1.2 Physics of ssDNA-SWCNT hybrid

SWCNT diameters are typically between 0.6 - 2 nm (depending on the chirality). The chirality is defined as the chiral vector (Ch)

$$Ch = n\overrightarrow{a_1} + m\overrightarrow{a_2} \quad (1)$$

where $\overrightarrow{a_1}$ and $\overrightarrow{a_2}$ are basis vectors while the pair of integers (n, m) is called chiral index. The geometry imposes a periodic boundary condition on the nanotube thereby leading to the quantization of the allowed electronic states. If $n - m$ is an integer multiple of number 3,

$$n - m = 3q \quad (2)$$

where q is an integer, then the nanotube is metallic, and otherwise it is semi-metallic or semiconducting. The range of electronic states of SWCNTs has led to many promising applications. Polydispersity and poor solubility in aqueous and non-aqueous solution impose a considerable challenge for their separation and assembly, which is required for many applications (Saito et al., 1998).

Pristine SWCNT require either covalent or non-covalent functionalization to enable an aqueous suspension, while still retaining their intrinsic electronic and optical properties. Many SWCNT applications rely on their noncovalent functionalization (Dresselhaus et al., 1996) with physiosorbed polymers, such that the sp^2 hybridization of the honeycomb carbon lattice of the SWCNT surface remains intact and fluorescent. Adsorbed polymers create a molecular corona around the SWCNT, which can facilitate the incorporation of SWCNT into bulk materials and cells. (Schmidt & Storsberg, 2015)

DNA is a naturally occurring polymer that plays a central role in biology. It is amphiphilic with a hydrophobic tail and hydrophilic head, which enables the ease of dissolution

of materials that have poor solubility and dispersibility. This unique property of DNA has inspired a search for its non-biological applications (Tu et al., 2009). Short single-stranded DNA (ssDNA) has emerged as the natural polymer of choice for non-covalently functionalized photoluminescent single-walled carbon nanotubes. In ssDNA, the hydrophobic side is attached to the hydrophobic end of SWCNT. However, double-stranded DNA (dsDNA) has no π stacking to interacting with SWCNT.

There have also been reports of polyaromatic adsorption π-π stacking, CH-π stacking and van der Waals forces in protein adoption, and lipid adsorption as observed by Mittal, (2011) and Bai et al., (2017).

Molecular recognition between complementary strands of a double-stranded DNA has been used to construct various geometric objects at the nanometer scale.

Figure 1.1 Helical wrapping model of ssDNA and SWCNT

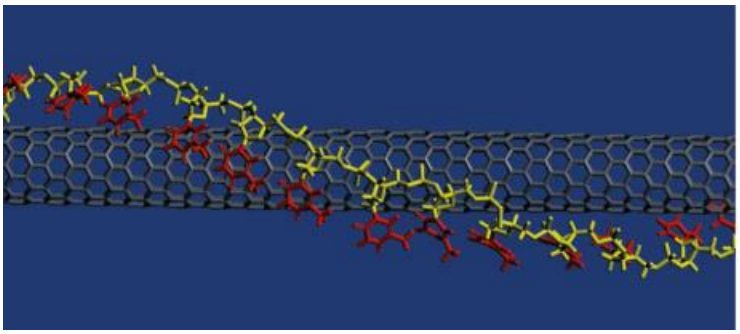

Note. (Zheng, M. et al., 2003). DNA-assisted dispersion and separation of carbon nanotubes.

A helical wrapping model has been proposed to describe the structure of DNA wrapped SWCNTs Ming Zheng and his team. The helical structure and stability of DNA on the tubes were influenced by the chemical and physical characteristics of SWCNTs and the ionic strength (Wang et al., 2013a) of the solution. Since the discovery of DNA's three-dimensional structure

by Watson and Crick in 1953, the DNA double helix's internal dynamics have been the subject of many theoretical and experimental investigations, not only from a biological or biochemical perspective, but also from a physical point of view (Mangham, 2016).This dynamic corresponds either to DNA zipping from the denatured to the duplex state, or its opening from the duplex to the single stranded state, or diffusion of denaturation bubbles (Watson & Crick, 1953).

Molecular modeling by Jagota's group suggested that DNA molecules hybridize with individual nanotubes by wrapping around them, the interaction being provided by π-stacking, with the plane of the aromatic nucleotide bases oriented parallel to the surface of the nanotube (Manohar et al., 2008). The aromatic nucleobases are believed to π-stack with the nanotube's side walls (Hughes et al., 2007).

M Zheng and his team also found that anion exchange chromatography provides a macroscopic means to assay for electrostatic properties of nanoscale ssDNA-SWCNT hybrids (Zheng et al., 2003a).

It has been reported that each of the four nucleobases (Guanine, Cytosine, Adenine, and Thymine) orient in distinct ways with respect to the single wall carbon nanotube's long axis (Hughes et al., 2007). It was also reported that various ssDNA polymers of alternating sequences facilitate the separation of nanotubes by their electronic properties (Zheng et al., 2003a). This suggests that the nanotube's electronic state and the base composition of the DNA determine the properties of the resulting DNA-nanotube hybrid (Tu et al., 2009). Many applications involving ssDNA/SWCNT will require controlling both the assembly and disassembly of the hybrid. The effectiveness of DNA/SWCNT hybrids as vehicles for gene or drug delivery hinges on the SWCNT's ability to release their cargo within the cell (Lin et al., 2004; Carbon Nanotechnologies Inc., 2005). Zheng and Diner reported on using DNA-SWCNT hybrids to

monitor electron transfer between small-molecule redox reagents and carbon nanotubes via ultraviolet-visible-near infra-red (UV/vis/NIR) absorbance spectroscopy (Zheng et al., 2003b). A ssDNA-SWCNT hybrid has also been used by several researchers for biosensing. For example, his group reports dopamine detection using DNA-wrapped SWCNTs in a self-doped polyaniline nanocomposite (Ali et al., 2008).

Figure 1.2. AFM image of (6,5) enriched fraction of DNA-SWCNT

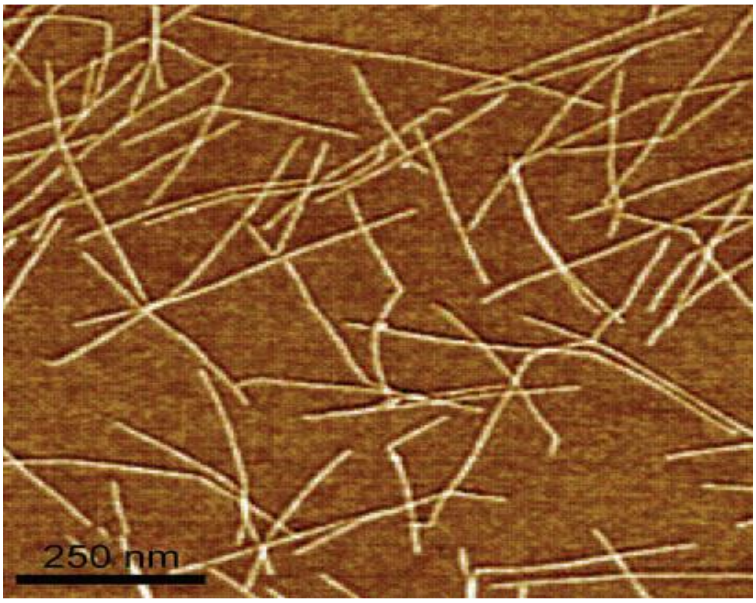

Note. Obtained by two step (SEC + IEX) chromatography (Zheng & Semke, 2007)

The formation of stable dispersions of SWCNTs formed by helical wrapping of ssDNA around the tubes makes SWCNTs highly compatible for *in vivo* systems. An example of the formation of a ssDNA-SWCNT hybrid can be seen in Figure 1.2 above.

The diameter of SWCNT is lower than the diffraction limit; therefore, it cannot be imaged by an optical microscope. Instead, Atomic Force Microscopes (AFMs) are often used to image these structures. An AFM image of a ssDNA-SWCNT gives information about the diameter of the carbon nanotube species, the length of the carbon nanotube if it is of interest, and

the motif of the hybrids. It also shows the level of separation of carbon nanotubes from its bundles. There are several reasons motivating the study of the ssDNA-SWCNT complexation. One of them is the insolubility or extremely poor solubility of SWCNTs, which imposes a considerable challenge when it comes to applications.

Thus, understanding the binding and unbinding of the DNA bases with SWCNTs, along with the factors that contribute to the stability of the ensemble, will be important in choosing the correct base composition, length, and solution conditions for the many potential applications of these hybrids. The activation energy of displacement of DNA was measured using a surfactant (Shankar et al., 2014; Hosoi et al., 2008). In fact, there is a strong relationship between recognition of DNA/SWCNT pairs and the activation energy for separation of both using a surfactant (Shankar et al., 2014).

Hydrogen-bond energies have been reported as 10.9 k_bT/bond and 3.4 k_bT/bond in vacuum and fully solvated states respectively (Roxbury et al., 2011b). Because DNA bases are only half solvated on a SWCNT sidewall, the energy for one bond can be expected to lie between these two values. We estimate a maximum binding energy of about 5.0 k_bT/bond because stitched structures are stabilized usually by two hydrogen bonds, and this term contributes about *-10* k_bT

The free energy G_{conf} due to stretching of the backbone can be approximated as:

$$G_{conf} = NK_bT = 7K_bT \quad (3)$$

Where N is the number of Kuhn length $l_{k,}$, k_b is the Boltzmann's constant, and T is the temperature.

However, for the ssDNA-SWCNT hybrid, a SWCNT has a curvature where we would like to introduce the contribution of electrostatic force into the wrapping force. The electrostatic

contribution U_{el} can be estimated as bending a line of charges to radius of curvature R, which are a defined distance b apart. U_{el} is then defined by

$$U_{el} = \frac{q^2 b e^{-\frac{b}{l_D}}}{4\pi\varepsilon\varepsilon_0(24R^2)} \quad (4)$$

with charge q, Debye screening length l_D, and dielectric constant ε.

The electrostatic contribution was estimated to be about

$$U_{el} \approx 0.1\ k_b T \quad (5)$$

It is expected that the electrostatic contribution will be added to the energy, but $0.1k_bT$ is assumed to be negligible for our consideration. Quantifying the binding strength through the measurement of DNA displacement from the surface of SWCNTs by surfactant molecules has shown experimentally that the addition or subtraction of one base from a recognition sequence strongly affects the relative ssDNA-SWCNT binding strength (Zheng, 2007). Stepanian and his group used both *ab initio* MP2 (second order Moller-Plesset perturbation theory) and DFT methods to study the stacking interaction of cytosine and the interaction energy between DNA and SWCNT in DNA-SWCNT complex formed. This interaction energy was reported to be < 42.1kJ/mol (71.1 K_bT)(Stepanian et al., 2008). Based on the foregoing, we can easily compare the hybridization energy that exists between two ssDNA with the adhesive energy in the form of free energy between the DNA and SWCNT, since they are of the same order of magnitude. Optical absorbance spectroscopy is a common and informative method for characterizing the excitonic properties of SWCNTs (Bozovic et al., 2000).

Through analysis of the characteristic SWCNT absorbance peaks, information about various properties of nanotubes, such as the nanotube chirality/diameter, the conductivity type, excitonic transition energy, evaluation of purity nanotubes etc., can be obtained. It was found

that SWCNTs for which $n = m$ has a finite density of states at the Fermi energy and display metallic electronic behavior. These structures are called “armchair” nanotubes because of their pattern of bonds around the circumference.

These diameter-dependent singularities appear due to the 1-D character of the nanotube electronic structure (Shankar et al., 2014). Based on tight-binding theory (Bozovic et al., 2000), the average nanotube diameter could be calculated from the spectrum, using the following equations: $E_{11S} = 2\alpha\beta/d$, $E_{22S} = 4\alpha\beta/d$ and $E_{11M} = 6\alpha\beta/d$, where α is C–C bond length (0.141 nm), β is the transfer or resonance integral between π-π-orbitals (2.9 eV), and d is the diameter of nanotube.

Optical absorption of carbon nanotubes strongly depends on the incident light polarization (Lefebvre et al., 2004). For light polarized parallel to the SWCNT axis, the preferential absorption at the band gaps was observed. Absorption for light polarized perpendicular to the tube axis is significantly weaker because, in this case, the optical transitions (Hartschuh et al., 2005) are strongly suppressed by the depolarization effect, in which the induced charges in the SWCNT weaken the electric field of light. For semiconducting SWCNTs, with diameters close to 1 nm, the first transition will appear in the NIR region, and the second one is observed in the visible. The width of the absorption line at the half maximum of the intensity is reported to be 25 meV (Rance et al., 2010). Thus, UV–vis spectroscopy can be used as an efficient spectroscopic tool for determining the average diameter of nanotube samples. Employing UV–vis spectroscopy, diameters of carbon nanotubes can be calculated from their plasmonic response. Rance et al., (2010) studied π-plasmon absorbance of a series of SWCNTs using complementary experimental and theoretical approaches; they deduced that π-plasmon

absorbance correlated with the nanotube diameter (d_{NT}). The relationship between the plasmon energy (E_p) and the nanotube diameter (d_{NT})was described as

$$E_p = 4.80 + \frac{0.70}{(d_{NT})^2} \quad (6)$$

Discovered by O'Connell et al., 2002, nanotube photoluminescence (PL) was observed in an aqueous micelle-like suspension of SWNTs after splitting nanotube bundles using a sonication treatment with surfactants (SDS), followed by ultracentrifugation. Micelles formed by surfactant molecules around nanotubes preventing the tubes from regenerating bundles. The decanted nanotube supernatant was a homogenous suspension, which is stable for many months. Emission from semiconducting SWCNTs is observed in the NIR range. PL from isolated nanotubes is richly structured and its absorption spectrum can be observed in the range of 900–1500 nm (Bozovic et al., 2000). Peak positions and their intensities are characteristic of the distinct chiral indices (n,m) of the specific nanotube species. Bands in the emission spectrum are red-shifted by about 5–8 meV, relative to those in the absorption spectrum that indicate a very small Stokes shift (Habenicht & Prezhdo, 2008). The band shape of the nanotube PL from individual SWCNT species was often described with a nearly Lorentzian function.

Interactions and deviations from the ideal nanotube structure can cause exciton mixing making some optically forbidden states weakly active (semi dark), rather than being strictly dark (Nie et al., 2012). Red shifts were explained by the dielectric screening of the electron–electron repulsion energy. It is known that a change in the environment of SWCNT will also cause a peak shift in the optical absorbance and photoluminescence, due to solvatochromic effect.

The Raman spectra of SWCNTs gives a lot of information about the 1D properties of carbon materials, such as their phonon and electronic structure, as well as information about their defects (Nie et al., 2012). In SWCNTs, the G band (usually the strongest Raman peak; typically

splits into many features around 1580 cm^{-1}), and the lower frequency radial breathing mode (RBM) band are both first-order Raman modes. The RBM is a unique phonon mode, appearing only in carbon nanotubes, and its observation in the Raman spectrum provides direct evidence that a sample contains SWCNTs.

The RBM is a bond-stretching out-of-plane phonon mode for which all the carbon atoms move coherently in the radial direction, and whose frequency ω_{RBM} is about 100–500 cm^{-1} (Berciaud et al., 2007). The RBM frequency is inversely proportional to the tube diameter d_{NT} and it is estimated using the following equation

$$W_{RBM} = \frac{221.7}{d_{NT}} + 13.4 cm^{-1} \quad (7)$$

In SWCNTs, the D-band at 1350 cm^{-1} and the G' -band at 2700 cm^{-1} are respectively due to one- and two-phonon, second-order Raman scattering processes.

In conclusion, the RBM is specifically used for the identification of the SWCNT chiralities present, while the D, G, and G' peaks are useful in the characterization and localization of SWCNTs in any sample.

1.3 Strategies for ssDNA-SWCNT wrapping

The preparation of the DNA-wrapped SWCNTs complexes consists of adding the SWCNTs to an aqueous solution of DNA and then mixing the components by stirring and/or sonicating in an ice-bath. M. Zheng et al., (2003) reported that single-stranded DNA interacts strongly with SWCNTs to form a stable ssDNA-SWCNT hybrid that effectively disperses SWCNTs in aqueous solution. More specifically, from the outcome of anion exchange–based DNA-SWCNT separation, optical absorption spectra changes from fraction to fraction using density-gradient separation is strongly dependent on the DNA sequence. (Zheng et al., 2007). In

a typical dispersion experiment, a DNA-SWCNT mixture was kept in an ice-water bath and sonicated for 120 min at a power level of 8 W.

Several researchers followed this procedure with slight modifications. For example, Nie et al., (2012) wrapped SWCNTs with ssDNA by dispersing 1mg of SWCNTs in PBS buffer (pH 7). The mixture was kept in an ice-water bath and sonicated for 2 h using a probe-type sonicator at a power of about 10 W. The resulting suspension was centrifuged at 10 000*g* for 1 h to remove large bundle SWCNT aggregations.

The supernatant was collected and re-centrifuged under similar conditions. Then, the SWCNTs in the supernatants were collected and filtered through a Millipore centrifugal filter with a molecular weight cutoff (100kDa) to remove excessive free oligonucleotides. M. Zheng and his team developed a low-energy fast route for generating arbitrary DNA-SWCNT hybrids. They found that the DNA/surfactant exchange reaction in methanol/water is rapid, gives high SWCNT recovery (on average over 90%) and enables the production of arbitrary DNA-SWCNTs from bile salt surfactant dispersed and processed SWCNTs.

1.4 Application of ssDNA-SWCNT hybrid

DNA-wrapped carbon nanotubes hold tremendous promise for nanotechnology. The formation of supramolecular complexes between DNA and SWCNTs recently has drawn much attention, since these hybrids can take advantage of the unique properties of the nanotubes and the remarkable recognition capabilities of DNA (Roxbury, 2011a). Compared to other polymers, DNA offers the advantage of defined length and sequence, high dispersion efficiency, (i.e., up to 4 mg/mL), and well-developed chemistries for further functionalization of the ssDNA-SWCNT hybrid, through either covalent or non-covalent functionalization (Hu et al., 2005).

Complexation of ssDNA with a chiral single-walled carbon nanotube exhibits surprising efficacy in various biological and non-biological applications. These include SWCNT dispersion and sorting, optical sensing, biosensing, and nano-electronic device design, among others. Bundled SWCNTs were effectively dispersed in water by sonication in the presence of ssDNA. Hu et al., (2005) used DNA functionalized single-walled carbon nanotubes for electrochemical detection by reporting the voltametric properties for an electrode made from ssDNA-SWCNT film, as well as detection of low-concentrations of dopamine in the presence of excess ascorbic acid. The individually dispersed ssDNA-SWCNTs adhered tightly to the substrate and formed a uniform, stable film, which was subsequently used for the electrochemical detection of dopamine.

The charge transfer properties of the ssDNA-SWCNT electrode were investigated by choosing Fe $(CN)_6^{4-}$/$Fe(CN)_6^{3-}$ as a redox pair for their voltametric responses. It was found that the redox reaction of Fe $(CN)_6^{4-}$/ $Fe(CN)_6^{3-}$ in 1 M KCl is a quasi-reversible reaction. The film made with the ssDNA-SWCNTs performed better in the detection of low dopamine concentrations in the presence of excess ascorbic acid. Zhao *et al.* prepared a reusable fluorescent sensor using DNA-SWCNT hybrids for highly sensitive and selective detection of Ag+ and cysteine (Cys) in aqueous solutions. During the incubation with Ag^+, Ag^+ will enhance stable duplex formation created by C–Ag^+–C (C=cytosine) coordination chemistry. This duplex weakens the interactions between DNA and SWCNTs, and thus activates the sensor fluorescence. Conversely, Cys will remove Ag^+ from C–Ag^+–C base pairs since it is a stronger ligand than Ag^+. It deactivates the sensor fluorescence by rewrapping the dye-labeled oligonucleotides around the SWNT. In this way, the fluorescence of a DNA/SWCNT sensor,

which signals on and off, can be used to detect aqueous Ag^+ and Cys respectively (Zhao et al., 2010).

In 2011, D'Souza et al. used ssDNA-SWCNT hybrids to measure electron transfer in self-assemblies of ion-paired porphyrins by employing (6,5) and (7,6) semiconductive SWCNTs. The donor-acceptor hybrids were bound together by ion-pairing between the phosphate groups of ssDNA on the surface of the SWCNT and positively charged porphyrin macrocycle ring's periphery. Photoinduced electron transfer from the excited singlet of porphyrin to SWCNTs and/or via ssDNA as an electron mediator has been established by performing the steady-state and time-resolved PL measurements, as well as with transient absorption studies.

Pirbhai et al., 2019 investigated the augmentation of C17.2 neural stem cell differentiation via uptake of low concentrations of ssDNA-wrapped single-walled carbon nanotubes. This study monitored the long-term impacts of SWCNTs on neural stem cell (NSC) survival and differentiation after exposure to low concentrations of SWCNTs. These cells are both able to potentially regenerate nervous system tissue and are shown to be tumor-tropic, with possible applications in anti-cancer therapies. In a bid to develop a reporter of endolysosomal lipid content, Jena et al., (2017a) identified a structurally defined DNA-carbon nanotube complex that responds optically to lipids. Carbon nanotubes were non-covalently functionalized with specific DNA oligonucleotides to facilitate separation using ion-exchange chromatography, resulting in suspensions of single-chirality DNA-nanotube complexes. The ss(GT)6-(8,6) complex was characterized by measuring the optical response to several classes of biomolecules and water-soluble lipid analogs, such as the mammalian cells, using near infrared and visible fluorescence microscopy. The near infrared emission from the nanotubes localized to the same

regions of the cell as the visible emission from Lysotracker, further supporting the endolysosomal localization of the nanotubes (Jena et al., 2017b).

1.5 General goals of research

Overall dissertation goal

To design and demonstrate that a DNA-wrapped SWCNT hybrid can act as a vehicle for the delivery of genetic and non-genetic materials into a cyanobacteria.

Overall dissertation hypothesis

"A DNA-wrapped SWCNT may serve as vehicle for the delivery of *nblA*, a non-bleaching peptide to the thylakoid membrane of a cyanobacteria, by interrupting the energy and electron transfer pathway to produce a designed bacterium.''

Rationale

Many hybrid forms of SWCNT/small peptides and ssDNA/small proteins have been reported, whereas there are relatively few reports of selective binding of ssDNA binding proteins onto ssDNA molecules adsorbed on SWCNT (Ojeda et al., 2015; Krusiński et al., 2010). The introduction of the *nblA*-ssDNA-SWCNT into the cyanobacteria achieved the delivery of *nblA* by interfering with the energy and electron transfer pathways. The kinetics of degradation of bacteria photoactivity are explained. Adenosine triphosphate production in the engineered bacteria is expected to be suppressed.

In the overall hypothesis, this research proposes the following specific aims:

Aim 1: Design and monitor the conformational changes that occur between two different and complementary ssDNA-SWCNT hybrids.

Goal 1: To demonstrate that the hybridization events of ssDNA-SWCNT hybrids can be monitored using FRET.

Hypothesis: The unzipping of DNA wrapped SWCNT hybrids and hybridization of two complementary ssDNA may be monitored using multiple experimental methods, including FRET.

Rationale: Fluorophores on the complementary ssDNA undergo FRET when they are as close as 10nm to each other. This process would ensure that unzipping from the corresponding SWCNT and subsequently hybridize with each other to form a helical structure. SWCNT goes into solution, leading to fluorescence quenching of the SWCNT.

Expected outcome: Aim 1 will result in a stable DNA-wrapped SWCNT formation at pH 7; while there will be a fluorescence quenching at a lower pH due to an unzipping of SWCNT from the DNA-wrapped SWCNT.

Aim 2: Conduct a kinetics study of non-genetically modified *S. elongatus* bacteria photoresponse using the nblA-ssDNA-SWCNT nanohybrid.

Goal 2: To investigate the delivery of the nblA-ssDNA-SWCNT hybrid into the thylakoid membrane of the *S. elongatus* bacteria and the degradation of phycobilisomes in the presence of *nblA.*

Hypothesis: ssDNA-SWCNT may deliver *nblA* peptide beside the phycobilisomes and interrupt the energy and electron transfer pathway, thereby suppressing ATP production.

Rationale: The C-terminus of *nblA* binds with the N-terminus on the phycocyanin to form a complex. This complex interrupts the energy and electron transfer pathway that facilitates the production of ATP in the bacteria. *nblA* may also mediate phycobilisome degradation by disrupting the structural integrity of the PC rod from within the rod (Nguyen et al., 2017). Alternatively, *nblA* could trigger phycobilisome degradation by interacting with some of its constituents, either by covalent or non-covalent binding, or by disruption of the phycobilisomes

via ionic interactions, rendering them susceptible to degradation. *nblA* may activate other genes that are involved in the PBS degradation process (Nguyen et al., 2017). However, since ATP is the end-product of the photosynthetic activity, we believe that ATP production will be reduced as soon as the light-harvesting ability of the phycobilisomes is reduced (Greenstein & Wert, 2019). Hence, ATP production will be lower in bacteria samples with the nblA-ssDNA-SWCNT hybrid compared to the bacteria without the nblA-ssDNA-SWCNT hybrid.

1.6 Dissertation Layout

This dissertation has been organized into six chapters. Chapter I begins with an introduction on nanomaterials for biological applications. It gives a brief background on single-walled carbon nanotubes as vehicles for genetic and non-genetic delivery systems. Chapter II presents a background of the basic tools relevant to the preparation of a stable DNA-wrapped SWCNT hybrid for a delivery system. The section presents a thorough literature review on Forster Resonance Energy Transfer, solvatochromism, and Manning Ossawa ion condensation as they affect a DNA-wrapped SWCNT hybrid system. Chapter III presents the approach and method for the preparation of ssDNA wrapped SWCNT hybrids. This section is followed by description of all the characterization techniques of the DNA- wrapped SWCNT hybrids and how the hybrid was affected by FRET. This chapter also mentions the various approaches to ATP quantification in bacteria. In Chapter IV, experimental sections for Aim 1 are discussed, (e.g., the design and monitoring of the interaction between two complementary ssDNA wrapped SWCNT nanohybrids using FRET as a tool). In Chapter V, results, and discussion of the kinetic study of non-genetic modification of *S. elongatus* bacteria photoresponse using the nblA-ssDNA-SWCNT nanohybrid is reported. Finally, in Chapter VI, the conclusion of this work and potential future direction is discussed.

CHAPTER II: BACKGROUND

2.1 Delivery systems in Biological Applications

Gene therapy is the process of delivering an external genomic material into a host cell to elicit a therapeutic improvement. There has been an increase in the prominence of gene delivery as this approach remains useful in the treatment of various genetic diseases (Conwell et al., 2005). Although gene therapy as a treatment for disease holds great promise, progress in developing effective clinical protocols has been slow. The problem lies in the development of safe and efficient gene-delivery systems. Genetic materials are transferred via a vector, which is a vehicle that is used for gene delivery of interest (Mali, 2013). The gene delivery system consists of three components—a plasmid-based gene expression, a system that controls the function of a gene within the targeting cell; a gene that encodes a specific therapeutic protein; and a gene delivery system that controls the delivery of the gene expression plasmid to a specific location within the body (Han et al., 2000; Mhato et al., 1999).

These systems can be classified into the viral, non-viral, and hybrid systems. The viral-mediated gene systems include the viruses that will be modified for replication-deficiency but can deliver DNA expression. Viral systems give a constant expression and an expression of therapeutic genes (Sullivan, 2003). Examples of viral gene-delivery vectors include the adenovirus, lentivirus, and retroviruses (Escors & Brecpot, 2010). Adenoviral systems isolated from human adenoid tissue cultures are well-characterized, relatively large, non-enveloped, unreplicated and infect cells rapidly with easier and shorter processes (Armendáriz-Borunda et al., 2011). Adenoviruses have been one of the most promising methods for high effectiveness in in-vivo gene therapy. However, the most serious problem in the use of Ad vectors is their tendency to cause strong immune and inflammatory responses at high doses (Navarro et al., 2008).

In a bid to improve the transfection process, non-viral gene delivery remains the most recent and it is being presented as the alternative. The system is dependent on its method of preparation, both physical and chemical. The chemical method makes use of natural or synthetic carriers such as dendrimers, polymers, or liposomes for the gene delivery inside the cells (Prokop & Davidson, 2007). Following is a description of the different methods of gene therapy.

2.1.1. Germline gene therapy

This technology is simple as it can be corrected by direct manipulation of germline cells with no targeting. It achieves a treatment for the individual and gametes carry some corrected genotype (Naverossadat et al., 2012). Germ line gene therapy introduces 'normal' human genes into the eggs or sperm of parents, or into the fertilized egg or early embryo of the offspring, thereby changing the child's genetic inheritance eventually (Wolf et al., 2019). The steps involved include: (a) Delivery of the gene to the nuclei which was taken from somatic cells at metaphase stage (Wolf et al., 2000); (b) ex vivo alteration of egg cells, following in vitro fertilization (Smith, 2004); (c) manipulation of embryonic stem cells of mouse during in vitro culture by different gene delivery systems (Hirabayashi et al., 2001); (d) Pronuclear microinjection of exogenous DNA solution by a glass needle (Gordon et al., 1980); and (e) Transgenic delivery into sperm cells by direct or indirect injection to testis or other parts of the genital system (John et al., 2011; Kevin & Corrado, 2005).

2.1.2. Somatic gene therapy

Somatic gene therapy is the process of inserting genes into the diploid cells of an individual; however, the genetic material is not passed into the progeny. It is a conservative but safer technique as it affects only the targeted cells (Nayerossadat et al., 2012). In-situ correction

would ensure appropriate regulation of the corrected gene with no damage to the remaining DNA (Williams & Orkin, 1986).

Described below are the three (3) types of somatic gene therapy:

***Ex vivo* delivery.** Ex vivo gene therapy involves the genetic modification of cells outside of the body, thereby producing therapeutic factors and their subsequent transplantation back into patients. Various cell types can be genetically engineered during the *ex vivo* delivery (Gowing et al., 2017), which is based on the genetic modification of cells *in vitro* followed by the transplantation of these cells to introduce a transient or stable graft to the desired patient population and thus replace defective cells and/or provide therapeutic proteins (Behrstock et al., 2005; Naldini, 2011). *Ex vivo* cell therapies depend on the isolation of stem, progenitor or differentiated cells from a patient or a normal donor to establish a transient or, more often, a stable graft of the infused cells and their progeny. This can be done to treat an inherited, infectious, or neoplastic disease, to regenerate a tissue or to deliver a biotherapeutic molecule to a disease site. One major advantage of *ex vivo* therapy is that there is no exposure of the patient to the gene transfer vector, hence the target cells of transduction can be selected, expanded and/or differentiated, before or after gene transfer, to improve efficacy and safety (Kay, 2011; Mingozzi & High, 2011)

***In situ* delivery.** In more specific terms, it is the administration of a generic material directly into a target tissue. Many systems have utilized the in-situ delivery system, but low efficiency of transduction is the main problem of this system, because in cancer therapy, one malignant cell can re-establish the tumor (Hu et al., 2007; Takefumi et al., 2005; Davis & Cooper, 2007).

***In vivo* delivery.** The genetic materials transfer directly into the targeting tissue through a viral or nonviral vector. This technique is the least advanced strategy at present but may potentially be the most useful. The problem with this technique is the insufficient targeting of vectors to the correct tissue sites; however, improvement in targeting and vector development remains the best approach to solve the problem (Nayerossadat et al., 2012).

2.1.3. Vector systems for gene delivery

Most of the employed gene therapy systems available today are viral vectors. These include among others, retrovirus, adenovirus, adeno-associated virus, herpes virus, pox virus, human foamy virus (HFV), and lentivirus (Huang et al., 2011). All viral vector genomes have been modified by deleting some areas of their genomes so that their replication becomes deranged, making them safer, but the system has some problems, such as a marked immunogenicity that causes induction of inflammatory system leading to degeneration of transducted tissue; as well as toxin production, including mortality, insertional mutagenesis, and their limitation in transgenic capacity size (Gardlik et al., 2005).

Adenoviral vectors. This remains the most used viral vector in cancer therapy. It consists of a double-stranded DNA genome and a protein shell (Haverossadat et al., 2012). The binding between the adenoviral particle and the cells through the protein, called capsid, can specifically recognize the target, delivering up to 38kB (Vorburger & Hunt, 2002). DNA particles and can be used for a large range of tissues (Thrasher et al., 2006). However, it has a short-term gene expression as it does not integrate into the host genome, even leading to death in some patients (Reid et al., 2003; Raper et al., 2003)

Adeno-associated vectors. Adeno-associated vectors (AAV) are safer than adenoviral vectors because of deficiency in their replication and pathogenicity. AAVs are not associated with any disease in human being. AAV can integrate into a specific site on chromosome 19 with no noticeable effects causing long-term expression *in vivo.* However, AAV have a complicated

process of vector production and limited transgene capacity of the particles (up to 4.8kb) (Lai et al., 2002; Flotte et al., 1996).

Retroviral vectors. Retroviruses have the potential to transfect dividing cells because they can pass through the nuclear pores of mitotic cells; this character of retroviruses make them proper candidates for *in situ* treatment (Anson, 2004; Frederic, 2007). Here, all the viral genes have been removed, creating approximately 8 kb of space for transgenic incorporation. Retroviruses are hence useful for *ex vivo* delivery of somatic cells because of their ability to linearly integrate into host cell genome (Nayerossadat, 2012).

2.2. Non-viral delivery system

Non-viral methods of gene delivery remain a very simple and, more importantly, a safer alternative to viral vectors because of the relatively simple quantitative production and their low host immunogenicity, hence they are attractive tools in gene therapy (Lundstrom & Boulikas, 2003). A non-viral, precisely defined molecule of DNA with the required gene, whose expression is dependent on the cell transcription and translation apparatus, creates the basis of such vectors. The main advantage is a virtually unlimited clone capacity, low toxicity and immunogenicity of non-viral vectors, and the ability of repeated application (Gardilik et al., 2005). Naked DNA is the simplest non-viral gene transfer technique. The naked plasmid DNA was used in several pre-clinical and clinical trials (Nishitani et al., 2000). By intramuscular injection, it secures a relatively low level of expression, but sufficient for use in DNA vaccination. DNA vaccination encoding viral antigens, in several animal experiments, caused an immune response which was protective against various infections (Molling, 1998).

One of the methods that improves DNA penetration of the cell is electroporation, a transmembrane potential induction by short electric impulses, which produce small pores in the membrane. Electroporation makes it easier for DNA to get into the cell. Successful use of electroporation was observed in transfecting muscles, brain, skin, liver, and tumors. Other known

physical methods of non-viral gene delivery techniques include DNA particle bombardment by a gene gun, hydrodynamic, ultrasound, and magnetofection, among others (Tupin et al., 2003).

2.2.1 Chemical nonviral delivery systems

The chemical non-viral delivery systems are more common that the physical non-viral systems. They are mostly nanomeric complexes containing negatively charges nucleic acid which is compacted by polycationic nanomeric particles from cationic liposome, micelle or polymers. The nanomeric complexes are stable enough to produce their bound nucleic acids from degradation and are strong enough to enter cells by endocytosis (Scherer et al., 2002). Cationic nonviral delivery systems have low toxicity and antigenicity because they are made of only biological lipids. They also possess long-term expression with less risk of insertional oncogenesis; however, it still has a low delivery efficiency. Cationic lipids are included in 6 subcategories, namely monovalent cationic lipids, polyvalent cationic lipids, guanidine containing compounds, cholesterol derivative compounds, cationic polymers: Poly(ethylenimine) (PEI), Poly-1-lysine (PLL), Protamine, lipid -polymer hybrid.

2.3 Förster Resonance Energy Transfer

The search for a non-toxic nonviral delivery system is an issue of concern. However, being able to deliver the therapeutic material with a great specificity remains more challenging. Hence, the search for a method that can establish the specificity of the target molecule is quite important. For this reason, the use of Förster Resonance Energy Transfer (FRET), a very useful tool, comes to mind.

2.3.1 Introduction to Förster Resonance Energy Transfer (FRET)

Förster Resonance Energy Transfer (FRET) is an electromagnetic phenomenon in which quantum energy is transferred non-radiatively from an excited donor fluorophore to an acceptor molecule within proximity (1–10 nm range). Single-molecule Förster resonance energy transfer (smFRET) serves as a molecular ruler that is ideally posed to study static and dynamic

heterogeneity in living cells (Sustarsic & Kapanidis, 2015). Single-molecule FRET, on the other hand, has been used extensively to study molecular structure, conformational changes, and dynamics *in vitro* (Ha et al., 1996; Hwang et al., 2009). However, it is found to be limited due to technical challenges. FRET measurements using fluorescent proteins are feasible in vivo (Miyawaki, 2011). FRET has also been used to study protein interactions, signaling cascades, and as biosensors (Lam et al., 2012; Grünberg et al., 2013). To achieve FRET, the fluorophores used for the in-cell FRET must have a background fluorescence, thereby achieving a good signal-to-noise ratio from the sufficient fluorophore brightness (Yang et al., 2012). A low brightness can be replaced by using a dye with higher excitation powers, but it leads to photobleaching (Bernas et al., 2004), which can be toxic to the living cell (Dixit & Cyr, 2003). When choosing a complementary FRET dye pair, it must exhibit sufficient spectral overlap and a Förster radius(R_0) in the desired distance range. Since autofluorescence decreases with an increasing wavelength (Billinton & Knight, 2001), red-infrared dye pairs are most appropriate (Fessi et al., 2012). Hydrophobic organic dyes must also be avoided to ensure an exact account of intracellular dynamics (Wurm et al., 2012).

The principle of FRET involves the non-radiative energy transfer process in which an energetically excited fluorophore (donor) transfers energy to another molecule (acceptor) through dipole–dipole coupling (through space). The excited acceptor molecule returns to the ground state by losing its energy via photon emission (in case, acceptor is a fluorophore), i.e., fluorescence. In the case of FRET, the ground state donor and the acceptor molecules are coupled energetically. The Jablonski diagram, shown below in Figure 2.2, explains the FRET process using donor/acceptor excitation and emission and their energetically coupled ground states. Irrespective of the photophysical characteristic of the acceptor, i.e., whether it is a

chromophore or fluorophore, the energy transfer process is called Förster resonance energy transfer. Förster resonance energy transfer is also occasionally referred to as fluorescence resonance energy transfer. For FRET to take place, the donor and acceptor must be at less than 10nm proximity. As illustrated in Figure 2.1, FRET occurs at the right image while it does not occur in the left image because the donor and acceptor are not in the required proximity.

Figure 2.1 Förster Resonance Energy Transfer Process

Note. Showing two complementary dye pair (Billinton & Knight, 2001)

Figure 2.2 Schematic representation of FRET

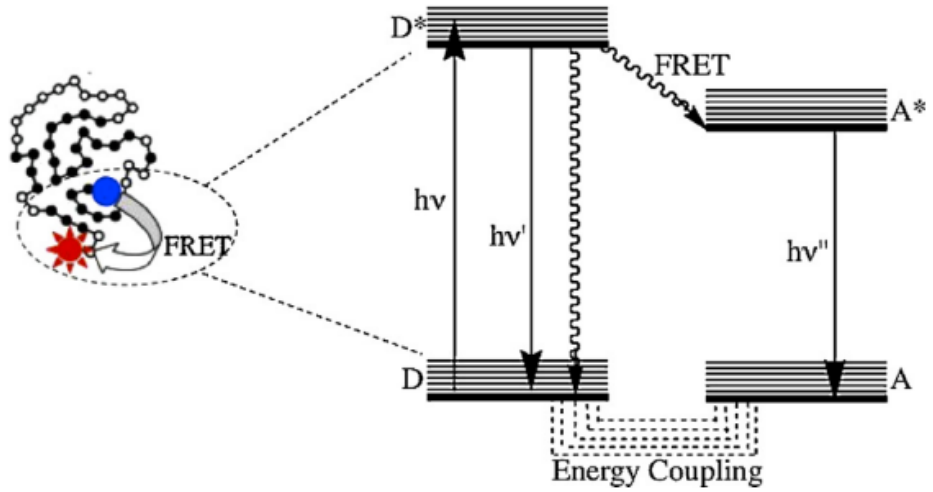

Note. Demonstrating the energy transfer from excited donor (D*) to acceptor (A) via nonradiative process. Energy transfer excites the acceptor from A to A* followed by radiative energy relaxation in terms of fluorescence. Solid and wavy arrows indicate the radiative and nonradiative processes, respectively.

FRET takes place as a 2-step process as shown in Fig 2.2. This involves the excitation of photons from the ground to excited state of the donor and the transfer of energy from excited donor to the acceptor molecule via a dipolar coupling between the donor emission and acceptor excitation dipole moments (Bullok et al., 2002).

Figure 2.3 Schematic representation of principle of Förster Resonance Energy Transfer based on distance.

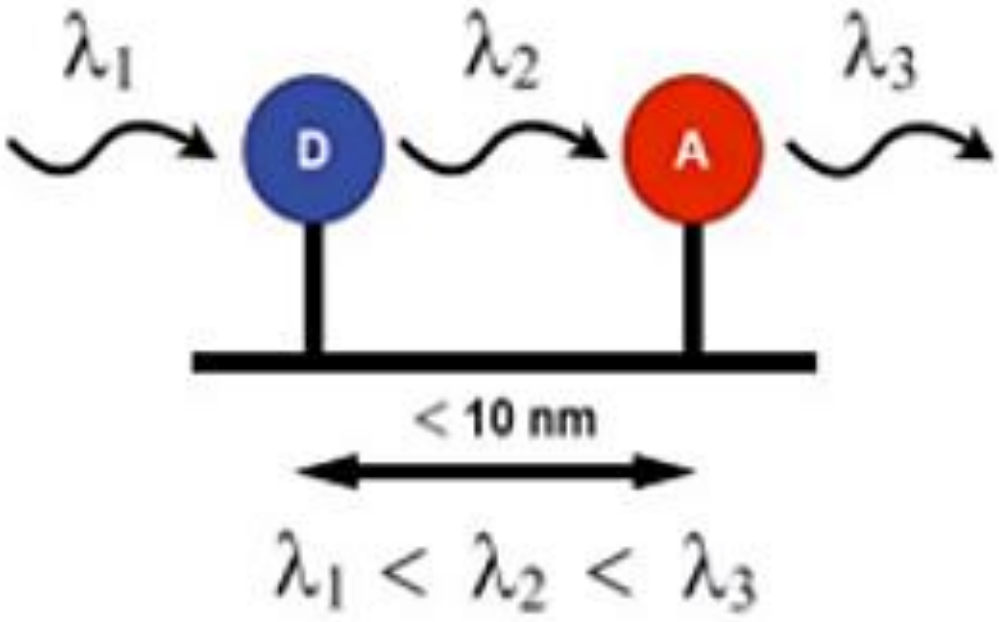

Note. (Kaur et al., 2020)

Figure 2.3 explains the importance of distance in FRET as it occurs when two molecules, donor and acceptor are in the range of less than 10nm. FRET efficiency (E_{FRET}) is expressed as the sixth power of the distance between two molecules (R), and it can be determined by the formula:

$$E_{FRET} = \frac{{R_0}^6}{{R_0}^6 + R^6} \quad (7)$$

where R_0, Föster radius is the characteristics distance at a 50% FRET efficiency. FRET efficiency varies from one FRET pair to another.

Figure 2.4 Graphical representation of spectral overlap J(λ) between donor fluorescence/emission (blue) and acceptor absorbance (red)

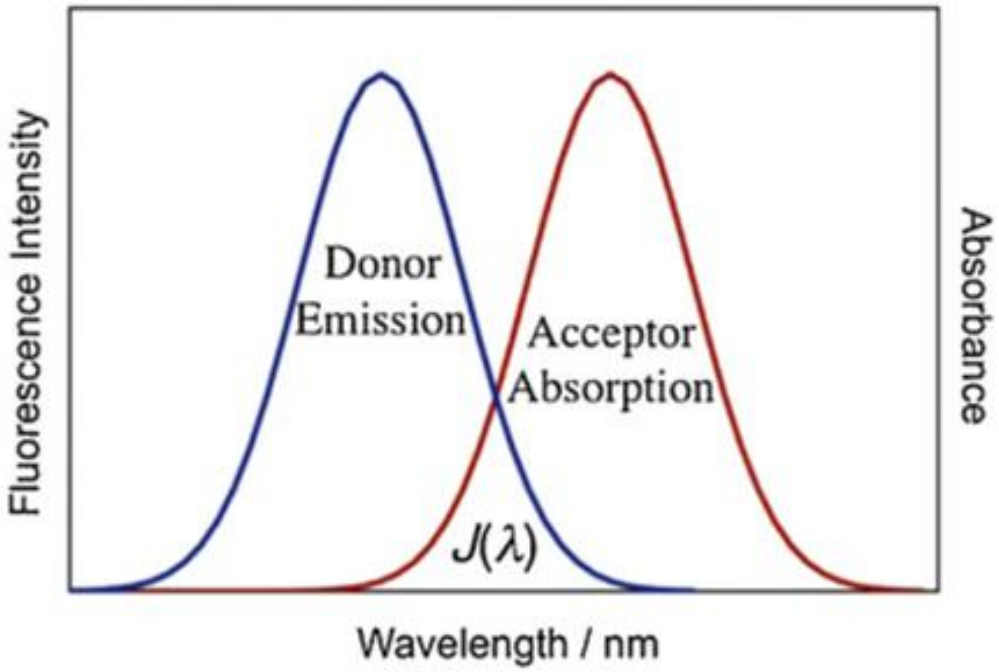

Note. (Bullock et al., 2002)

As shown in Figure 2.4, the spectral overlap remains very important in FRET, as it gives an idea of how the donor emission wavelength overlaps the acceptor absorption wavelength. When the distance is close to R_0, FRET serves as a molecular ruler due to higher precision in the measurement and data interpretation. R_0 in an aqueous solution is determined by equation 7, with the parameters:

$$R_0 = [8.79 \times 10^{-5}(\kappa^2 \eta^{-4} Q_D J(\lambda))]^{1/6} \text{ Å} \quad (8)$$

where K^2 represents the angle between the two fluorophore dipole moments (also called orientation factor), Q_D is the donor quantum yield and ŋ is the refractive index of the medium. The dipole-dipole interaction, K^2 is usually assumed to be 2/3. J(λ) is the spectral overlap integral between the normalized donor fluorescence, $F_D(\lambda)$, and the acceptor absorption spectra (which is a direct measure of the molar extinction coefficient, εA(λ)). J(λ) is also determined by the equation:

$$J(\lambda) = \frac{\int F_D(\lambda)\varepsilon_A(\lambda)\lambda^4 d\lambda}{\int F_D(\lambda) d\lambda} mol^{-1}cm^{-1}nm^4 \quad (9)$$

FRET efficiency, E_{FRET}, can be determined either from the fluorescence intensity (I_{DA}: intensity of donor in presence of acceptor and I_D: intensity of donor only) or the lifetime (τ_{DA}: lifetime of donor in presence of acceptor and τ_D: lifetime of donor only) of the donor molecule as given below:

$$E_{FRET} = 1 - \frac{I_{DA}}{I_D} \quad \text{and} \quad E_{FRET} = 1 - \frac{\tau_{DA}}{\tau_D} \quad (10)$$

FRET efficiency is affected by the molecular brightness of fluorophore (ψ= ϒσQW(0), where ϒ is the detection efficiency of the fluorescence emission, σ is the absorption cross-section at the excitation wavelength, Q is the fluorescence quantum yield, and W(0) is the laser intensity at the center of the point-spread function), stoichiometry ratio between fluorophores. To avoid a situation where the fluorophores with low brightness interfere with the background noise and the measurement, the FRET pair must be of comparable brightness. The brightness-related parameters were modified by Muller et al in 2005 to give the equation below:

$$E_{FRET} = \frac{I_{DA}}{\alpha I_{DA} + I_{AD}} \quad (11)$$

I_{AD} is the fluorescence intensity of acceptor in the presence of a donor and ˛ ȧ is the detection-correction factor (ȧ= (Υ_A,R $Q_A/\Upsilon_{D,G}$ Q_D). $\Upsilon_{A,R}$ and $\Upsilon_{D,G}$ are the detection efficiencies of acceptor and donor in red and green channels respectively, and Q_A is the fluorescence quantum yield of acceptor.

2.3.2 Current applications of Förster Resonance Energy Transfer

Due to its remarkable distance sensitivity and the capacity to be used in living cells, FRET has been extensively applied in probing real-time protein conformational changes during protein function and the underlying bioprocess mechanisms that occur in the system (Stryer, 1978). FRET is a useful biophysical tool to quantify molecular dynamics, including protein–protein interactions, protein–DNA interactions, and protein conformational changes both in vitro and in vivo systems. FRET has been used to study RNA folding (Gell et al., 2008), DNA bending and DNA-protein interactions (Dragan et al., 2008). For example, FM/TMRM pair (Fluorescein maleimide / tetramethyl rhodamine maleimide) has been used to stoichiometrically label (i.e., with different concentrations of donor and acceptor resulting in a biased binomial donor-acceptor distribution) the S3–S4 linker and observed that S4 twists during activation (Glauner et al., 1999).

Based on the FRET distances between the sites (of interest) in a protein, characterization of intermediate states can be carried out. The distance distribution probabilities in intermediates reveal the compactness of the protein and consequently the conformational changes during the folding process. FRET analyses revealed that the interaction between Fibronectin domains (III A and III B) exposes the binding sites in solution through conformational changes in Fibronectin III (Karuri et al., 2009). Fluorescence lifetime imaging microscopy (FLIM) and FRET have been successfully applied to study biomolecular interactions in the analysis of protein-protein. For example, FLIM-FRET method was used to quantify the homologous interactions between the

FP-labeled basic leucine zipper (BZip) domain of C/EBPα. Then the heterologous interactions between the C/EBPa BZip domain and HP1a are quantified using the FRET-FLIM method (Day, 2014). The lifetime for the BZip domain labeled with Turquoise was determined in regions of heterochromatin and it was also used for the study of conformational changes in the analysis of binding sequences (Banning et al., 2010; Krusinki et al., 2010). FLIM-FRET methods were also employed to directly measure the displacement (or lack of displacement) of full-length Bcl-2 family proteins in live mammalian cells (Pemberton et al., 2019). FRET also showed how ATP dose-dependently inhibits membrane-bound SNARE protein syntaxin-1A (Syn-1A) binding to sulfonylurea receptors, which releases the inhibition of $K_{(ATP)}$ channel activity (Kang et al., 2011). In multimeric channels with arbitrary subunit assembly, the total apparent FRET efficiency can be calculated from a binomial distribution, from which the real FRET efficiency can be derived. For example, this strategy has been used to investigate the relative arrangement of SUR1 and Kir 6.2 in K_{ATP} channels (Wang et al., 2013b).

FRET has been used for the quantitative analysis of cell material interfaces for both two and three-dimensional adhesion substrates. Using pyrene and coumarin, FRET has been used for the study of the core-shell nanoparticles complex systems (Chavex et al., 2009). FRET shows the interaction between TRPV4 and F-actin, which might play a role in sensing hypotonicity and the onset of regulatory volume decrease (Becker et al., 2009). Recently, FRET also helped to set up the link between the tumor suppressor protein Numb and TRPV6, shedding light on another potential mechanism on the involvement of ion channels in tumorgenesis (Kin et al., 2013).

In recent decades, sensors that are based on FRET principles have been developed. They have become powerful tools in the monitoring and identification of cellular molecular dynamics, cellular physiology, and cell-cell interactions. A FRET biosensor typically is composed of an acceptor fluorophore, a donor fluorophore, a ligand domain, a sensor domain, and linkers between them. The sensor domain is designed to respond to a specific signal by changing its conformation. The ligand domain then binds to the conformation-changed sensor domain, which

by changing the distance between the acceptor and donor fluorophores generate the needed FRET changes (Ma et al., 2014). A widely used example of a FRET biosensor is the intracellular Ca^{2+} indicator which contains calmodulin as the sensor domain, M13 as the ligand domain, CYP/YFP as the FRET fluorophore pair. When there is an increase in the concentration of Ca^{2+}, calmodulin binds to M13, thereby bringing CFP and CYP closer to yield an increased FRET signal (Miyawaki et al., 1997). This FRET biosensor was ultimately designed for the treatment of muscle disorders (Guhathakurta et al., 2018). The major approaches commonly applied to the design of FRET-based biosensors include, (i) the interaction between the sensor domain and the ligand domain upon cellular stimulation which results in an increased FRET signal due to a shortening of distance between donor an acceptor (Komatsu et al., 2011); (ii) the possibility of FRET pair simultaneously attaching to one molecule at close positions and continuously .generating a positive FRET (Kohl et al., 2002); and (iii) an intramolecularly labelled biomolecule with two fluorophores labeled at a distance beyond FRET sensitivity, thereby undergoing a conformational change upon stimulation, and leading to the initiation of FRET (Kajihara et al., 2006).

FRET was discussed in this dissertation because it serves as a major tool to monitor the conformational changes that are expected during the hybridization of the two complementary ssDNA used for this work.

2.4. Solvatochromism

2.4.1 Introduction to Solvatochromism

Both chemical and physical properties of a chromophore in organic molecules of a solvent influence the energy, intensity, and shape of its UV-vis absorption spectrum (Baraldi et al., 2003; Morley et al., 1998; Hammam & El-Nahas, 1998; Pinheiro & de Melo, 2011) because of the electronic transitions of a solute. Hantzschlater named this phenomenon solvatochromism (Catalán & Del Valle, 2014; El-Ayaan et al., 2001). Solvatochromism has been established as a

powerful tool to investigate the local polarity in macrosystems (Bauer et al., 2008; Marini et al., 2010). Analysis of the solvatochromism from absorption and fluorescence maxima is becoming the simplest and most widely used method to estimate the ground and excited-state dipole moments of molecules (Kawski, 2002).

Knowledge of the permanent electric dipole moment of a molecule can provide a wealth of information, such as the efficacies of quantum chemically derived wave functions and electron correlation treatments, for understanding the physicochemical processes, and for designing efficient non-linear optical materials (Mitchell et al., 2008). To effectively describe solvatochromism in terms of dielectric constant and refractive index, Onsager's reaction field theory provides the basic framework (Onsager, 1936; Mataga et al., 1956).

The field theory asserts that when the liquid solvent surrounds a solute molecule, the solvent can affect the solute molecule by its polarity. When this occurs, the electrons in the solvent instantaneously adapt to a new charge distribution upon electronic excitation. The instantaneous electronic response is reflected in the optical refractive index (ŋ), while the electronic and molecular motions are reflected in the dielectric constant (ε) (Yu et al., 2002). The following equations emphasize the relationship between instantaneous refractive index or slower dielectric response: Lippert-Mataga (eq. (12)) (Talone et al., 2016), Bilot-Kawski (eq. (13)) (Bilot & Kawski, 1962), Bakhshiev(eq. (14)) (Aggarwal & Khurana, 2015) and McRea's (Eq. (15)) (Józefowicza

$$\widetilde{\nu_A} - \widetilde{\nu_g} = \frac{2(\mu_e - \mu_g)^2}{4\pi\varepsilon_0 hca^3}\Delta F_1 + Constant;\ \ \Delta F_1 = \frac{\varepsilon-1}{2\varepsilon+1} - \frac{1}{2}\left(\frac{n^2-1}{2n^2+1}\right) \tag{12}$$

$$\frac{\widetilde{\nu_A} - \widetilde{\nu_g}}{2} = -\frac{2(\mu_e{}^2 - \mu_g{}^2)}{4\pi\varepsilon_0 hca^3}\Delta F_2 + Constant;\ \ \Delta F_2 = \left[\frac{\varepsilon-1}{\varepsilon+2} - \frac{n^2-1}{n^2+2}\right]\frac{2n^2+1}{2(n^2+2)} + \frac{3}{2}\left[\frac{(n^4-1)}{(n^2+2)^2}\right] \tag{13}$$

$$\widetilde{\nu_A} = \frac{\mu_g(\mu_e - \mu_g)}{4\pi\varepsilon_0 hca^3}\Delta F_4 + Constant;\ \ \Delta F_4 = \frac{\varepsilon-1}{\varepsilon+2} - \frac{n^2-1}{n^2+2} \quad (14)$$

$$\widetilde{\nu_A} - \widetilde{\nu_g} = \frac{2(\mu_e - \mu_g)^2}{4\pi\varepsilon_0 hca^3}\Delta F_3 + Constant;\ \ \Delta F_3 = \frac{2n^2+1}{n^2+2}\left[\frac{\varepsilon-1}{\varepsilon+2} - \frac{n^2-1}{n^2+2}\right] \quad (15)$$

where $\widetilde{\nu_A}$ and $\widetilde{\nu_e}$ are the energy of the absorbance and emission maximum in wavenumbers, mg and me are the dipole moments in the ground and excited singlet state, ε is the solvent dielectric constant, ε_o is permittivity of vacuum is the solvent refractive index, *h* being Planck's constant, ΔFi corresponds to the solvent polarity function, and c, the velocity of light in vacuum.

Figure 2.5. Normalized absorption and emission spectra of p-aminobenzoic acid (PABA) in cyclohexene, chloroform, dichloroethane and acetonitrile at room temperature

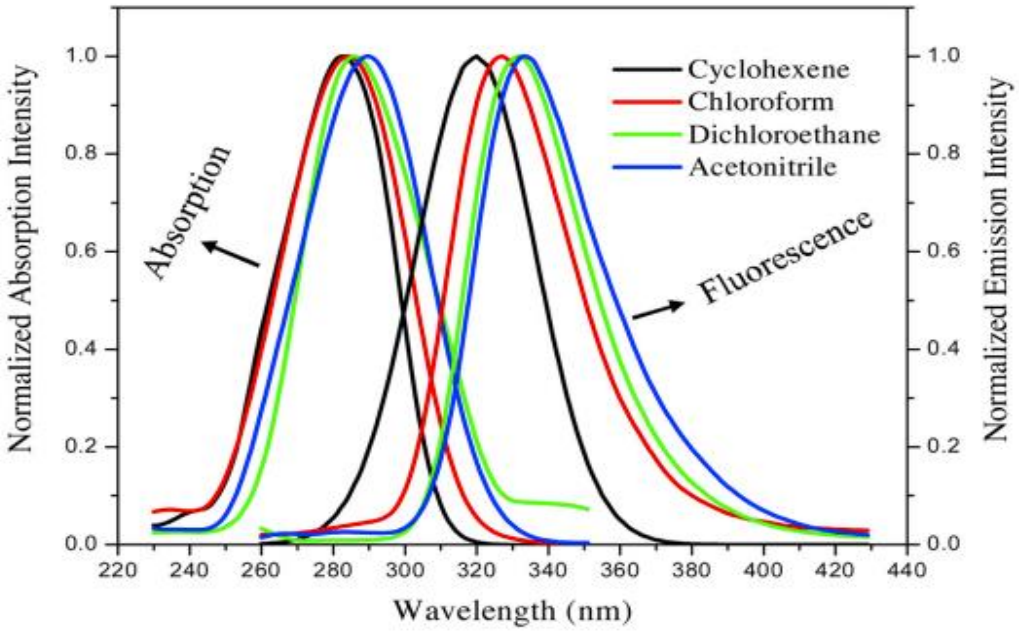

Note. (Demissie et al., 2017)

In Figure 2.5, the molecule shows a solvatochromic shift for both absorption and emission. With a greater response in the emission, it shows a charge transfer character of the

emitting state. Positive solvatochromism is observed from non-polar to polar solvents, thereby indicating a progressive stabilization of the excited state compared to the ground state. This is because the excited state has a larger dipole moment than the ground state. A blue shift was also observed by a suggestion of additional specific solvent effect because of the ability of carboxyl group to be deprotonated. The charge separation between amino acid and carboxy moiety which can be enhanced also caused a blue shift (Demissie et al., 2017).

2.4.2 Kamlet–Taft dipolarity/polarizability

Solvent polarity-polarizabilities provides a measure of the ability of the medium to stabilize a charge or a dipole by virtue of its dielectric effect (Kamlet et al.,1977; Kamlet et al., 1979a; Kamlet et al., 1979b) π* values are very nearly proportional to molecular dipole moments in most nonhalogenated aliphatic solvents (specifically excluding dioxan and hexamethylphosphoramide (Kamlet et al., 1977)

For σ—π* or π —π* , only nonchlorinated aliphatic solvents, polychlorinated aliphatic, or aromatic solvents (Kamlet et al., 1977) is represented as

$$XYZ = XYZ_0 + a\alpha + b\beta + SPPE \quad (16)$$

XYZ is the reaction rate or equilibrium, a and b are measures of susceptibility of XYZ to changing solvent acidity or basicity.

When considering all the solvents, the equation becomes

$$XYZ = XYZ_0 + s(\pi^* + d_\delta) \quad (17)$$

where $_\delta$, a polarizability correction term is 0.0 for nonchlorinated aliphatic solvents, 0.5 for polychlorinated aliphatic, and 1.0 for aromatic solvents.[109].

$E_T(1)$ values have been reported in 30 nonhydrogen-bonding solvents for which x* values are known. Least-squares correlation equations are as follows: (a) for 16 non-chlorinated aliphatic solvents, except dioxan (Manning, 1969a)

$$E_T = 50.6 - 8.07x^* \text{ kcal/mol} \quad (18)$$

with r (the correlation coefficient) = 0.981 and σ (the standard deviation) = 0.56 kcal/mol; (b) for 29 solvents of all types, except dioxan.

2.4.3 Physical basis of Solvatochromism

During the theoretical treatments of electronic spectra, the assumption is that there are isolated molecules which experimentally exist in gas phase at low pressures or when the spectrum is recorded in very dilute solutions of the dye probe in non-interacting solvents. Thus, both solute-solute and solute-solvent interactions must be considered. The effect of the medium on the spectral properties of the solute molecules can be broadly divided into two categories—general solvent-solute interactions and specific interactions (Nigam &Rutan, 2001).

This interaction involves three types of electrostatic forces namely (i)dipole-dipole, (ii) dipole-induced dipole, and (iii) induced diploe-induced dipole. When the dipole moment of the molecule increases upon excitation, as is the case for π-π* transitions, a more dipolar or polarizable solvent will serve to stabilize the excited state more than the ground state as shown in Fig. 2.6(a). The separation between the ground and excited state energies decreases, causing a positive solvatochromism or a bathochromic and the absorption spectrum shifts to the red region. The magnitude of this shift depends on the change in the probe molecule's dipole moment during the excitation process (Nigam &Rutan, 2001).

Conversely, a hyperchromic (blue) shift occurs (as shown In Fig.2.6 (b) in molecules whose dipole moment decreases in the excited state compared to the ground state, thereby

stabilizing the ground state energy in polar solvents. This leads to negative solvatochromism with n-π* transitions.

Figure 2.6 Schematic qualitative representation of solvent effects on the electronic transition energy of dipolar solutes in polar solvents

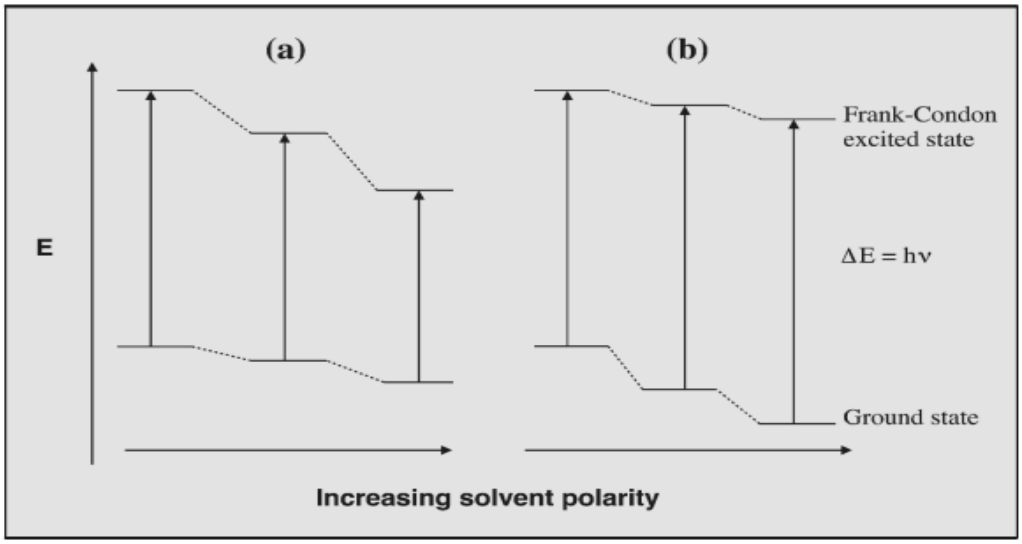

Note. (Nigam &Rutan, 2001).

In Figure 2.6, positive solvatochromism occurs when the UV visible transition energy shifts to lower energy (longer wavelength) as the solvent polarity is increased. However, in negative solvatochromism, the UV-visible transition energy shifts to higher energy (shorter wavelength) as the solvent polarity is increased.

Specific interactions are the specific chemical interactions that occur between the chromophore and the solvent. These interactions include hydrogen bonding, charge transfer interactions and complexation. These interactions give rise to substantial changes in the electronic spectrum of the molecule. For example, hydrogen bonding interactions experience a reduction in its electronic state energy caused by the electrostatic interaction of a positively polarized hydrogen atom of the solvent with a lone pair of electrons. When the electron density migrates from the basic atom, hydrogen bond formation opposes this migration, and it then leads

to a blue shift with an increase of the hydrogen bonding capacity of the solvent. On the contrary, when the charge migration occurs towards the basic atom upon excitation, a red shift is observed with an increasing hydrogen bonding capacity of the solvent (Nigam &Rutan, 2001).

2.4.4 Solvent Effects on Fluorescence spectra

During the creation of excited state of a molecule in solution, the excited state molecule interacts with the surrounding solvent molecule to a varying degree. The time scale for fluorescence is much longer than that for absorption spectroscopy, and over this period, the solvent molecules have a chance to rotationally reorient to stabilize an excited state dipole moment. This effect is called solvent relaxation and leads to a reduced energy of the excited state of the molecule in a dipolar solvent. After the emission of radiation, the excited molecule returns to its ground state electronic configuration. The energy of this initial ground state is therefore usually larger than the equilibrium ground state as shown in Figure 2.7.

Figure 2.7 Solvent effects on electronic state energies.

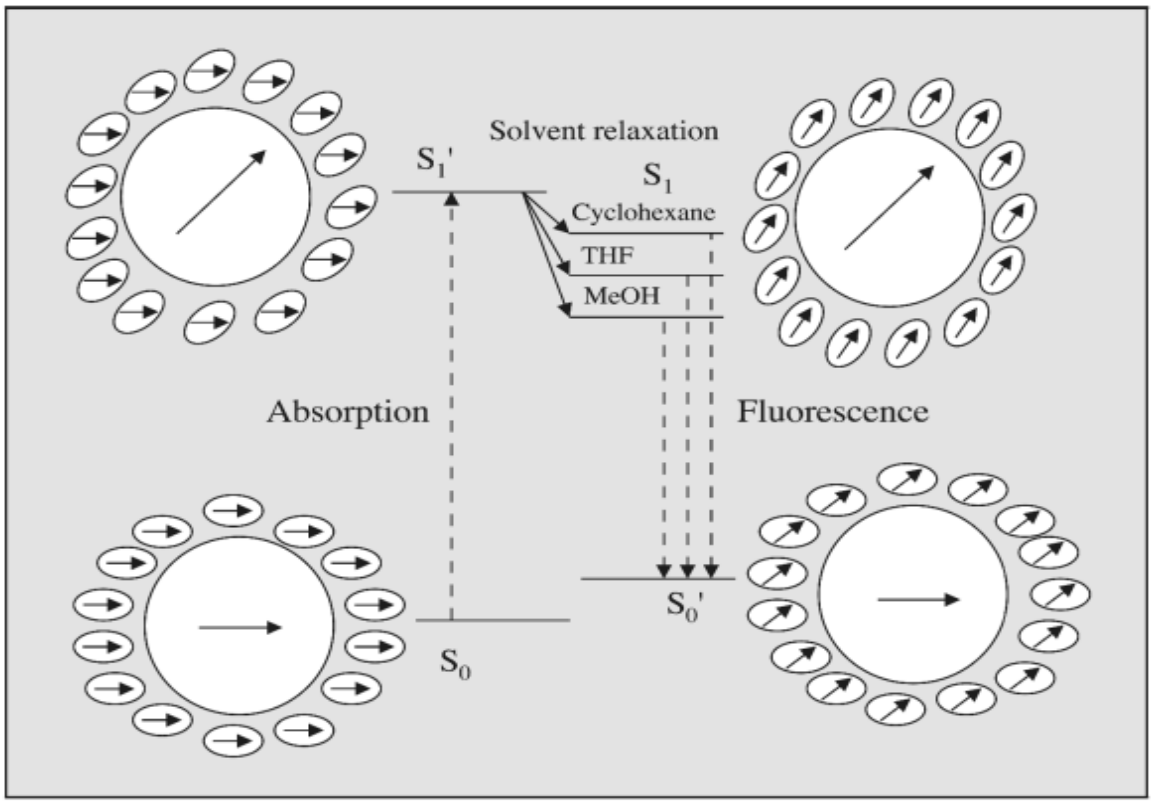

Note. S_0 is the ground state, S_1 is the excited state, dashed line: radiative process, solid lines: non-radiative processes (Jablonski diagram showing solvent relaxation process) (Nigam &Rutan, 2001).

Figure 2.7 also shows that, although the electronic configurations of the solvent molecules in the solvation sphere have had a chance to reorient, the solvent molecules themselves do not have time to rotationally reorganize over the time scale of fluorescence emission.

The Onsanger field theory further describes the energy of the interaction of a non-polarizable spherical dipole of a specific radius on a surrounding dielectric. There exists a division line between the contributions of the dielectric polarization into (i) the change in the energy of the interaction of the dipole and the dielectric upon excitation of the solute to an excited state with a different dipole moment (orientation component) and (ii) the instantaneous electronic polarization of the dielectric surroundings (the electronic component) (McRae, 1957).

2.4.5 Current applications of Solvatochromism

Mixed solvents are employed in various processes to have better control over the polarity of the system; Hence allowing for the proper and better fine-tuning of the selectivity and reaction yield of the chromatographic systems. Solvent exchange models have been used in the transition energy of E_T (30) indicator such as 4-nitroanisole, 4-nitroaniline, and N, N- diethyl-4-nitroaniline in binary hydroxylic solvents (Ortega et al., 1996). The indicators were used to compute the E_T (30), and Kamlet–Taft π*, α, β, solvatochromic parameters of the mixtures. The enhancement of the water structure caused by the addition of small amounts of alcohols to water has been studied (Buhvestov et al., 1998)

Solvatochromism has been extensively used for the characterization of polymers. Brady and his team used solvatochromism to characterize the polymers used as gas chromatographic stationary phases (Brady et al., 1984). The use of the Kamlet–Taft methodology for the characterization of various polymers was explored by Paley et al. (Sadaoka et al., 1992). The solvatochromic measurements were sensitive to the presence of water in the polymer matrix due to variations in the relative humidity. Hence, humidity and ammonia gas sensors were developed using poly(methyl)methacrylate and poly (ethylene oxide) films and it made it easier to quantify the concentration of water in organic solvents by using the strong solvatochromic sensitivity of betaine indicator dyes (Kumoi, 1970).

Solute-solvent interaction in supercritical fluids also remains one great application of solvatochromism based on the low density around the solute molecule. This is because the solvatochromic indicator dyes are very sensitive to these density fluctuations. For example, Sasaki *et al* 1999 studied the low density around phenol blue in supercritical carbon dioxide. Biswas et al., 1999 also concluded that the local densities around the solute were similar for the supercritical ethane, carbon monoxide, and chloroform in the presence of Coumarin 153, a fluorescent dye.

Recently, there has been an effort to use nanoscopic or microscopic assemblies in solution to confer a local structure. This gave rise to the study of micelles, which are spherical assemblies of surfactant molecules arranged in a hydrophobic core and a hydrophilic head group surrounding the core. Many researchers have studied the dipolarity-polarizability of these assemblies using solvatochromism. For example, π* values of sodium dodecyl sulfate (SDS) and dodecyl trimethylammonium bromide (DTAB) micelles were investigated, using several Kamlet-Taft indicators. It was found that the environment experienced by the indicator dye was slightly

less polar than water. SDS micelles showed higher HBD acidity relative to DTAB, and DTAB micelles had slightly more HBA basicity than the SDS micelles (Vitha et al., 1997; Vitha & Carr, 1998).

In this dissertation, our plan is to use solvatochromism to study the interactions that exist within the platform that we design and fabricate for genetic and non-genetic deliveries.

To further understand the science behind micelle formation as a major determinant for the organized media, there is need to understand the Manning Ossawa ion condensation effect and the underlying principles.

2.5 Manning Ossawa ion condensation effect

One of the major theoretical tools for predicting the distribution of small, mobile ions around polymers, colloids, biomolecules and biomembranes in solution is the Poisson-Boltzmann (PB) theory. However, for the sub-class of solution electrostatics problems that involve charged rods, the Manning theory of counterion condensation (CC) remains a very popular and viable alternative (Manning, 1969a; Manning, 1969b). CC arose because of the mathematical difficulties experienced in the use of PB theory. The Manning theory of counterion condensation approach treats the distribution of counterions around highly charged polyelectrolytes in terms of the linear charge density parameter $\varepsilon_\zeta = l_B/b$, where $l_B = e^2/4\pi\varepsilon_0\varepsilon kT$ is the Bjerrum length (l_B = 7.13 A at 25°C in water), and b is the axial distance between successive charges fixed to the polyelectrolyte chain. Manning considered highly charged polyelectrolytes, ($\varepsilon_\zeta > 1$, and counterions with valency z_i. Counterion condensation theory then assumes that the non-condensed counterions are distributed according to the linearized PB equation.

There are two theories attributed to the counterion condensation theories. The first condensation theory (CC1) (Manning, 1969a) modeled the polyelectrolyte chain as a charged rod

(having finite thickness) or a line charge (infinitely thin), with counterions condensing onto the rod surface or onto the line charge as a radial δ-function. The second condensation theory (CC2) (Manning, 1969b) assumes that the polyion is represented as a linear array of point charges, with a finite cylindrical volume around it, V_p per point charge, and the condensed counterions are uniformly distributed as a radial step function. CC theory is very simple, and it has succeeded in explaining the colligative properties of polyelectrolyte solutions (Manning, 1969a; Manning 1969b; Record et al., 1976; Record et al., 1978; De Gennes et al., 1976). A salt-free ionic surfactant solution remains ideal for the demonstration of counterion condensation phenomenon. At a point where the surfactant concentration is smaller than the critical micelle concentration (cmc), micelles do not exist.

CHAPTER III: APPROACH AND METHODS

The chapter discusses the sample preparation approach for the stable ssDNA wrapped SWCNT hybrids, as well as several characterization methods used in this work. The ssDNA in general is a biopolymer whose monomeric part is a nucleotide composed of three units: deoxyribose sugar, negatively charged phosphate group and a nucleobase. There are four nucleobases: Adenine (A) and Guanine (G), which are purines with two aromatic rings each, and Thymine (T) and Cytosine (C), which are pyrimidines with one aromatic ring each. The free phosphate end of the strand is called the 5' end and the free hydroxyl group end is called the 3' end. Every nucleotide has a hydrophilic part (i.e., the phosphate group) and a hydrophobic part (i.e., the aromatic nucleobase.)

The ssDNA is thus amphiphilic and has surfactant-like properties. The SWCNT surface possess hydrophobic properties; therefore, nanotubes produce aggregates when placed in an aqueous solution. Poor dispersion is a major limiting factor for most SWCNT applications. To make SWCNTs soluble, there is a need to wrap them with amphiphilic molecules such as surfactants, single-stranded DNA, or proteins. The hydrophobic parts of the amphiphilic molecule interact with the hydrophobic surface of the SWCNT, and the hydrophilic regions render the resulting hybrid water-soluble. In case of single-stranded DNA, the hydrophobic aromatic rings in the bases are thought to attach non-covalently on the SWCNT surface via π-stacking. Each of the resulting ssDNA-SWCNT hybrids is negatively charged. SWCNT have characteristic optical transition energies associated with their (n,m) chirality, as discussed in Chapter 2. They also exhibit solvatochromic shift, whereby the SWCNT excitonic transition energy depends on the surrounding solvents and adsorbed molecules. For example, when ssDNA

adsorbed onto SWCNT are replaced by surfactant molecules such as sodium deoxycholate (DOC), a PL blueshift is observed. This can be traced using optical measurement techniques such as SWCNT photoluminescence and absorbance spectroscopy.

3.1 Methodology of sample preparation:

3.1.1. Making biopolymer-SWCNT hybrid

Method 1. *Direct wrapping procedure.* ssDNA (Integrated DNA Technologies, Iowa IA, USA) and SWCNT (CoMoCat, Sigma Aldrich's Louis MO, USA) were mixed in a 19.75 mg to 0.1 mg weight ratio in a 1 mL volume of dissolved in cacodylate buffer. The mixture was sonicated using UPS200St with Vial Tweeter (Hielscher Ultrasound Technology. Teltow, Germany) on ice for 90 min at 40 W. The sonicated sample was then centrifuged at 16300 × g for 15 min (accuSpin micro17, Fisher Scientific., Lenexa, KS, USA), to remove large particulates, undispersed SWCNTs, and other residual impurities, after which the supernatant was collected and used for subsequent experiments. The supernatant was sonicated again for 90 min before removing the free DNA that did not take part in the wrapping process. Four different ssDNA sequences were used for this project to give four different hybrids.

Method 2. *Surfactant exchange method for wrapping SWCNT.* 300uL of DOC-SWCNT sample was placed in an Eppendorf tube, and 50uL of 25%(m/v) Polyacrylamide (PAM) was added and thoroughly mixed using a vortex mixer. 60uL of GT15 DNA sequence was added and thoroughly mixed via vortex mixer. 180uL methanol was added and mixed 3 times to ensure the DOC replacement. Following this, 1200uL IPA was added to the mixture to ensure the DOC removal. The mixture was then centrifuged at 17,000g for 2 minutes and the filtrate was removed to ensure the complete removal of the IPA, methanol, and DOC, leaving behind the DNA-wrapped SWCNT. The pellets were dispersed into 150uL DI followed by sonication for about 10

minutes. IPA was further added, followed by centrifugation, decantation and redispersion into 150uL DI. This process was observed three times. A few drops of 5N NaCl were added to the redispersed solution.

Table 3.1. Sequences of the ssDNA samples used for this research.

	DNA Sequence	**Name**
1	5’-GTGTGTGTGTGTGTGTGTGTGTGTGTGT-3’	GT15
2	5’-ACACACACACACACACACACACACACAC-3’	CA15
3	5’-GTGTGTGTGTGTGTGTGTGTGTGTGTGT-Alexa488-3’	488GT15
4	5’- Alexa546-ACACACACACACACACACACACACAC-3’	546CA15
5	5’-GGAGACCGACCGGGCAGATGAACTTCAGGCATT-3’	DNA Sense
6	5’-AATGACCCTGAATCATCTGCACCACCGCACGCTCC-3’	DNA Antisense
7	5’GGAGACCGTGACCGGTGGTGCAGATGAACTTCAGGGTCAT T-Alexa488-3’	DNA Sense488
8	5’-Alexa546-AATGACCCTGAAGTTCATCTGCACCACCGGTC ACGGTCTCC-3’	DNA Antisense546

3.1.2 Preparation of nbla-GT15-SWCNT hybrid by incubation

To prepare nbla-GT15-SWCNT hybrid starting with the earlier prepared GT15-SWCNT sample, the 2uL of 0.1mg/L *nblA* peptide solution was carefully transferred into 0.5mL of 0.03mg/L GT15-SWCNT solution. The mixture was incubated for 30 minutes at 29^{o}C and 100rpm. The SWCNT photoluminescence spectra at 570nm excitation wavelength were taken to verify stability of new hybrid structure.

3.1.3 S. elongatus bacteria culture conditions

S. elongatus was grown in BG-11 medium at 29°C with shaking at 100 rpm in the ratio 99:1. Cultures were maintained in a Benchmark Incu-Shaker mini outfitted with 4 compact fluorescent lamp (CFL), natural-spectrum bulbs from Lithonia Lighting China, rated at 128 W. 10 mL of bacteria culture was transferred in a 25-ml conical flask which was covered with a cork. The pores in the cork allow for CO_2 and O_2 exchange needed for photosynthesis. All assays were conducted using biological nine replicates. Cell growth was monitored by measuring the optical density at 750 nm (OD_{750}).

3.1.4 ATP Extraction and Quantification

A hot water ATP extraction from the control *S. elongatus* bacteria and *S. elongatus* bacteria with nblA-GT15-SWCNT hybrids were made. We used the Kinase glo assay reagent to quantify the Relative Light Units (RLU) where the luminescence is directly proportional to the amount of ATP present in a kinase reaction between 0 to 2µM. Serial dilutions of ATP standard within the 0 to 2µM linear range were prepared and an ATP standard calibration curve was made. The extracted samples were used for the ATP quantification. 10µL of each ATP standard with known concentrations and the extracted samples were transferred into the 96-well white

plate, 10µL Kinase-Glo^{TM} reagent was added to each sample in triplicates. These samples were incubated at room temperature for 10 minutes and the luminescence was read using the Infinite M200 Pro Tecan Plate reader.

3.2 Characterization Methods

3.2.1 Optical Characterization of hybrid structures

Figure 3.1 Optical properties of the hybrid structure showing the (a) SWCNT absorption spectrum (b) SWCNT PL/PLE map

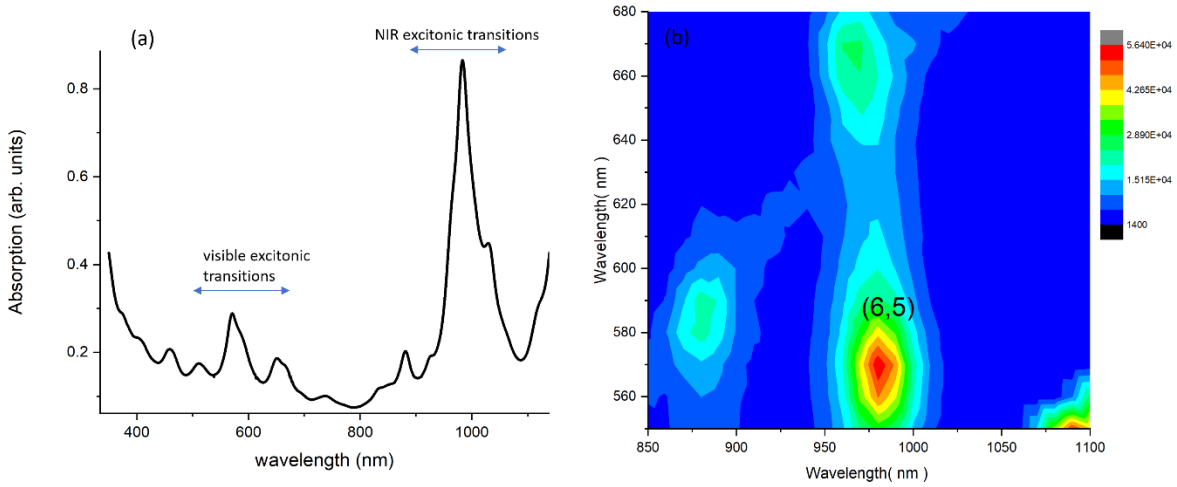

To check for the effectiveness of wrapping, initial absorbance, and photoluminescence, spectra of the DNA-SWCNT dispersion were measured as shown in Figure 3.1. A UV/Vis/NIR spectrophotometer (Agilent Cary 6000i) was used to collect the absorbance spectrum from 400–1300 nm of the SWCNT dispersion in a quartz microcuvette. Thus, we covered all major excitonic transitions in SWCNTs. A prominent NIR peak was observed at 992 nm, indicative of the first excitonic transition (E_{11}) for the (6,5)-SWCNT, majority chirality for CoMoCat nanotubes. Furthermore, a two-dimensional excitation/emission NIR photoluminescence map (Horiba Yvon Jobin Fluoro-Max 4 Fluorometer) DNA-SWCNT hybrids were measured. The excitation and emission ranges were 500–600 nm and 850–1100 nm (due to the limitation of our

equipment with silicon detector) respectively. We also kept a narrow excitation band and a wide emission band to ensure a proper data capture. To achieve high sensitivity, the integration time of the instrument was increased to 1s. Please note that there were no electronic transitions in ssDNA and Alexa Flour dyes, only in SWCNTs: the dominant peak corresponded to (6,4)-SWCNT and (6,5)-SWCNT with excitation/emission pair of 590/880 nm and 569/992 nm respectively.

Figure 3.2 Raman spectrum of (a) SWC NT after wrapping SWCNT with ssDNA

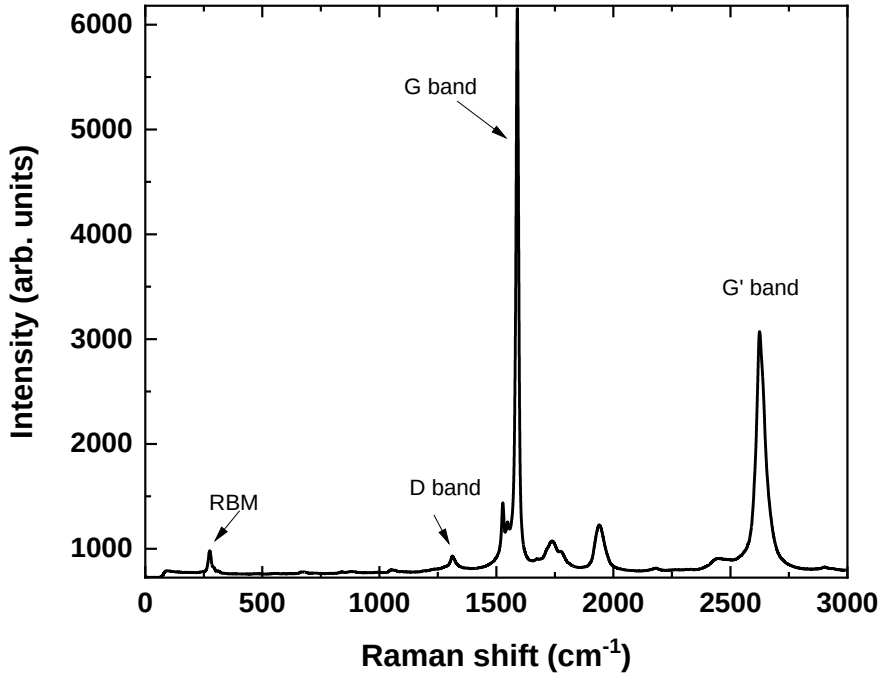

Note. (532 nm excitation)

Raman spectroscopy confirmed that the functionalization process does not significantly modify SWCNT structure.

The characteristic Raman bands of carbon nanotubes are expressed by two strong peaks centered at *ca.* 1580 cm^{-1} and 2700 cm^{-1} (G and G' bands respectively), and RBM peak around 300 cm^{-1} (Figure 3.2).

SWCNT Raman bands can be used to localize nanotubes**.** In a bid to visualize SWCNTs in bacteria, the sample was prepared by diluting up to 10 times with DI water. The final solution was centrifuged for 5 minutes at 1000 rpm. These washing steps were done five times to remove the bacterial growth media completely. After the washing, the bacteria were drop cast on a thoroughly washed Si/SiO_2 substrate. Horiba Raman system (Horiba Instruments, Atlanta, USA) was used for the spectroscopy, 100X objective with grating 1200T and 532nm laser excitation sources.

3.2.2. Scanning Electrons Microscopy Imaging

The samples were imaged with a scanning electron microscope (Zeiss Auriga FIB/FESEM), using an accelerating voltage of 5 kV, and a working distance of 5 mm. Sample was deposited on Si/SiO_2 substrate.

Figure 3.3 Scanning electron microscopy of (a) SWCNT in water (b) SWCNT after wrapping SWCNT with ssDNA

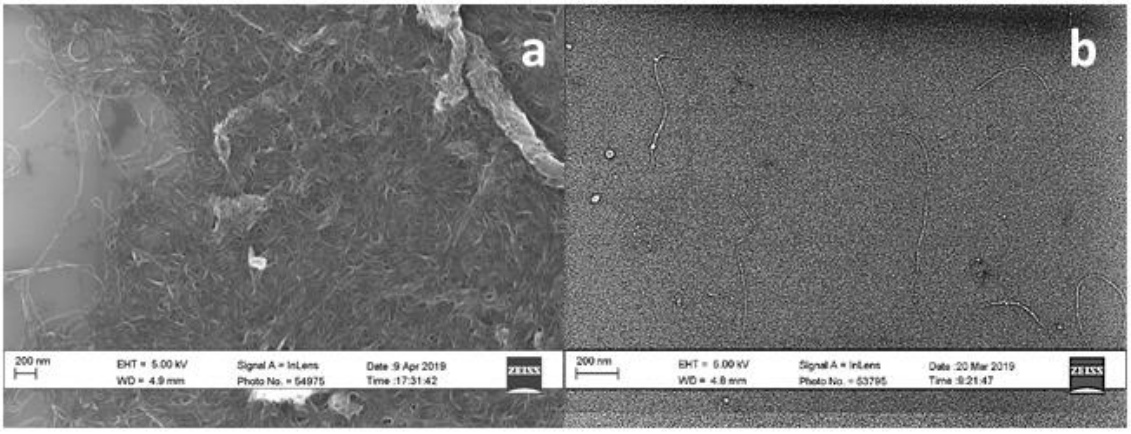

Note. (Adesina 2019, Unpublished).

3.2.3. Atomic Force Microscopy Imaging

To study length distribution, effectiveness of wrapping, and DNA-SWCNT nanocrystal formation, we used Atomic Force Microscope (AFM) to probe the sample. 1mL of ssDNA-SWCNT solution was deposited onto a piece of mica substrate, rinsed with water and dried before measurement with nitrogen. Tapping mode was used to acquire the images under ambient conditions using MFP-3D Origin+ Asylum Research AFM from Oxford Instruments, Concord, MA Asylum MFP-3D Origin+ AFM with the Si tips coated with Al (TAP300AL-G probe, Budget Sensors).

Contact potential difference (CPD) for ssDNA-SWCNT sample was measured by Kelvin probe force microscopy (KPFM) using amplitude modulation (AM-KPFM). In this case, we probed by a conductive Pt/Ir-coated tip (EFM, Nanoword), while silver paint was used for grounding.

3.2.4. Cryo-Electron Microscopy Imaging

To localize SWCNT in bacteria, cryo-EM imaging was carried out. Low-dose images were collected on ThermoFisher Talos Arctica 200 keV cryo-TEM equipped with a Gatan K3 camera.

3.3 Experimental steps for hybridization event

Step 1: SWCNT wrapped with 488GT15.

Step 2: SWCNT wrapped with 546CA15.

Step 3: Solutions were mixed, and hybridization was observed.

Conformational change was traced by FRET between dyes (due to DNA hybridization) and SWCNT PL quenching, due to unwrapping and bundle formation. (Tabakman et al, 2010)

Figure 3.4 Schematic diagram for hybridization event involving two individually wrapped ssDNA-SWCNT hybrid

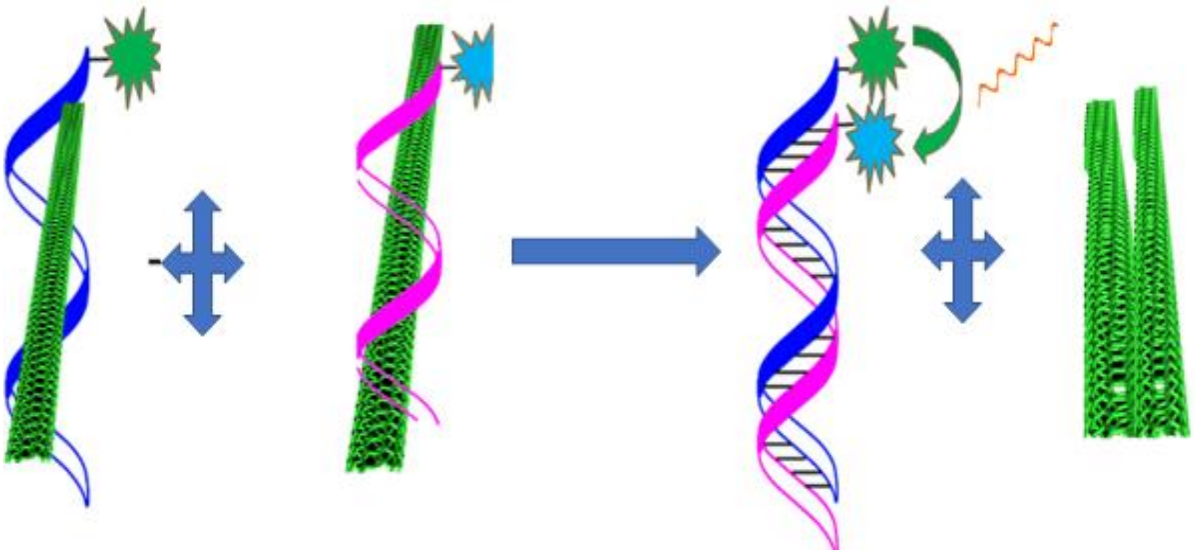

First, we monitored hybridization by FRET without SWCNTs upon mixing complementary GT15 and CA15 as a proof-of-concept and control experiment.

CHAPTER IV: MONITORING CONFORMATIONAL CHANGES IN OLIGONUCLEOTIDE BASED NANOCRYSTALS USING FRET

4.1 Design of experiment

Figure 4.1 Flow chart highlighting the methodology used for achieving Aim 1

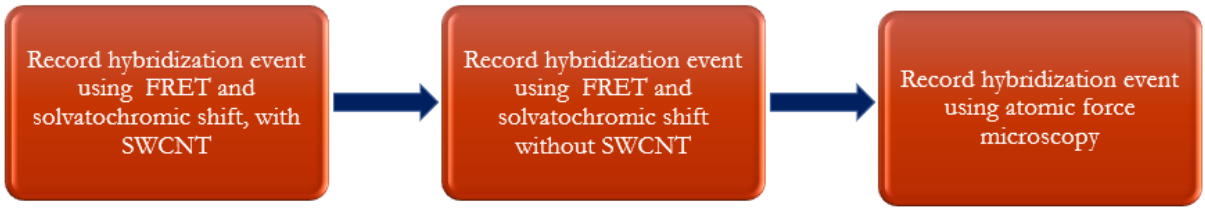

4.2 Results and discussion

4.2.1 ssDNA-SWCNT Hybrid conjugation

The value for the first excitonic band gap was calculated using fitting of the absorption data(shown in Figure 4.2) by a Lorentz function and summarized in Table 4.1. Information about the concentration of carbon nanotubes in the hybrids can also be deduced from the intensity of (6,5) SWCNT absorption peak at 992 nm (Khripin et al, 2012) as shown in Table 4.1. The results of analysis of the absorption data showed that ssDNA-SWCNT solution presented 6 NT species in the GT15-SWCNT, with two different ssDNA. This goes along with the SWCNT absorption peaks reported by Zheng, Ming, et al,2003 and Tu et al, 2003. First excitonic (E_{11}) and second excitonic(E_{22}) energy levels reported here were determined after Lorentz fitting.

Table 4.1 Lorentz fit showing the various chirality found in SWCNTs after wrapping with two different ssDNA.

	Chiralities	**E_{11}**		**E_{22}**	
		Nm	**Ev**	**nm**	**Ev**
488GT15-SWCNT	6,4	889	1.395	585	2.119
	9,1	928	1.336	691	1.794
	6,5	996	1.245	566	2.191
	7,5	1041	1.191	645	1.922
	10,2	1077	1.151	737	1.682
	7,6	1131	1.096	648	1.913
546CA15-SWCNT	6,4	889	1.395	585	2.119
	9,1	929	1.335	691	1.794
	6,5	999	1.241	566	2.191
	7,5	1041	1.191	645	1.922
	10,2	1077	1.151	737	1.682
	7,6	1130	1.097	648	1.913

Figure 4.2 Absorption spectra showing the various SWCNT chiralities in (a) 488GT15-SWCNT (blue) (b)546CA15-SWCNT(red) (c) DNA Sense488-SWCNT(purple) and (d)DNA Antiense546-SWCNT (olive)

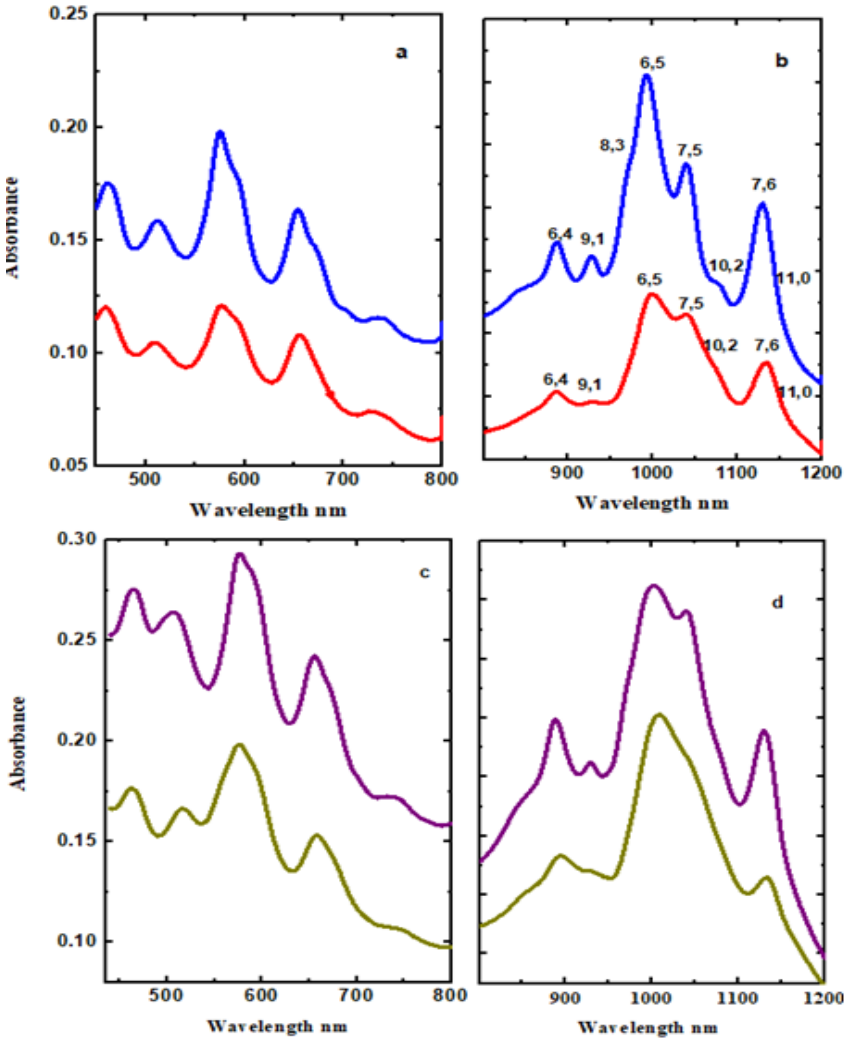

The influence of tip sonication duration on the spectral characteristics of SWCNTs in aqueous suspension with single-stranded DNA (ssDNA) was studied by NIR luminescence, NIR absorption, and Raman spectroscopy. It is worth noting that, despite using ultrasonication to solve agglomeration of SWCNT, the ultrasonic energy can also induce direct damage to the individual SWCNT.

The DNA GT15(blue) as shown in Figure 4.2(a,b) is the sequence that wrapped SWCNT most effectively, considering the FWHM of its peaks in the absorption spectrum. The absorption spectra in Figures 4.2(a) and 4.2(b) were found to have broad spectra which indicates that the SWCNT did not effectively wrap. The two remaining DNA sequences used in this research also exhibited same broad spectra as shown in Figures 4.2(c) and 4.2(d) which made them inapplicable for further use. From these results, we can conclude that the SWCNTs can be wrapped effectively by biopolymers presented above.

The AFM topography images presented on Figure 4.3 (left and middle images) show well separated DNA-SWCNT hybrids. However, we were not able to resolve helical DNA patterns on the surface of SWCNTs. The calculated length distribution of the CA15-SWCNT and GT15-SWCNT reveals additional damage (nanotube chopping) introduced by prolonged sonication time for CA15-SWCNT (Figure 4.3 right panel). The SEM image shown in Figure 3.3 also shows the individually separated DNA-SWCNT tube (left), compared to an agglomerate of poorly dispersed SWCNT in water (right).

Figure 4.3 AFM image of GT15-wrapped SWCNT (left), CA15-wrapped SWCNT (middle) and the SWCNT length distribution. (right, n>62)

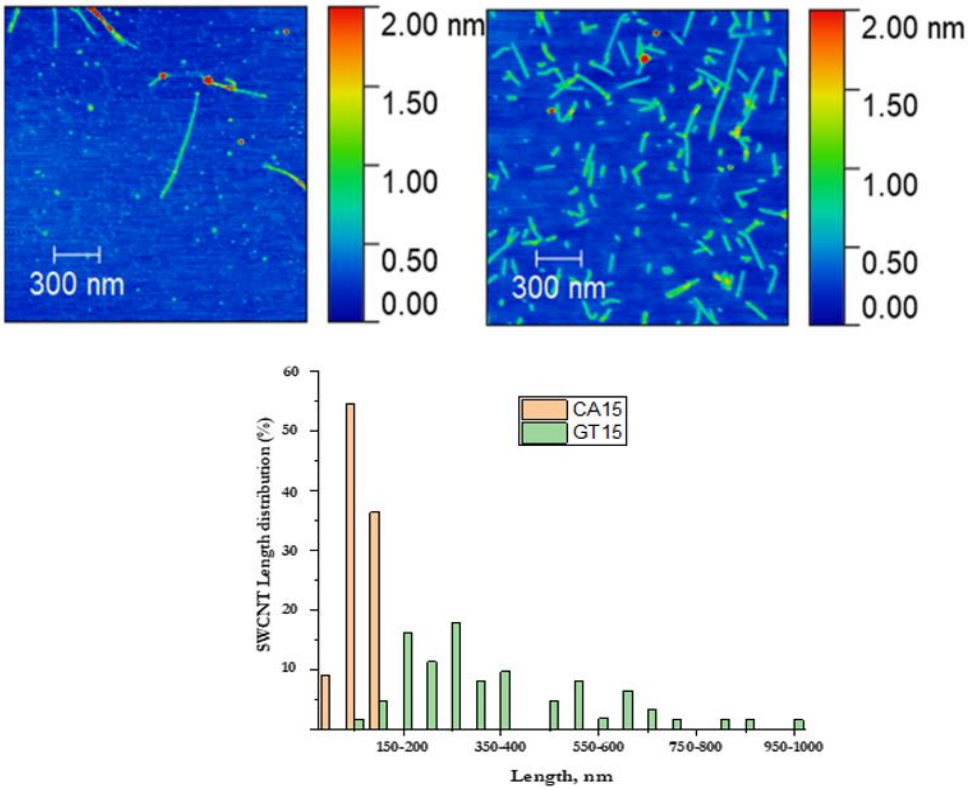

As shown in Figure 4.3, the length distribution for CA15-wrapped SWCNT and GT15-wrapped SWCNT is found to be 88±37 nm and 360±196 nm, respectively. The AFM data showed that GT15-wrapped SWCNT is at least three times longer compared to the CA15-wrapped SWCNT hybrid (sonication time was increased for CA15-wrapped SWCNT before achieving the wrapping).

4.2.2 FRET Experiment

Förster resonance energy transfer (FRET) is an efficient method to record structural changes in DNA. FRET is widely utilized as it has applications in biology and medical sciences due to its ability to monitor the hybridization event of two single-stranded DNA to form a duplex. Here, we report the ability of SWCNTs wrapped with complementary ssDNA labeled

with Alexa Fluor™ dyes to initiate DNA hybridization upon mixing two individually wrapped DNA-SWCNT hybrid solutions. The hybridization results in FRET from donor Alexa Fluor488 to acceptor Alexa Fluor546. It should be also accompanied with reduction of the SWCNT PL intensity and exciton lifetimes (quenching of SWCNT PL) and bundle formation, due to increase of non-radiative decay rate in bundles (Perebeinos et al, 2008)

In contrast, we observed an unexpected enhancement of the SWCNT NIR emission. The atomic force microscopy measurements reveal changes in optical responses of SWCNTs with the nano-tree and nano-brush assemblies' formations. A 2-step FRET was observed, and this was because of the energy being transferred from the donor to the dye acceptor at 568nm in resonance excitation wavelength of (6,5)-SWCNT. Our observed phenomena and the experimental design can potentially be exploited in intracellular gene delivery applications.

Figure 4.4 (left) fluorescence of 488GT15 at 488 nm excitation and fluorescence of 546CA15 at 546nm excitations: (right) fluorescence of the mixed solution at 488nm excitation wavelength showing the FRET

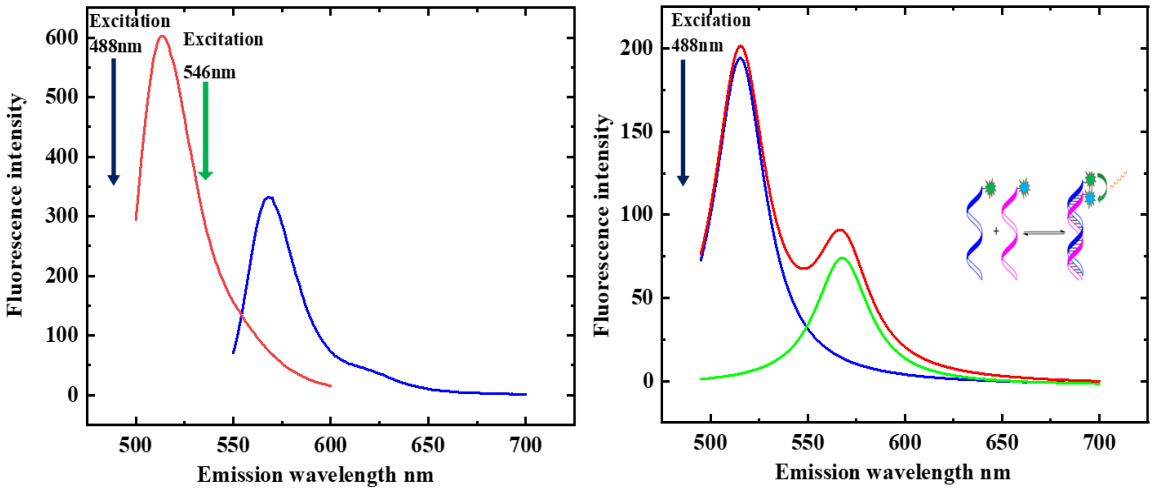

Compared to traditional dyes, Alexa Fluor™ dyes are brighter, more photostable, and more pH resistant between pH 4 and 10. A reduction in the pH of the system leads to the unbundling of the SWCNT from the DNA-SWCNT hybrid. This leads to a fluorescence quenching as shown in appendix A in the appendices section. For example, when the pH of the system was reduced from 7 to 5, there was about 86% fluorescence quenching during a 488nm excitation. At 570nm excitation, about 69% fluorescence quenching was observed.

The image on the left panel of Figure 4.4 presents resonant excitation of both dyes, while the right panel shows FRET recorded upon hybridization. We repeated the same experiment for ssDNA-SWCNT samples (as shown in Figure 4.4). 0.5 mL 0.03mg/L each of two complementary ssDNA-SWCNT hybrids were mixed and FRET monitored formation of DNA duplex. Despite using different dyes with same concentration, their FRET efficiencies were found to be different.

GT15 desorption from the SWCNT surface may not be thermodynamically favorable, due to the high free energy cost of bare SWCNTs in buffer solution and high binding strengths

between 5'-$(GT)_n$-3' and SWCNTs as shown in Figure 4.5. Therefore, GT15-CA15 or sense-antisense strand hybridization can be initiated from CA15 (antisense) side.

Figure 4.5 (Lomzov, A.A. et al., 2015). Molecular dynamics for the formation of a helical dsDNA formation from two ssDNA

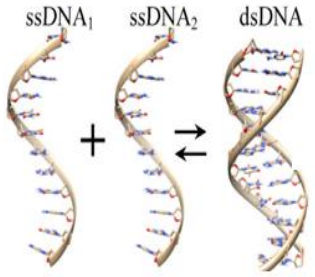

Considering the difference in length of SWCNTs species wrapped with complementary ssDNA, we should see the formation of nanoscale patterns formed by partially bundled and partially wrapped nanotubes.

Figure 4.6 represents comparison of fluorescence ssDNA-SWCNT hybrids under resonant and non-resonant excitations. Difference in fluorescence intensity for the same concentrations can be explained by differences in dye fluorescence quantum yields

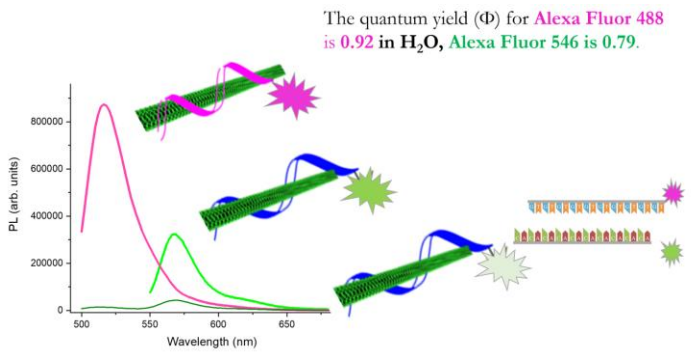

Figure 4.6 shows both resonant and non-resonant emissions of DNA-wrapped SWCNT. The pink spectrum represents the resonant emission of alexa fluor 488 with quantum yield of 0.92 while that of alexa fluor (green) has a quantum yield of 0.79. The spectrum (olive) is the non-resonant emission which is almost zero.

FRET transfer efficiency, E was calculated as the relative fluorescence of the donor in presence (I_{DA}) and absence (I_D) of the acceptor after fitting fluorescence peaks with Lorentz function.

$$E = 1 - \frac{I_{DA}}{I_D} = 16.6 \pm 1.9\%(2\sigma)$$

Transfer efficiency was found to be $16.6 \pm 1.9\%$ (2σ). A solvatochromic shift of 2.5 nm was also observed, due to the change in the nearest DNA's dielectric environment.

The addition of competing ions into a system contributes to fluorescence quenching, as observed when zinc chloride was added to the system as shown in appendix B. It was expected that multivalent metal ions (Zn, Tb) in the medium change the dielectric enviroment and lead to blue solvatochromic shift in SWCNT emission spectrum. In this research, 6nm blue shift was observed in SWCNT PL in the presence of Terbium chloride, $TbCl_3$. (See appendix C)

Figure 4.7 Upon real time hybridization of 488GT15-SWCNT and 546CA15-SWCNT (after mixing), a blue shift was observed, due to the change in dielectric constant of the dsDNA nearest environment

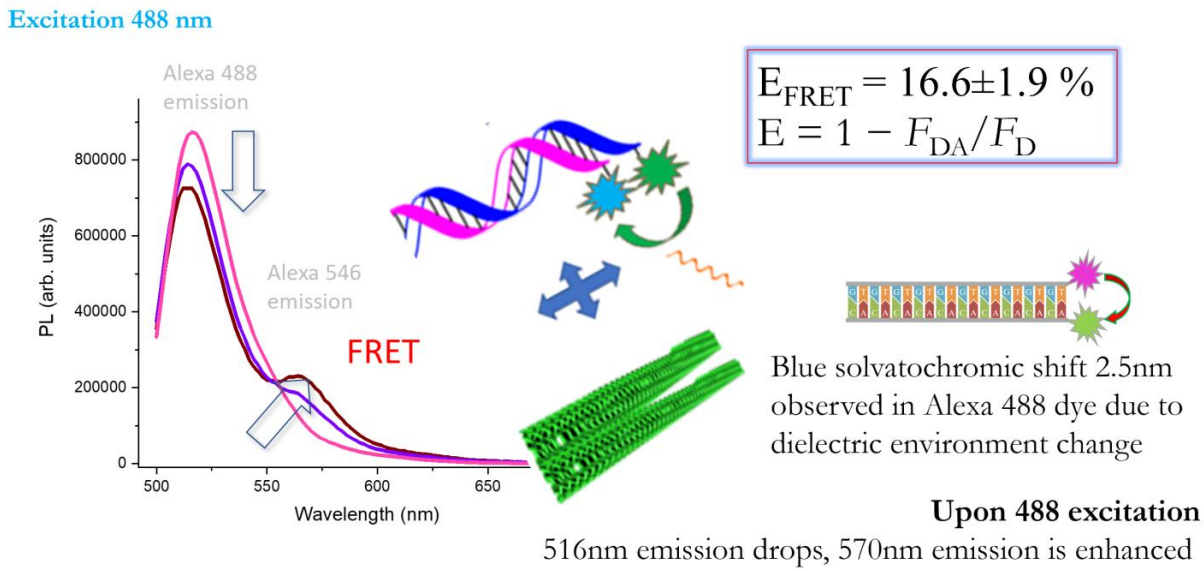

We found that mixing of two SWCNT complexes wrapped with complementary ssDNA resulted in formation of nanostructures 488GT15-SWCNT-SWCNT-546CA15 (will be discussed later). The labeled 546CA15 emission maximum is at 570 nm, which is in resonance with the (6,5) SWCNT excitonic band. It leads to a double energy transfer, meaning that the energy is being transferred from 488GT15 to the acceptor 546CA15, and then further transferred to the SWCNT. For this reason, there was not an appreciable increase in the intensity of the acceptor. This provided an insight into what happened to the SWCNT intensity as shown in Figure 4.8 (left), where an increase in SWCNT intensity was observed, versus the expected PL quenching. Figure 4.7 shows a little blue shift (2.5nm) due to a decrease in dielectric constant introduced by SWCNT partial bundling.

Figure 4.8 Enhancement in PL Intensity of SWCNT before and after hybridization and unzipping of 488GT15-SWCNT and 546CA15-SWCNT hybrids

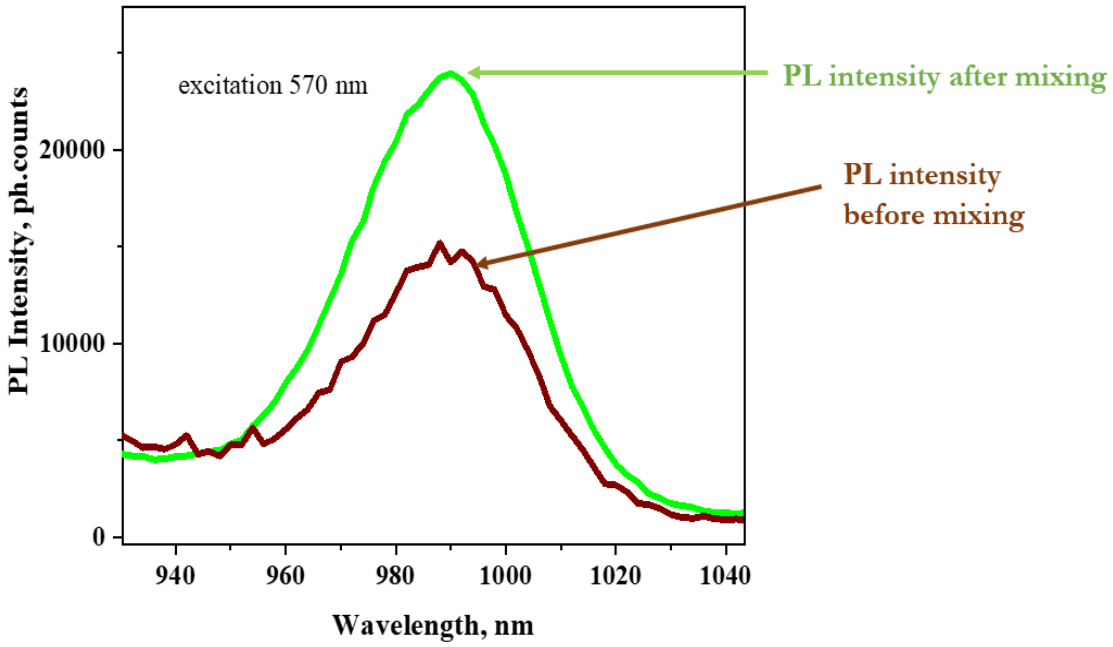

Figure 4.8 shows an enhancement in the photoluminescence of SWCNT despite an expected quenching of SWCNT. This observation is consistent with a 2-step FRET process, as the energy is first transferred from the excited donor to the acceptor, and it was further transferred to the SWCNT.

4.3 Surface properties of ssDNA-SWCNT hybrids

Figure 4.9. AFM images of mixed samples of 488GT15-SWCNT and 546CA15-SWCNT during hybridization and nano-tree formation

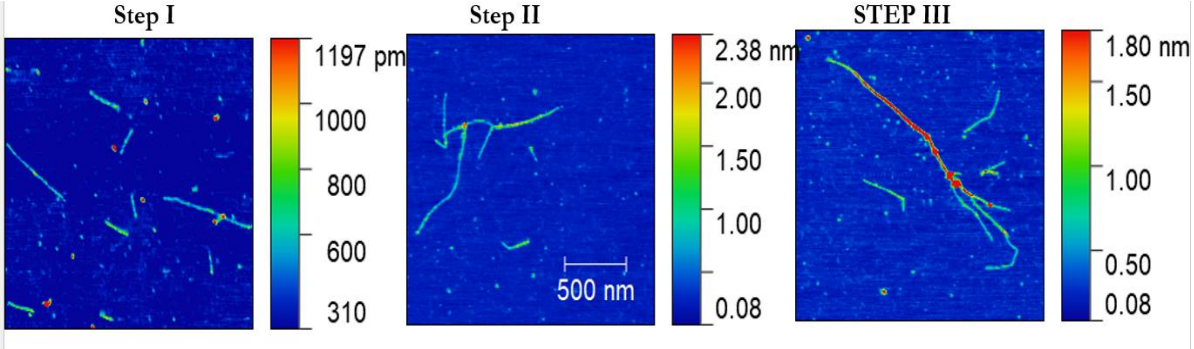

Atomic force microscopy was used to prove formation of nanostructures upon mixing samples of 488GT15-SWCNT and 546CA15-SWCNT. In Figure 4.10, a Step I shows the mixture of CA15-wrapped SWCNT nanohybrids with shorter lengths, and GT15-wrapped SWCNT with longer lengths. The image labelled Step II shows a form of rearrangement starting to occur in the mixed sample after a few minutes, When the sample was left standing for 10 minutes and visualized under the AFM, the image labelled Step III was observed. This sequence shows the steps involved in the formation of nanostructures; SWCNT nano-treesAn AFM analysis carried out on the nanotree SWCNT hybrid shown on Step III. This analysis showed the hight of the SWCNT moiety to be three times the normal 0.75 nm diameter of a (6,5)-SWCNT. This observation supports the formation of SWCNT bundles with hybridized DNA assisting in the enhancement of SWCNT photoluminescence.

CHAPTER V: KINETIC STUDY OF NON-GENETIC MODIFICATION OF *S. ELONGATUS* BACTERIA PHOTORESPONSE USING nblA-GT15-SWCNT HYBRID

5.1 Introduction

Photosynthesis is a vital part of human life, contributing to food production and the clean air we breathe. Hence, researchers endeavor to enhance various photosynthetic organisms, such as cyanobacteria. For example, Wang et al. in 2020, enhanced the light coverage of photosynthetic bacteria for photosynthesis augmentation using conjugated polymer nanoparticles (CNPs). [1] However, little work has been reported on how to suppress the photoresponse of a cyanobacteria. The lack of work provides the motivation for the present work. Here, we attempted to deliver a *nblA* peptide into cyanobacteria and monitor the bacteria's photosynthetic response.

Aim 2: To study the kinetics of non-genetic modification of *S. elongatus* bacteria photoresponse using the nblA-ssDNA-SWCNT nanohybrid.

Goal 2: To investigate the delivery of nblA-ssDNA-SWCNT hybrid into the thylakoid membrane of the *S. elongatus* bacteria and the degradation of phycobilisomes in the presence of *nblA.*

Hypothesis: ssDNA-SWCNT may deliver the *nblA* peptide to the phycobilisomes and interrupt the energy and electron transfer pathway, thereby suppressing ATP production.

Rationale: The C-terminus of *nblA* binds with the N-terminus on the phycocyanin to form a *nblA*-phycobilisome complex (Brandenburg and Klahn, 2020). Therefore, the *nblA* complex interrupts the energy and electron transfer pathway that facilitates the production of ATP in the bacteria. *nblA* may also mediate phycobilisome degradation by disrupting the structural integrity

of the PC rod from within the rod (Nguyen et al., 2017). Alternatively, *nblA* could trigger phycobilisome degradation by interacting with some of its constituents–either by covalent or non-covalent binding. This can also be achieved by disrupting the phycobilisomes via ionic interactions, rendering them susceptible to degradation. *nblA* may activate other genes that are involved in the PBS degradation process (Nguyen et al., 2017). However, since ATP is the end-product of the photosynthetic activity, we believe that ATP production will be reduced as the light-harvesting ability of the phycobilisomes is reduced (Greenstein & Wert, 2019).

Prediction: ATP production will be lower in bacteria samples with the nblA-ssDNA-SWCNT hybrid, when compared to the bacteria without the nblA-ssDNA-SWCNT hybrid.

5.2 Design of experiment for Aim 2

Figure 5.1. Step by step approach and steps to be taken to achieve Aim 2.

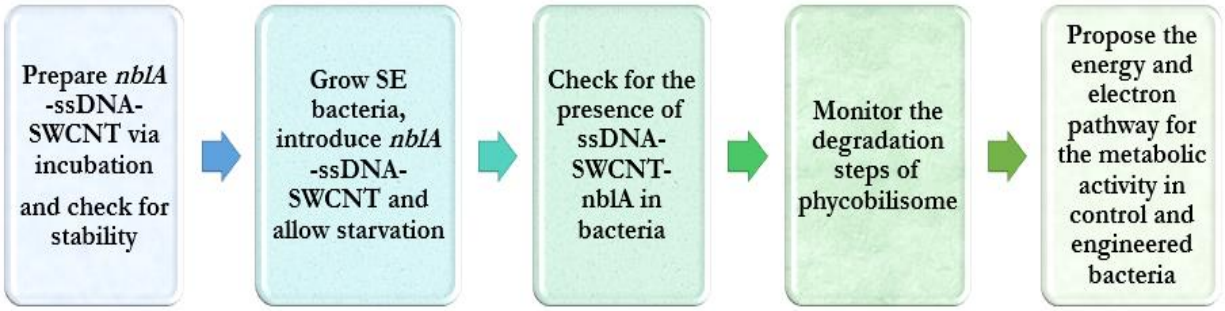

5.3 Preparation of nblA-GT15-SWCNT hybrid

Figure 5.2 shows the comparison between the fluorescence spectra of the GT15-SWCNT and nbla-GT15-SWCNT hybrids. In the process of incubating the GT15-SWCNT hybrid with the *nblA* peptide, there was a need to verify the stability of the final hybrid formed. Consequently, we compared the photoluminescence (PL) of the hybrid nblA-GT15-SWCNT hybrid (in green) with that of the GT15-SWCNT hybrid (in red).

Figure 5.2. Comparison between the PL spectra of GT15-wrapped SWCNT hybrid with nblA (green spectrum) and without nblA (red spectrum).

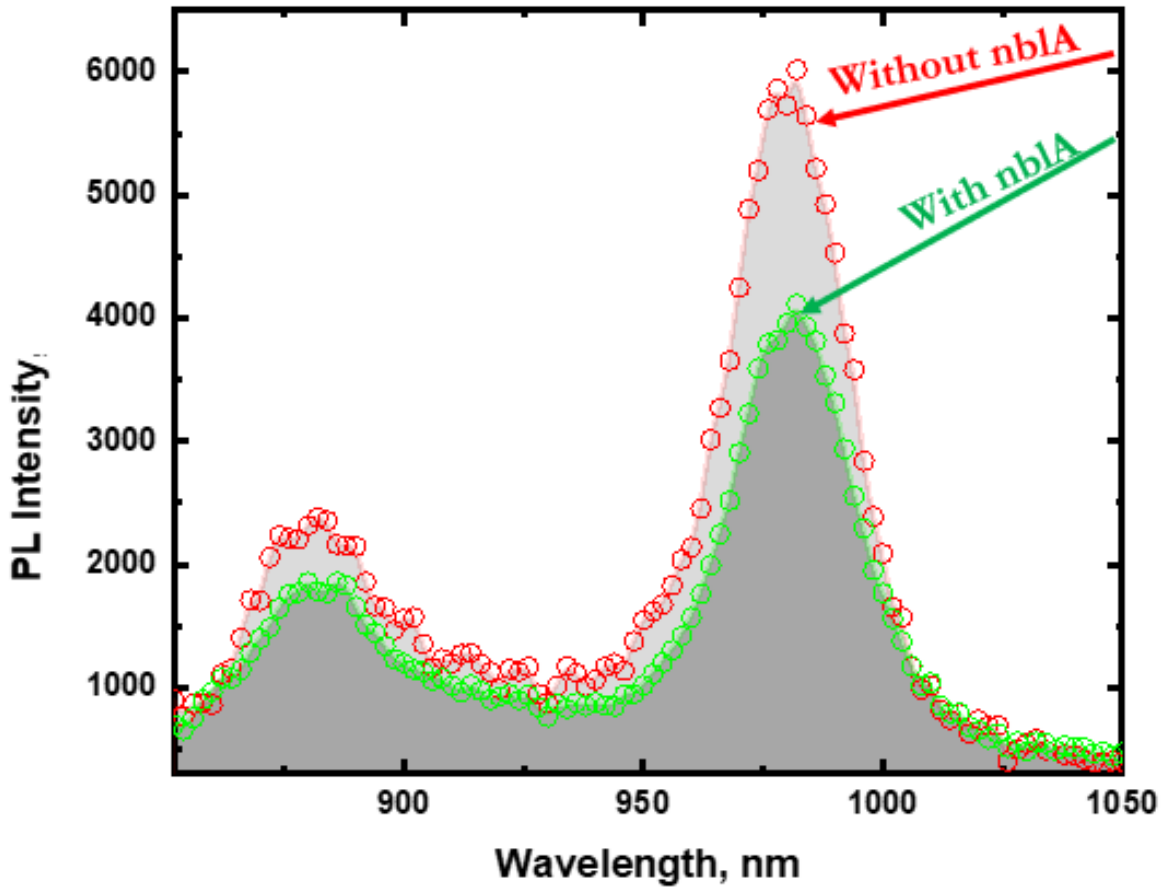

However, after fitting the data using a Lorentzian fit, we observed ~1nm red shift. Due to the resolution limit of the spectrometer used for this measurement, we cannot conclude that the shift is significant. This is consistent with the work of Dziuba et al., (2016), in which the fluorescence spectra of DNA^{FL} were measured either with or without p53CD_GST. The protein bound DNA^{FL} showed only a modest blue shift in the fluorescence spectrum (Dziuba et al.,

2016). Based on the alignment of the PL peaks, we found that the hybrid is physically stable, and the properties were preserved after 30-minute incubation.

The molecular dynamics (MD) simulation, shown in Figure 5.3, suggests the molecular mechanism of single-stranded DNA binding protein (SSB) association with ssDNA. This simulation establishes that nblA, GT15 and SWCNT can make a stable hybrid. This assertion is supported by the PL measurements reported by Maffeo & Aksimentiev, 2017, who also studied DNA's association with a single-stranded DNA binding protein.

Figure 5.3. Molecular dynamics image of the formation of a nblA-GT15-SWCNT hybrid

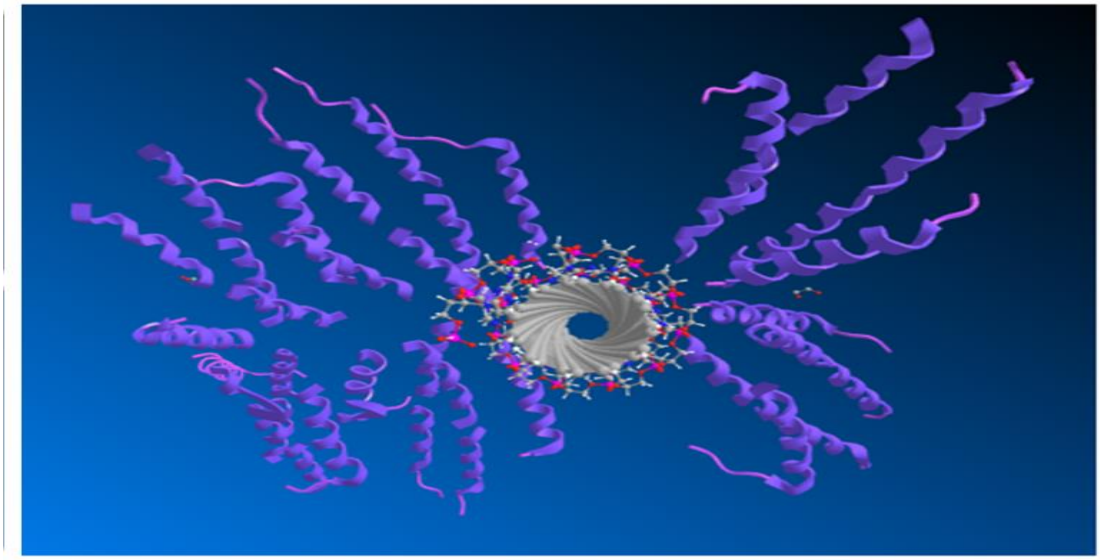

They report that SSB wrapped the ssDNA with high affinity to protect it from degradation and prevented the formation of a secondary structure. Nii et al., (2014) report that protein molecules attach to ssDNA-SWCNT hybrids via covalent bonding, by chemical modification of the 5′- or 3′ termini of the DNA molecules attached to the SWCNT.

5.4 S.elongatus bacteria growth

The samples of S. elongatus bacteria were prepared by following protocol described in Chapter 3.1.3. By day 14, we observed an increase in the bacteria color intensity. Chlorosis commenced on day 0, as shown in Figure 5.4. At this point, the bacteria entered starvation mode. As the chlorophyll and phycobilisome pigments started to deplete, a yellow-green coloration was observed.

Figure 5.4. Images of S. elongatus bacteria - before the onset of chlorosis; day 7 when the nblA-GT15-SWCNT hybrid was introduced into a bacteria sample.

On day 13, we observed the onset of chlorosis onset. The rightmost images show S. elongatus bacteria incubated with nblA-GT15-SWCNT hybrid solution and the S. elongatus bacteria control sample on day 22

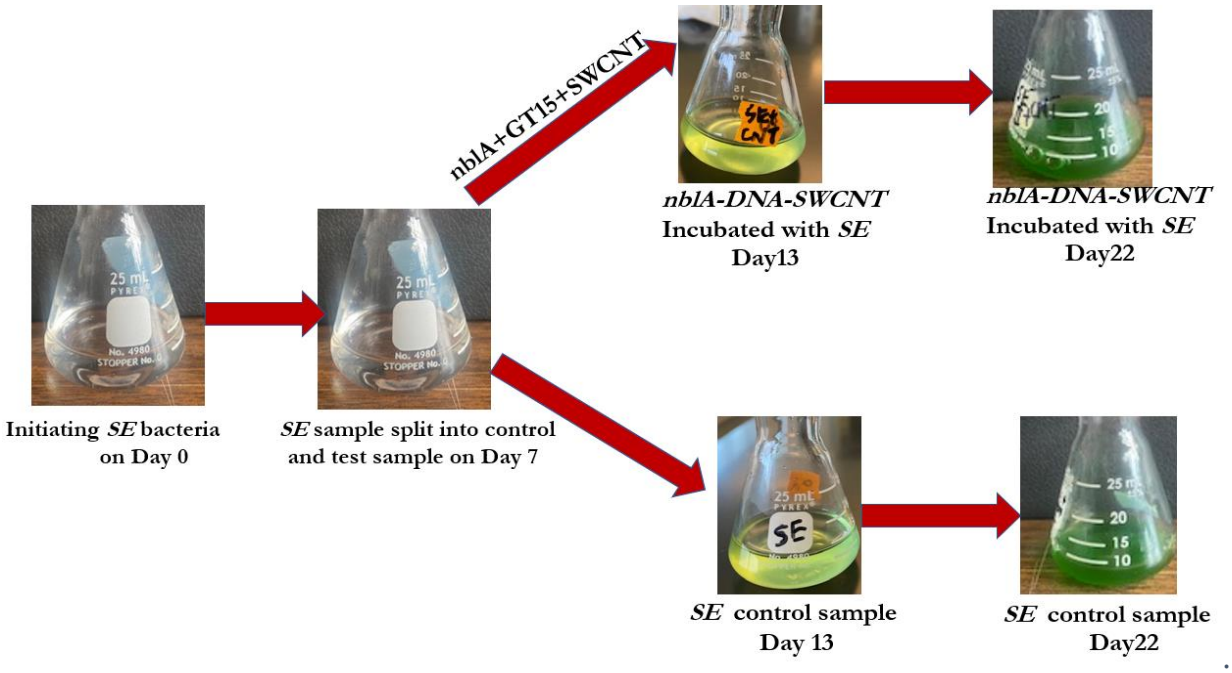

Despite the continued increase in the fluorescence intensity of the bacteria, the chlorosis continued with a consistent depletion and degradation of phycobilisomes. Visually, on day 22,

the samples appeared similar, suggesting little macroscopic difference in the level of phycobilisome degradation.

5.5 Cellular uptake of nblA-GT15-SWCNT hybrid using *S. elongatus* bacteria

The confirmation of SWCNT of functionalized SWCNT (*f*-SWCNT) uptake, while suggestive, warrants further high-resolution studies. However, SWCNT cellular uptake can be explained by three predominant mechanisms—endocytosis, phagocytosis, or pinocytosis. This experiment sought to establish that cellular uptake of the nblA-GT15-SWCNT hybrid can take place using any of these processes, i.e., endocytosis, phagocytosis, or pinocytosis. To establish that the nblA-GT15-SWCNT hybrid was able to enter *S. elongatus* bacteria, we performed Raman spectroscopy on the sample, as shown in Figure 5.5.

5.5.1 Localization of SWCNT in bacteria with Raman Spectroscopy

Figure 5.5. (a) Two Raman spectra taken at the points marked as a blue and red star respectively; (b) S. elongatus bacteria incubated autofluorescence map; (c) Heat map of the SWCNT G' Raman peak intensity

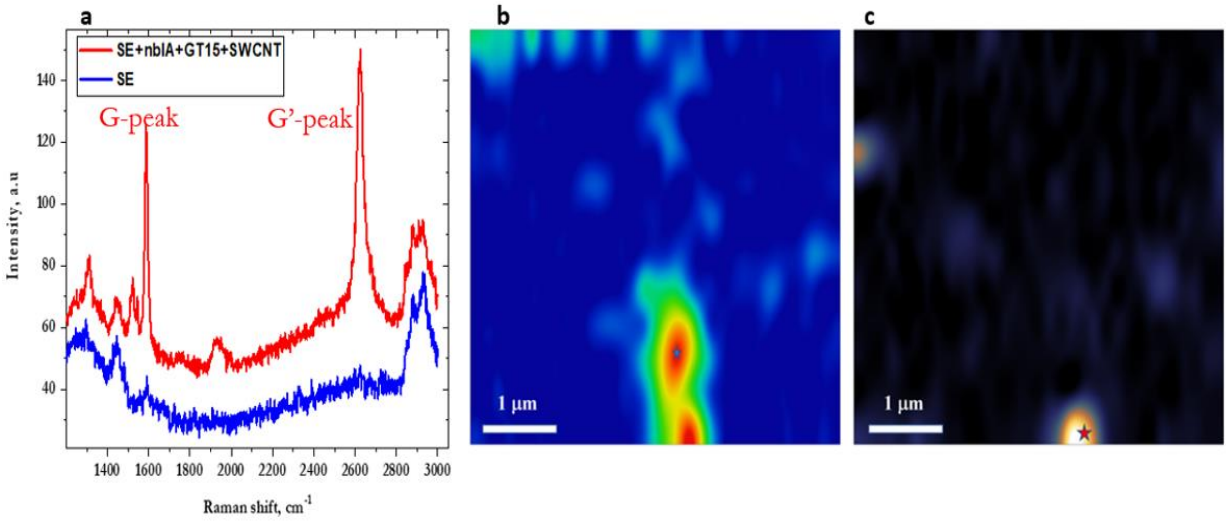

Raman hyperspectral imaging was used to probe the presence of SWCNTs in the bacteria. In general, SWCNTs can be identified by representative Raman features on the hyperspectral map, specifically the G-band and G′-band, which are two major peaks shown on the Raman spectrum for a SWCNT spin-coated onto an Si/SiO_2 substrate (Figure 3.2). Although these peaks are intense, in the presence of bacteria we expect to see additional false positives around the SWCNT G-band due to the C-C bond stretching lines in bacteria proteins and DNA. Therefore G'-band SWCNT filter was chosen to plot Raman maps.

To prepare samples, we followed a protocol previously discussed in Chapter 3.2. The Raman hyperspectral maps in Figure 5 represent the spatial distribution of bacteria autofluorescence (b) and intensity of SWCNT G' band (c). We can clearly observe the location

The blue and red curves in Figure 5(c) are two spectra taken in locations marked as blue and red stars in (b) and (c). The blue spectrum shows multiple Raman lines which are characteristic to bacteria and SWCNT, while the red spectrum does not contain Raman lines of SWCNT. Although colocalization of bacteria and SWCNT was observed, due to diffraction limited resolution we cannot conclude the internalization of SWCNT in bacteria.

5.5.2 Characterization using SEM

Figure 5.6. Scanning electron microscopy image of S. elongatus bacteria fed with the nblA-GT15-SWCNT hybrid solution

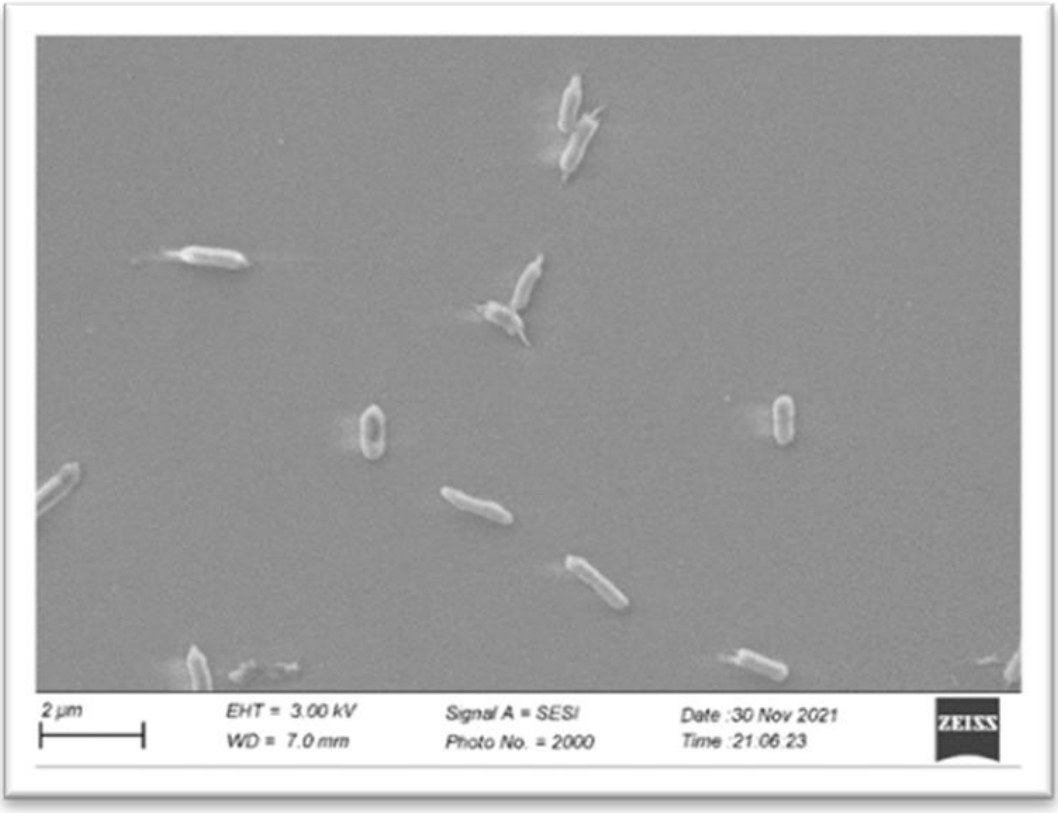

The SEM image in Figure 5.6 suggests that the shape of bacteria was preserved despite incubation with the nblA-GT15-SWCNT hybrid.

We saw a co-localization of SWCNTs with the bacteria, which suggests that the nblA-GT15-SWCNT hybrid enters the bacteria. However, further cryo-electron microscopic studies are warranted to establish the exact nature of the SE-nblA-GT15-SWCNT -bacteria interaction, as shown in Figure 5.7

5.5.3 Characterization using Cryo-EM

In the cryo-EM image, shown in Figure 5.7(a), the white circles show the suggested route the nblA-GT15-SWCNT nanohybrid followed to enter the SE bacteria membrane. Since the bacteria and SWCNT compositions are dominated by carbon, they have comparable intensities, which made them hard to resolve. The green image with the red arrows shows the faint image of what may be a SWCNT penetrating the SE bacteria outer membrane.

Figure 5.7. Cryo-EM image of S. elongatus bacteria fed with nblA-GT15-SWCNT hybrid solution

This image suggests that the nblA-GT15-SWCNT hybrid can be internalized by the

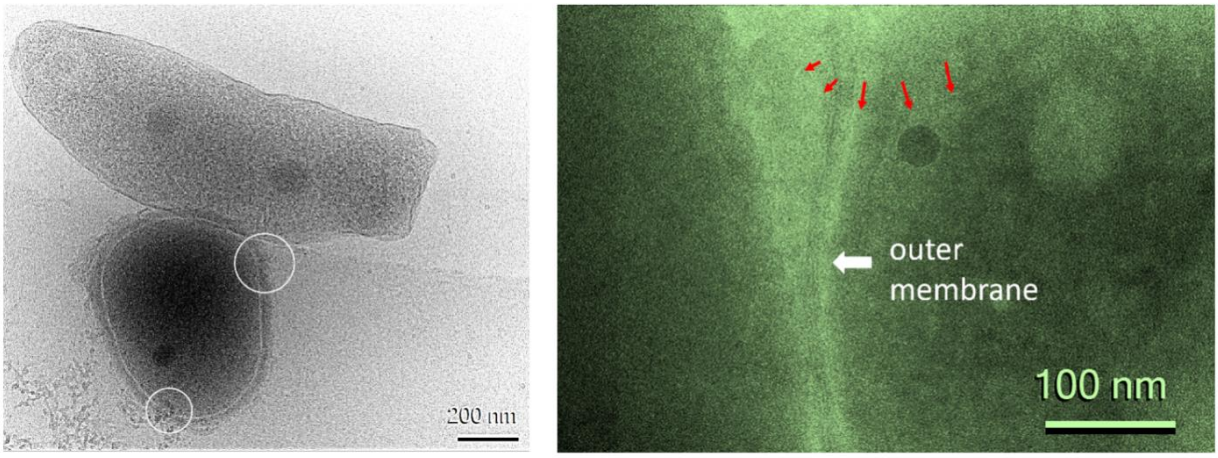

bacteria. However, conclusive evidence for membrane penetration requires future higher-resolution studies.

5.6 Kinetics of degradation of phycobilisomes in *S. elongatus* bacteria

It is poorly understood how the *nblA* peptide leads to phycobilisome degradation. The *nblA* shows no sequence similarity to proteins with known functionality and it exhibits no detectable proteolytic activity. Evidence suggested that *nblA* could tag or disrupt phycobilisomes, rendering them susceptible to degradation (Collier & Grossman, 1994). Others report that *nblA* binds to phycobiliproteins from the filamentous cyanobacterium Tolypothrix PCC 7601, and preferentially to phycocyanin and phycoerythrin (Luque et al., 2003). Phycobilisome degradation induces a blue green to yellow green color change in the cells, referred to as bleaching or chlorosis. It has also been reported that *nblA* binds via a conserved region at its C terminus to the α-subunits of phycobiliproteins, the main components of phycobilisomes (Karradt et al., 2008).

Alternatively, *nblA* could trigger phycobilisome degradation by interacting with some of its constituents, either by covalent or non-covalent binding, or by disruption of the phycobilisomes via ionic interactions between the C-terminal in *nblA* and N-terminal in phycobilisomes, rendering them susceptible to degradation. The *nblA* also may activate other genes that are involved in the phycobilisome degradation process (Grossman et al., 1993).

Phycobilisomes degrade naturally. Nagarajan et al., (2019) report that about 80% of the phycobilisomes in each cell degrade in six hours under optimal light and CO_2 conditions. However, we observed a faster than natural phycobilisome degradation rate when the nblA-GT15-SWCNT hybrid was incubated with the bacteria.

Figure 5.8. Fluorescence Intensity of cyanobacteria (SE) at resonance excitation of Phycolibisome (548 nm) at the beginning of starvation

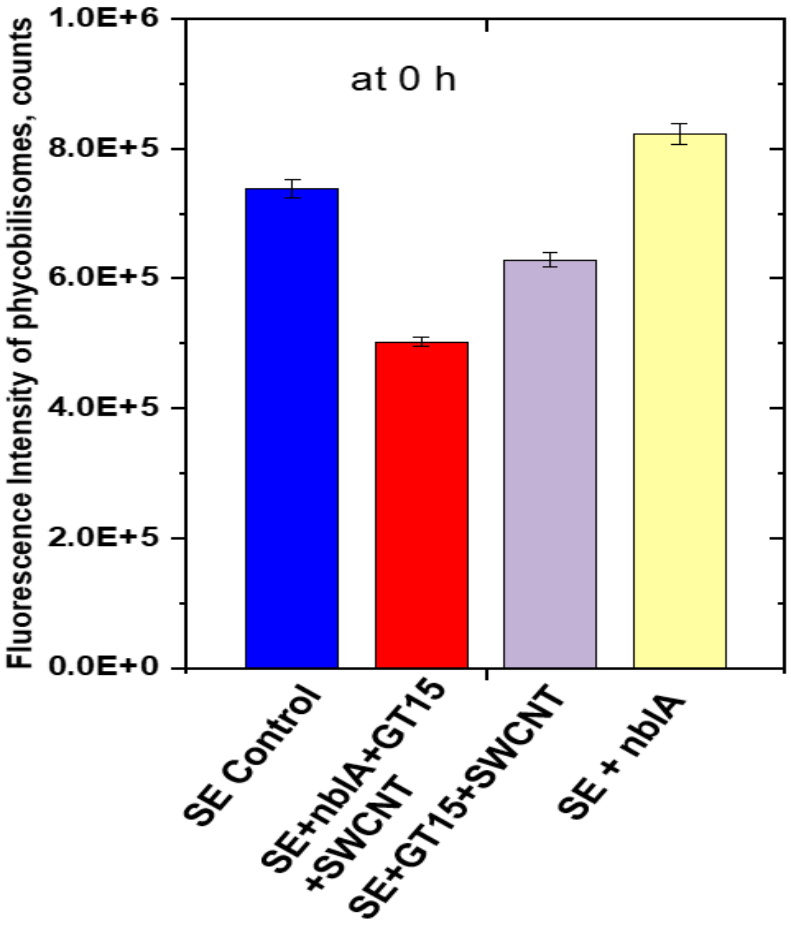

Note. (blue) control cell; (red) cell modified with nblA-GT15-SWCNT hybrid;(violet), cell directly modified with *nblA* (yellow, negative control). It is worth noting that the modified cell showed a significant drop of fluorescence activity (error bar at ±2σ). The data plotted here are extracted from the maximum fluorescence intensity of phycobilisome (as represented in Appendix E).

Figure 5.8 provides a comparison of the fluorescence intensity of phycobilisomes excited at the resonance wavelength of 548nm for four samples, i.e., the SE bacteria(control), SE incubated with ordinary *nblA* peptide, SE incubated with GT15-SWCNT, and lastly SE incubated with nblA-GT15-SWCNT hybrid. We observed that the SE with the nblA-GT15-SWCNT hybrid showed the lowest fluorescence intensity, which indicates the highest phycobilisome degradation among these samples. Hence, we proceeded with this hybrid system for our studies. The other two samples (i.e., SE incubated with *nblA* via normal addition with no delivery vehicle, and the addition of GT15-SWCNT hybrids) exhibit considerably lower degradation compared to the nblA-GT15-SWCNT hybrid. We observed an increase in fluorescence intensity in the sample with added nblA. This observation may be because nblA was unable to reach the phycobilisomes by itself and, instead, it serves as food for the bacteria, thereby enhancing bacterial growth and increasing in fluorescence activity. Hence, our studies focused on comparing control sample (i.e., SE with the SE incubated) with nblA-GT15-SWCNT hybrid sample.

Figure 5.9: Mean first order degradation profiles of phycobilisomes in S. elongatus

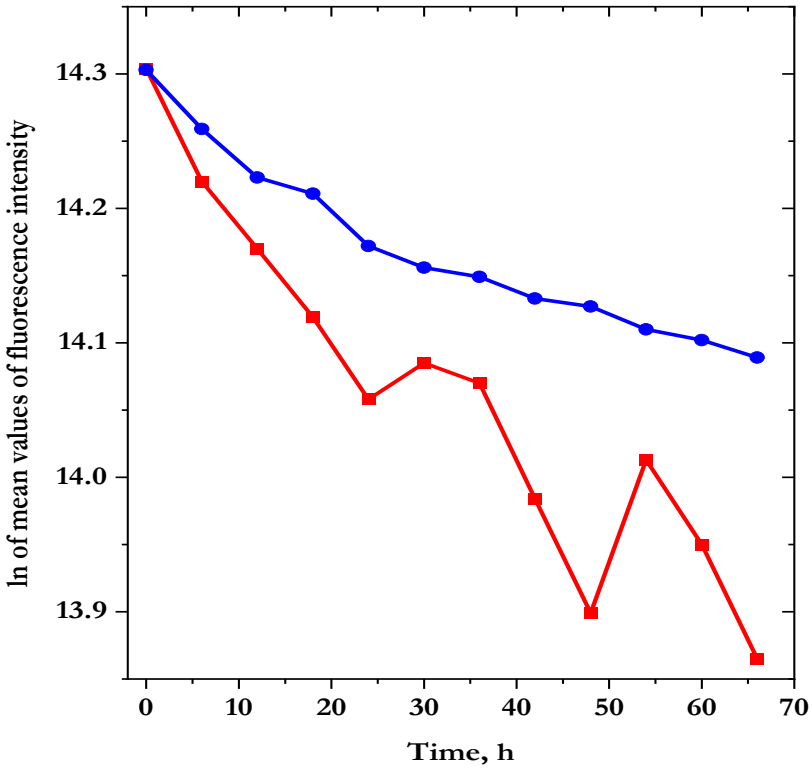

Note. (blue plot) and S. elongatus bacteria fed with nblA-GT15-SWCNT hybrid solution (red plot), (0-66 h after peak fluorescence). For each data point, n=9.

By comparing the test and control samples 0-66 h after peak fluorescence in Figure 5.9, we observed that, qualitatively, the degradation rate of the sample with the hybrid was greater than the degradation rate for the control sample, as shown. Hence, the presence of nblA-GT15-SWCNT hybrid increased the rate of phycobilisome degradation in the bacteria, as shown by the phycobilisome fluorescence in the experiment. In addition to the faster phycobilisome degradation in SE incubated with nblA-GT15-SWCNT hybrid, we also observed a zigzag degradation pattern over short time intervals, with low variability. This pattern may be attributed

to the DNA present in the sample serving as short term nutritional support for the bacteria, leading to a zigzag pattern of growth and decay.

Figure 5.10: Fitting parameters Slope (s_m), $s_m + 2\sigma$ and $s_m - 2\sigma$ for the degradation of phycobilisomes in S. elongatus bacteria with nblA-GT15-SWCNT hybrid(red) and without nblA-GT15-SWCNT hybrid(blue) at 0-66 h after the peak fluorescence based on data from Figure 5.9.

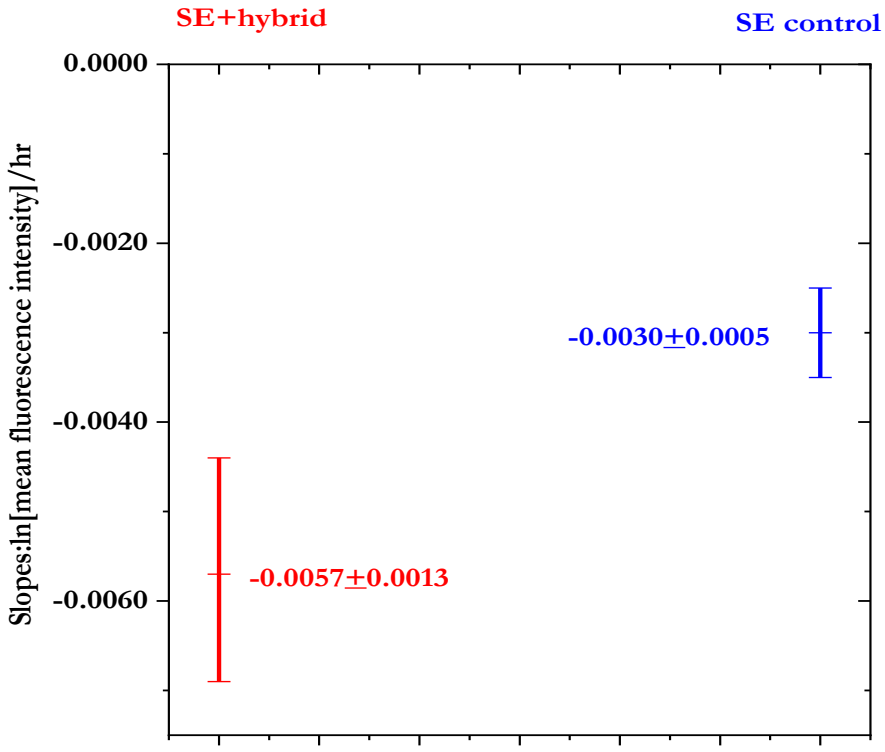

Based on the results of the plots shown in Figure 5.9, Figure 5.10 shows the values for the slope of the control and test both samples over 66 hours past the peak fluorescence. These data demonstrate that the long-term rate of fluorescence degradation is significantly faster, with 95% confidence, for the SE incubated with nblA-GT15-SWCNT hybrid than the corresponding rate for the SE control.

Consequently, the presence of the nblA-GT15-SWCNT hybrid adversely impacts phycocyanin fluorescence.

Figure 5.11. Short term kinetics of degradation of phycobilisomes in S. elongatus (blue) and S. elongatus bacteria fed with nblA-GT15-SWCNT hybrid solution (red) (0-24 h after peak fluorescence. For each data point, n=9.

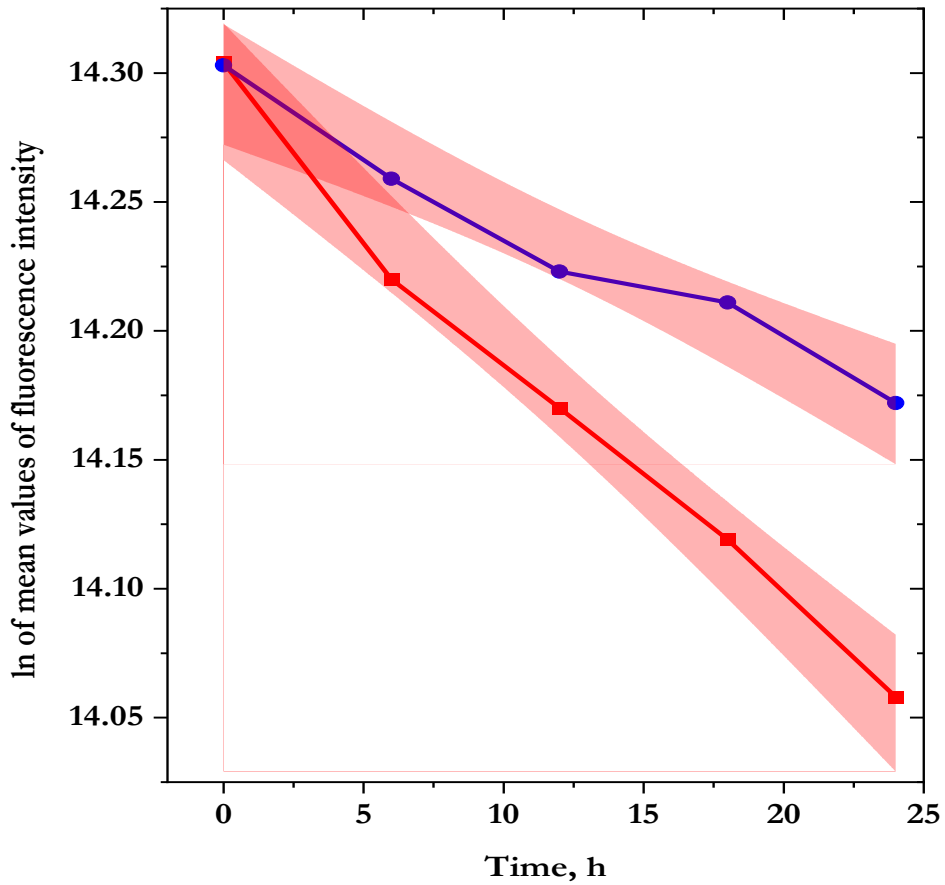

Figure 5.11 compares the initial first-order fluorescence (phycobilisome) degradation rates within the first 24 hours of peak fluorescence for control and hybrid samples. For these samples, the initial degradation rates differ significantly, as demonstrated by the diverging and nonoverlapping 95% confidence intervals, based on Origin analysis. Specifically, the fluorescence of the hybrid system degrades significantly faster than that of the SE control.

Figure 5.12: Fitting Slope (s_m), $s_m + 2\sigma$ and $s_m - 2\sigma$ for the degradation of phycobilisomes in S. elongatus bacteria(blue) with and without nblA-GT15-SWCNT hybrid (red) at 0-24 hr. after the peak fluorescence based on data from Figure 5.11.

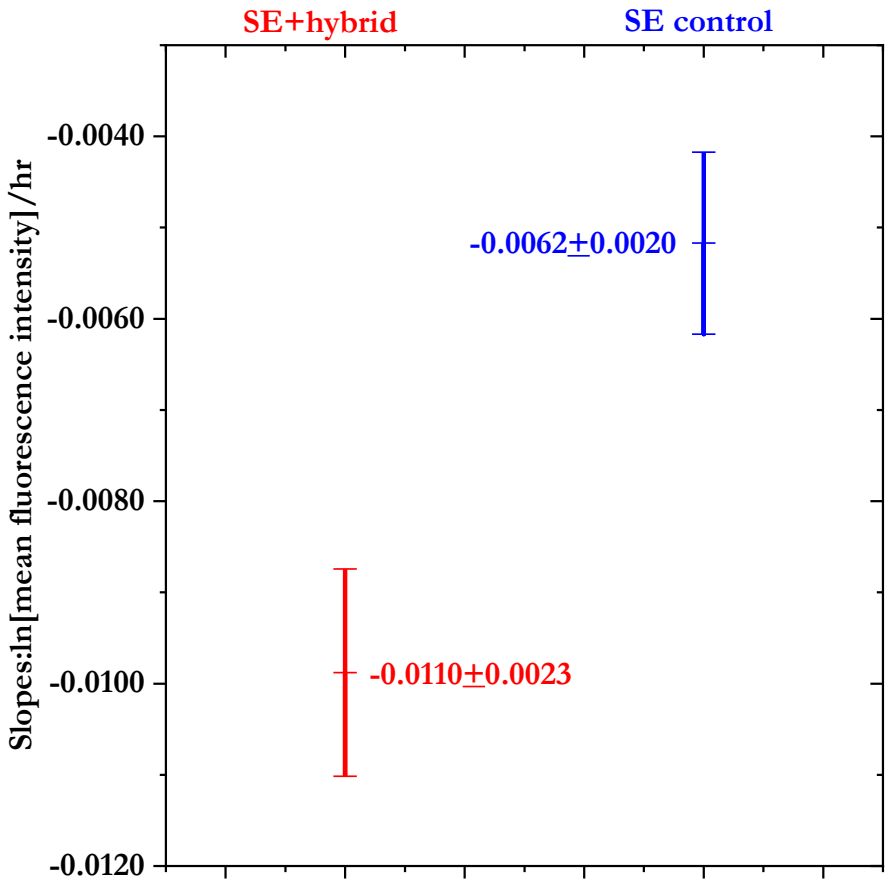

As shown in Figure 5.12, even within the first 24 hours of post-peak fluorescence, the fluorescence of the hybrid system degrades about twice as fast as that of the control, i.e., SE alone, with 95% confidence. The relative degradation rates of the hybrid to the control system appear to be relatively constant over the short-term and longer-term trials, though the initial short-term degradation rates for both systems appear to be faster than those for the longer-term trends, i.e., over 66 hours.

5.7 Metabolic activity of *S. elongatus* bacteria with and without nblA-GT15-SWCNT hybrid

Berla proposed that, during the process of electron transport, energy is transferred from a phycocyanin (PC) donor to an allophycocyanin (APC) acceptor, which serves as the terminal energy acceptor (Berla et al., 2015). At Photosystem II (PSII), a water splitting event occurred and hydrogen ions produced are used for the protonation of NADP at Photosystem I (PSI). Here, the electrons are excited by light for a reduction to NADPH, as shown in Figure 5.13.

The presence of the nblA-GT15-SWCNT hybrid appears to interrupt energy transfer and changes/increases the rate at which phycobilisomes are degraded. This occurs because of a complex, and yet to be elucidated, formation that exists between the C-terminal of the *nblA* and N-terminal of the phycocyanin. The *nblA* hybrid-phycobilisome complex, indicated in Figure 5.13, may simply decrease the efficiency of phycobilisome absorbance or photoluminescence. This interaction appears to inhibit the water splitting process, which protonates the system, and attenuate ATP production.

Additional support for this assertion can be obtained from adenosine triphosphate (ATP) quantification to monitor its level of depletion. We believe that the residual ATP in the bacteria samples reflects the energy present in the bacteria during and after chlorosis. Since ATP serves as an indicator for energy derived from the chlorophyll, we correlate ATP levels and trends with phycobilisome degradation.

Figure 5.13. Proposed energy and electron transfer pathway during the delivery of nblA peptide into S. elongatus bacteria and ATP depletion

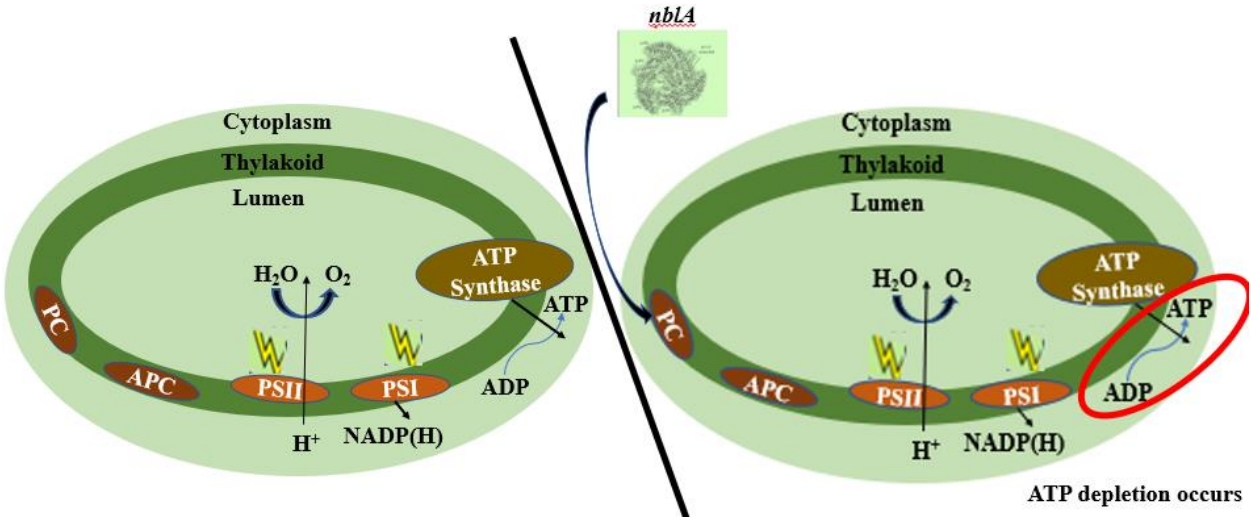

This work suggests that the delivery of nblA into SE bacteria, using GT15-SWCNT as a vehicle to localize the nblA in the phycocyanin (PC) component of the phycobilisome. This process inactivates the PC and effectively blocks the subsequent electron transfer that leads to ATP production.

We used the Colony Forming Units (CFU) method and other cell counting techniques to quantify the amount of cellular ATP. However, we found these techniques to be inappropriate because they only estimated the number of live bacteria. A bacterium with an almost completely degraded phycobilisome is expected to have less ATP because of ATP depletion.

Figure 5.14. Comparison between the (a) slopes of degraded phycobilisomes in control bacteria and modified bacteria (0-66 hr) and (b) the observed concentrations of ATP (µg/mL) in control bacteria and modified bacteria at 66 hr.

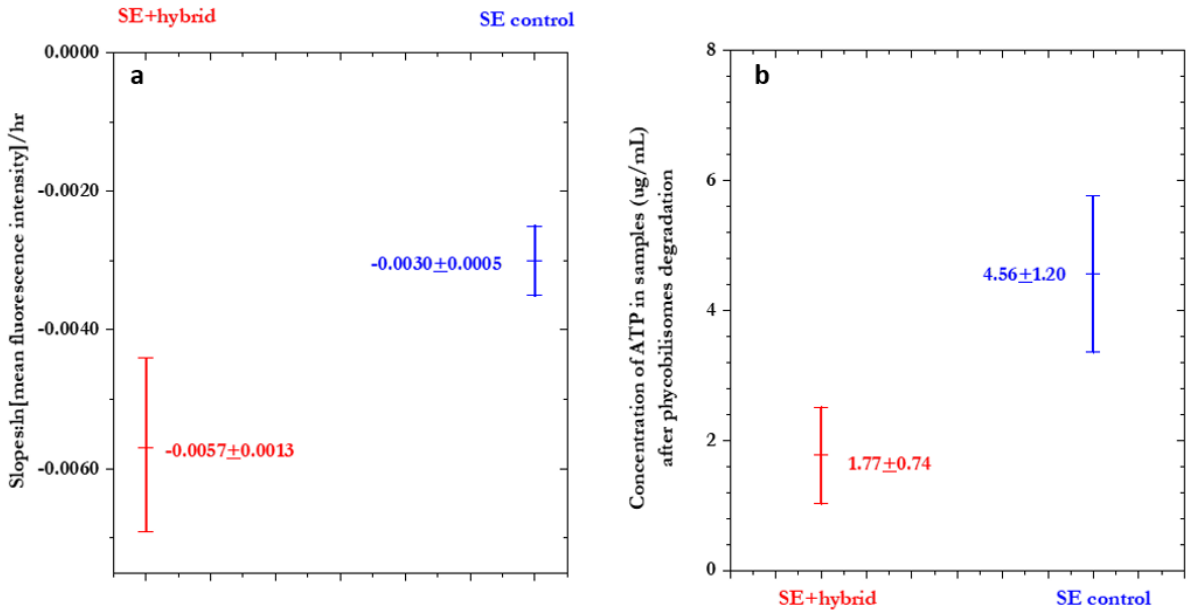

We chose to prepare a standard calibration curve using a Kinase-glo assay. The concentration of ATP found in *S. elongatus* bacteria was found to be 4.56 (±1.20, 2σ) µg/mL, while 1.77 (±0.74, 2σ) µg/mL ATP was found in the bacteria with nblA-GT15-SWCNT hybrid.

The ratio of hybrid and control fluorescence degradation rates, shown in Figure 5.14a, appear to be inversely proportional to the corresponding relative observed rates of ATP production, shown in Figure 5.14b. Specifically, the roughly 2X increase in the hybrid fluorescence degradation rate versus that of the SE control corelates with roughly a 2X decrease in ATP production for the hybrid system versus the SE control. These results suggest that the hybrid's interaction with phycobilisomes, 'PC', serves to decrease the photoluminescence efficiency and sufficiently explains the attenuated ATP production in the hybrid system. This

finding supports our prediction that the hybrid bacterium would exhibit a lower concentration of ATP than that of the SE control system.

Based on the proposed energy transfer pathway, we can infer that the nblA peptide delivered into or onto *S. elongatus* bacteria inhibits the light-harvesting capability of the phycobilisome. This early-stage event thereby inhibits subsequent energy transfer and harvesting activities. Specifically, we observed that the hybrid system reduced ATP energy production roughly by half.

5.8 Discussion

Our initial hypothesis asserted that the DNA wrapped SWCNT would deliver *nblA* peptide into the phycobilisome of the *S. elongatus* bacteria. Our results from Raman spectroscopic, scanning electron and cryo-electron microscopic studies suggest (due to resolution limits) that the SWCNT carried and delivered the *nblA* into or onto the bacteria. The other hypothesis was that the presence of the *nblA* peptide inhibits phycobilisome fluorescence and attenuates the subsequent energy and electron transfer process, which suppresses ATP production. The results generally support the hypothesis. The quantified ATP in bacteria samples (n=3) incubated with the nblA-GT15-SWCNT hybrid solution expressed a lower amount of ATP, i.e., 1.77 ±0.74(2σ) μg/mL compared to the amount of ATP present in the control bacteria samples (n=3), i.e., 4.56 ±1.20(2σ) μg/mL.

This table summarizes the comparisons between predicted and observed outcomes.

Table 5.1. Predictions

Prediction #	**Prediction**	**Result**	**Prediction confirmed or refuted**
1	GT15-SWCNT hybrid delivers *nblA* peptide into the phycobilisomes	Washed bacteria samples show the hybrid is either in or on the bacteria. Faint path of entry shown by cryo-EM suggests that the hybrid entered the bacteria.	Suggestive, but inconclusive, as a higher resolution method may be needed.
2	Hybrid interrupts the energy and electron transfer pathway to ATP.	Kinase-glo assay for ATP quantification shows a higher amount of ATP in bacteria control sample and a reduced ATP in bacteria with nblA hybrid	Supports the hypothesis.

In conclusion, this work demonstrates the feasibility of a non-genetically modified process to impact the performance properties of photosynthesis, in bacteria, such as *S. Elongatus*. Future studies will explore the general nature of this process in other living tissue, e.g., plants, and whether it can be applied to tune in desirable cellular properties.

CHAPTER VI: CONCLUSIONS AND FUTURE DIRECTIONS

6.1 Conclusions

The primary goal of this research was to develop a delivery system that can offer the following possibilities:

(a) To demonstrate that the hybridization events of ssDNA-SWCNT hybrids can be monitored using FRET and solvatochromism, even in the presence of other external factors, such as pH and competing ions.

(b) To establish the entry of a nblA-GT15-SWCNT nanohybrid leading to designed bacteria properties.

Even though the photosynthetic activities of cyanobacteria have been reported to have been enhanced, a reduction in its photo response has never been reported. Therefore, the major focus of the dissertation was aimed at studying the process of delivering a peptide that has the potential to inactivate the light-harvesting and/or energy transfer capability of the phycobilisomes in the *S. elongatus* bacteria. The manipulation of the light-harvesting capability of the phycobilisomes in the *S. elongatus* bacteria was achieved in three stages: the choice of the vehicle for the delivery, the design of the delivery, and the evaluation of the phycobilisomes degradation based on its mechanism and rate of degradation. The summary of the dissertation research findings is presented below.

Aim 1 of the dissertation research work was to design and monitor the conformational changes that occur between two different and complementary ssDNA-SWCNT hybrids using FRET. We successfully used FRET and solvatochromism to study the conformational changes that occur during DNA unzipping and hybridization events. We prepared nanotree and nanobrush assemblies from two complementary ssDNA-SWCNT nanohybrids. This formation

was studied using AFM imaging as presented in the dissertation. We correlated the enhancement of SWCNT photoluminescence with nanohybrid formation.

Aim 2 was targeted at investigating the delivery of nblA-GT15-SWCNT hybrid into the thylakoid membrane of the *S. elongatus* bacteria. Overall, we established the entry or proximity of nblA-GT15-SWCNT nanohybrids leading to designed bacteria properties. Specifically, ATP production in the designed bacteria sample was suppressed by about 50%. This aligned with our assumption that *S. elongatus* bacteria with the hybrid is expected to reduce ATP production because of a modified photoresponse in the engineered bacteria.

6.2 Recommendations for future research

The research presented in this dissertation has established many promising opportunities for future research. This section thereby emphasizes some of the research activities that can be implemented in the nearest future, as they pertain to studying the engineering of biological materials using a ssDNA-SWCNT hybrid.

6.2.1 Use of other DNA strands and SWCNT chiralities

In this study, SWCNT with about 350nm was used for the experiment. In as much as we were only able to speculate that the SWCNT entered the bacteria, we reported the degradation of phycobilisomes using the *nblA* peptide that was delivered to the phycobilisomes. Hence, in a bid to improve this process, a shorter SWCNT with higher diameter may be a potential candidate. For example, SWCNT (9,8) with diameter 1.17nm, (8,8) with diameter 1.10nm, (9,9) with diameter 1.24nm will have the potential to carry and deliver the peptide or any other therapeutic agent more conveniently. We propose the use of other strands of ssDNA since we know that the strength of DNA-wrapped SWCNT is dependent on the ssDNA strand or sequence used for the fabrication of the delivery platform.

6.2.2 Repeating experiment with another bacteria class

This research focused mainly on the delivery of *nblA* into a cyanobacteria because we were more focused on observing and monitoring the effect that it would have on the light-harvesting capability of phycobilisomes after the delivery of *nblA.* However, it will be a great research opportunity to deliver other therapeutic material into another class of bacteria or algae and monitor its end products to see if the hybrid can be employed for any bacteria. An organism with a faster growth rate should also be considered for the purpose of reducing the duration of this experiment.

6.2.3 Proof of concept for in vivo delivery of ssDNA in cancer cells

Using the approach in Aim 1, a real *in vivo* delivery of DNA sequences is to be delivered in cancer cells to study the specificity of the delivery system proposed.

6.2.4 Further studies on photoresponse enhancement

While we were able to achieve a decreased photoresponse of the bacteria using the *nblA* peptide delivery using DNA-SWCNT, we propose that another, yet to be defined, peptide, or other biological agent may be used to engineer towards an increased photoresponse of the bacteria.

REFERENCES

Ali, S. R., Parajuli, R.R, Balogun, Y., Ma, Y., &He, H.A. (2008). Nonoxidative Electrochemical Sensor Based on a Self-Doped Polyaniline/Carbon Nanotube Composite for Sensitive and Selective Detection of the Neurotransmitter Dopamine: A Review *Sensors (Basel). 8*(12): 8423-8452.

Anson, D.S. (2004). The use of retroviral vectors for gene therapy-what are the risks? A review of retroviral pathogenesis and its relevance to retroviral vector-mediated gene delivery. *Genet Vaccines Ther*,2,9.

Armendáriz-Borunda, J., Bastidas-Ramírez, B. E., Sandoval-Rodríguez, A., González-Cuevas, J., Gómez-Meda, B., & García-Bañuelos, J. (2011). Production of first generation adenoviral vectors for preclinical protocols: amplification, purification and functional titration. *Journal of bioscience and bioengineering*, *112*(5), 415–421.

Bai, L., Bai, Y., & Zheng.J. (2017). Improving the filler dispersion and performance of silicone rubber/multi-walled carbon nanotube composites by noncovalent functionalization of polymethylphenylsiloxane. *Journal of Materials Science.52*(12), 7516-7529.

Banning, C., Votteler, J., Hoffmann, D., Koppensteiner, H., Warmer, M., Reimer, R., Schindler, M. (2010). A Flow Cytometry-Based FRET Assay to Identify and Analyse Protein-Protein Interactions in Living Cells. *PLoS ONE*, *5*(2), e9344.

Baraldi, I., Brancolini, G., Momicchioli, F., Ponterini, G., & Vanossi, D. (2003). Solvent influence on absorption and fluorescence spectra of merocyanine dyes: a theoretical and experimental study. *Chemical Physics*, *288*(2-3), 309–325.

Bauer, M.., Rollberg, A.., Barth, A.., & Spange, S. (2008). Differentiating between dipolarity and polarizability effects of solvents using the solvatochromism of barbiturate dyes. *European Journal of Organic Chemistry*, 4475–4481.

Becker, D., Bereiter-Hahn, J., & Jendrach, M. (2009). Functional interaction of the cation channel transient receptor potential vanilloid 4 (TRPV4) and actin in volume regulation. *European Journal of Cell Biology 88*(3), 141-52.

Behrstock, S., Ebert, A., McHugh, J., Vosberg, S., Moore, J., Schneider, B., … Svendsen, C. N. (2005). Human neural progenitors deliver glial cell line-derived neurotrophic factor to parkinsonian rodents and aged primates. *Gene Therapy*, *13(*5), 379–388.

Berciaud, S., Cognet, L., Poulin, P., Weisman, R.B., Lounis, B. (2007). Absorption spectroscopy of individual single-walled carbon nanotubes. *Nano Lett*. 7, 1203–1207.

Berla, B. M., Saha. R., Maranas.C.D., & Pakrasi. H.B. (2015). Cyanobacterial Alkanes Modulate Photosynthetic Cyclic Electron Flow to Assist Growth under Cold Stress. *Sci. Rep*. **5**, 14894.

Bernas, T., Zarebski, M., Cook, R.R., Dobrucki, J.W., Cook, P.R. (2004). Minimizing photobleaching during confocal microscopy of fluorescent probes bound to chromatin: role of anoxia and photon flux. *J Microsc*, 215,281-296.

Billinton, N., & Knight, A.W. (2001). Seeing the wood through the trees: a review of techniques for distinguishing green fluorescent protein from endogenous autofluorescence. *Anal Biochem,29*1(2),175-97.

Bilot, L., & Kawski, A. (1962). Zur theorie des einflusses von Lösungsmitteln auf die elektronenspektren der molecule. Z. *Naturforsch*, 17A, 621–627.

Biswas, R., Lewis, J. E., & Maroncelli, M. (1999). Electronic spectral shifts, reorganization energies, and local density augmentation of Coumarin 153 in supercritical solvents. Chemical Physics Letters, 310(5-6), 485–494.

Bozovic, I., Bozovic, N., Damnjanovic, M. (2000). Optical dichroism in nanotubes. *Phys. Rev. B.* 62, 6971–6974

Brady, J.E., Bjorkman, D., Herter, C., & Carr, P. (1984). Solvatochromic investigation of polarizable polymeric liquids. *Anal. Chem,56*(2), 278-283.

Buhvestov,, U., Rived, F., Rafols,, C., Bosch, E., & Roses, M. (1998). Solute–solvent and solvent–solvent interactions in binary solvent mixtures. Part 7. Comparison of the enhancement of the water structure in alcohol–water mixtures measured by solvatochromic indicators. *J. Phys. Org. Chem*, *11*(3), 185-192.

Bullok, K. E., Dyszlewski, M., Prior, J. L., Pica, C. M., Sharma, V., & Piwnica-Worms, D. (2002). Characterization of novel histidine-tagged Tat-peptide complexes dual-labeled with (99m)Tc-tricarbonyl and fluorescein for scintigraphy and fluorescence microscopy. *Bioconjugate chemistry*, *13*(6), 1226–1237.

Carbon Nanotechnologies Inc. Product Description, HiPco Single-Walled Carbon Nanotubes. (2005). Houston, TX: *Carbon Nanotechnologies Inc.*

Catalán. J., Del Valle, J.C. (2014). A spectroscopic rule from the solvatochromism of aromatic solutes in nonpolar solvents. *J. Phys. Chem. B*, 118,5168–5176.

Chávez, J. L., Jiang, H., & Duran, R. S. (2009). A study of the compartmentalization of core–shell nanoparticles through fluorescence energy transfer of dopants. Nanotechnology, *21*(5), 055703.

Chen, C. L., Kuo, L. R., Lee, S. Y., Hwu, Y. K., Chou, S. W., Chen, C. C., Chang, F. H., Lin, K. H., Tsai, D. H., & Chen, Y. Y. (2013). Photothermal cancer therapy via femtosecond-laser-excited FePt nanoparticles. *Biomaterials*, *34*(4), 1128–1134.

Collier, J. L., & Grossman, A. R. (1994). A small polypeptide triggers complete degradation of light-harvesting phycobiliproteins in nutrient-deprived cyanobacteria. *The EMBO journal*, *13*(5), 1039–1047.

Conwell, C., Huang, L., In, K., Taira, K., Kataoka, T. & Niidome (ed). (2005). Recent Progress in Non-viral Gene Delivery. Non-viral Gene Therapy Gene Design and Delivery. *Springer* Verlag Tokyo. Japan; pp: 3-11

D'Souza, F., Das, S.K., Zandler, M.E., Sandanayaka, A.S.D., &Ito, O. (2011). Bionano donor-acceptor hybrids of porphyrin, ssDNA, and semiconductive single-wall carbon nanotubes for electron transfer via porphyrin excitation. *J. Am. Chem. Soc,* 133, 19922–19930.

Davis, P. B., & Cooper, M. J. (2007). Vectors for airway gene delivery. *The AAPS Journal*,*9*(1), E11–E17.

Day, R. N. (2014). Measuring Protein Interactions Using Förster Resonance Energy Transfer and Fluorescence Lifetime Imaging Microscopy. *Microscopy and Microanalysis*,*20*(S3), 2130–2131.

De Gennes, P. G., Pincus, P., Velasco,, R.M., & Brochard, F. (1976). Remarks on polyelectrolyte conformation. *J. Physique. 37*(12), 1461-147

Demissie,, E.G., Mengesha, ET., & Woyessa, G.W. (2017). Modified solvatochromic equations for better estimation of ground and excited state dipole moments of *p*-aminobenzoic acid (PABA): Accounting for real shape over hypothetical spherical solvent shell .*Journal of Photochemistry and Photobiology A: Chemistry*, 337, 184-189.

Dixit, R., & Cyr, R. (2003). Cell damage and reactive oxygen species production induced by fluorescence microscopy: effect on mitosis and guidelines for non-invasive fluorescence microscopy. *Plant J*, 36,280-290.

Dragan, A.I., Privalov, P.L. (2008). Use of fluorescence resonance energy transfer (FRET) in studying protein-induced DNA bending. *Methods Enzymol.* 450,185-99.

Dresselhaus, M. S., Dresselhaus, G., &Eklund, P. C. (1996).Science offullerenes and carbon nanotubes: their properties and applications,*Academic press, San Diego.*

Dziuba, D., Pospíšil, P., Matyašovský, J., Brynda, J., Nachtigallová, D., Rulíšek, L., … Hocek, M. (2016). Solvatochromic fluorene-linked nucleoside and DNA as color-changing fluorescent probes for sensing interactions. *Chemical Science, 7*(9), 5775–5785.

El-Ayaan, U., Murata, F., & Fukuda, Y. (2001). Thermochromism and solvatochromism in solution. *Monatsh. Chem*, 132,1279–1294.

Escors, D., & Brecpot, K. (2010). Lentiviral vectors in gene therapy: their status and future potential. *Archivum Immunologiae et Therapia Experimentalis*;58;107–119.

Fessl, T., Adamec, F., Polı´vka, T., Foldynova´-Trantı´rkova´, S., Va´ cha, F., Trantı´rek, L. (2012). Towards characterization of DNA structure under physiological conditions in vivo at the single-molecule level using single-pair FRET. *Nucleic Acids Res, 40*(16), e121.

Flotte, T., Carter, B., Conrad, C., Guggino, W., Reynolds, T., Rosenstein, B., et al. (1996) A phase study of an adeno-associated virus-CFTR gene vector in adult CF patients with mild lung disease. *Hum Gene Ther*,7,1145-59

Franco-Molina, M. A., Mendoza-Gamboa, E., Sierra-Rivera, C. A., Gómez-Flores, R. A., Zapata-Benavides, P., Castillo-Tello, P., Alcocer-González, J. M., Miranda-Hernández, D. F., Tamez-Guerra, R. S., & Rodríguez-Padilla, C. (2010). Antitumor activity of colloidal silver on MCF-7 human breast cancer cells. *Journal of experimental & clinical cancer research: CR*, *29*(1), 148.

Frederic, D.B. (2007) Retroviral integration and human gene therapy. *J Clin Invest*,117, 2083-6

Gardlík, R., Pálffy, R., Hodosy, J., Lukács, J., Turna, J., & Celec, P. (2005). Vectors and delivery systems in gene therapy. *Med Sci Monit, 11*(4):RA110-21.

Glauner K.S., Mannuzzu, L.M., Gandhi, C.S., & Isacoff, E.Y. (1999). Spectroscopic mapping of voltage sensor movement in the Shaker potassium channel. *Nature*. *402*(6763),813-817.

Gordon, J.W., Scangos, G.A., Plotkin, D.J., Barbosa, J.A., Ruddle, F.H. (1980). Genetic transformation of mouse embryos by micro-injection of purified DNA. *Proc Natl Acad Sci USA*, 77,7380-4.

Gowing, G., Svendsen, S., & Svendsen, C. N. (2017). Ex vivo gene therapy for the treatment of neurological disorders. *Progress in Brain Research*, 99–132.

Greenstein, K. E., & Wert, E. C. (2019). Using rapid quantification of adenosine triphosphate (ATP) as an indicator for early detection and treatment of cyanobacterial blooms. *Water Research*, 154, 171–179

Grossman, A. R., Schaefer, M. R., Chiang, G. G., & Collier, J. L. (1993). The phycobilisome, a light-harvesting complex responsive to environmental conditions. *Microbiological reviews*, *57*(3), 725–749.

Grünberg, R., Burnier, J.V., Ferrar, T., Beltran-Sastre, V., Stricher, F., van der Sloot, A.M., Garcia-Olivas, R., Mallabiabarrena, A., Sanjuan, X., Zimmermann, T., et al. (2013). Engineering of weak helper interactions for high-efficiency FRET probes. *Nat Methods*, 10,1021-1027

Guhathakurta, P., Prochniewicz, E., Grant, B. D., Peterson, K. C., & Thomas, D. D. (2018). High-throughput screen, using time-resolved FRET, yields actin-binding compounds that modulate actin-myosin structure and function. *The Journal of biological chemistry*, *293*(31), 12288–12298.

Ha, T., Enderle, T., Ogletree, D.F., Chemla, D.S., Selvin, P.R., & Weiss, S. (1996). Probing the interaction between two single molecules: fluorescence resonance energy transfer between a single donor and a single acceptor. *Proc Natl Acad Sci USA*, 93, 6264-6268.

Habenicht, B.F., & Prezhdo, O.V. (2008). Nonradiative quenching of fluorescence in a semiconducting carbon nanotube: a time-domain ab initio study. *Phys. Rev. Lett.* 100, 197402–1– 197402–4.

Hammam, E., & El-Nahas, A.M. (1998). Theoretical Study on Photophysical and Photochemical Properties of a Merocyanine Dye. *J. Phys. Chem A*, 102, 9739-9744

Han, S.O., Mahato, R.I., Sung, Y.K., & Kim, S.W. (2000). Development of biomaterials for gene therapy. *Mol Therapy*, 2, 302–17.

Hartschuh, A., Pedrosa, H.N., Peterson, J., Huang, L., Anger, P., Qian, H., Meixner, A.J., Steiner, M., Novotny, L., &Krauss, T.D. (2005). Single carbon nanotube optical spectroscopy. *Chem. Phys. Chem*. 6, 577–582.

He, H., Huy, LA., Dramou, P. et al. (2013) Carbon nanotubes: applications in pharmacy and medicine. *BioMed Research International*, 578290

Hirabayashi, M., Takahashi, R., Ito, K., Kashiwazaki, N., Hirao, M., Hirasawa, K., et al. (2001). A comparative study on the integration of exogenous DNA into mouse, rat, rabbit, and pig genomes. *Exp Anim*;,50,125-31.

Hirlekar R, Yamagar M, Garse H et al. (2009) Carbon nanotubes and its applications: a review. *Asian Journal of Pharmaceutical and Clinical Research* 2: 17–27.

Hosoi, H., Nakamura, M., Yamada, Y., Sueoka, K., & Mukasa, K. (2008). Surface potential imaging of SWCNT-FET devices by scanning Kelvin probe microscopy. *Journal of Physics: Conference Series*, *100*(5), 052085.

Hu, C., Zhang, Y., Bao, G., Zhang, Y., Liu, M., & Wang, Z. L. (2005). DNA Functionalized Single-Walled Carbon Nanotubes for Electrochemical Detection. *The Journal of Physical Chemistry B*, *109*(43), 20072–20076.

Hu, W.W., Wang, Z., Hollister, S.J., & Krebsbach, P.H. (2007). Localized viral vector delivery to enhance in situ regenerative gene therapy. *Gene Ther*,14,891–901.

Huang, Y., Liu, X., Dong, L., Liu, Z., He, X., & Liu, W. (2011). Development of Viral Vectors for Gene Therapy for Chronic Pain. *Pain Research and Treatment*, 1–8.

Hughes, M.E., Brandin, E., &Golovchenko, J. A. (2007). Optical absorption of DNA-carbon nanotube structures. *Nano Lett*. *7*(5):1191-4.

Hwang, L.C., Hohlbein, J., Holden, S.J., Kapanidis, A.N. (2009). Single-molecule FRET: methods and biological applications. *Handbook of Single-Molecule Biophysics*, 129–163.

Jena, P.V., Galassi, T.V., Roxbury, D., &Heller, D.A. (2017a). Review—Progress toward Applications of Carbon Nanotube Photoluminescence. *ECS J. Solid State Sci. Technol. 6(*6): M3075–M3077.

Jena, P.V., Roxbury, D., Galassi, T.V., Akkari, L., Horoszko, C.P., Iaea, D.P., Budhathoki-Uprety, J., Pipalia, N. H., Haka, A.S., Harvey, J.D., Mittal, J., Maxfield, F.R., Joyce, J. A., &Heller, J. A. (2017b). A carbon nanotube optical reporter maps endolysosomal lipid flux. *ACS Nano,* 11, 11, 10689-10703.

John, P.L., Kevin, C., & Joaquin, G. (2011) Sperm and testis mediated DNA transfer as a means of gene therapy. *Syst Biol Reprod Med*. 57,35-42.

Józefowicza ,M., Milartb, P., & Heldt, J.R. (2009). Determination of ground and excited state dipole moments of 4,50 -diamino [1,10 :30 ,100-terphenyl]-40 ,60 -dicarbonitrile using solvatochromic method and quantum-chemical calculations. *Spectrochim. Acta Part A,* 74, 959–963.

Kajihara, D., Abe, R., Iijima, I., Komiyama, C., Sisido, M., Hohsaka, T. (2006). FRET analysis of protein conformational change through position-specific incorporation of fluorescent amino acids. *Nat Methods*.*3*(11):923-929

Kamlet, M. J., & Taft, R. W. (1979b). Linear solvation energy relationships. Part 1. Solvent polarity–polarizability effects on infrared spectra. *J. Chem. Soc., Perkin Trans, 2* (3), 337–341.

Kamlet, M. J., Abboud, J. L., & Taft, R. W. (1977). The solvatochromic comparison method. 6. The .pi.* scale of solvent polarities. *Journal of the American Chemical Society, 99*(18), 6027–6038

Kamlet, M. J., Hall, T. N., Boykin, J., & Taft, R. W. (1979a). Linear solvation energy relationships. 6. Additions to and correlations with the. pi.* scale of solvent polarities. *The Journal of Organic Chemistry*, *44*(15), 2599–2604.

Kang, Y., Zhang, Y., Liang, T., Leung, Y.M., Ng, B., Xie, H., Chang, N., Chan, J., Shyng, S.L., Tsushima, R.G., & Gaisano, H.Y. (2011). ATP modulates interaction of syntaxin-1A with sulfonylurea receptor 1 to regulate pancreatic beta-cell KATP channels. *Journal of Biologic Chemistry 286*(7), 5876-83.

Karradt, A., Sobanski, J., Mattow, J., Lockau, W., & Baier, K. (2008). NblA, a Key Protein of Phycobilisome Degradation, Interacts with ClpC, a HSP100 Chaperone Partner of a Cyanobacterial Clp Protease. *Journal of Biological Chemistry, 283*(47), 32394–32403

Karuri, N.W., Lin, Z., Rye, H.S., & Schwarzbauer, J.E. (2009). Probing the conformation of the fibronectin III1-2 domain by fluorescence resonance energy transfer. *Journal of Biological Chemistry 284*(6), 3445-3452.

Kaur, A., Kaur, P., & Ahuja, S. (2020). Förster resonance energy transfer (FRET) and applications thereof. Analytical Methods, 12(46), 5532–5550.

Kawski A. (2002). On the estimation of excited-State dipole moments from solvatochromic shifts of absorption and fluorescence spectra, *Z. Naturforsch* ,57a ,255–262.

Kay, M. A. (2011). State-of-the-art gene-based therapies: the road ahead. *Nature Rev. Genet*, 12, 316–328.

Kevin, S., & Corrado, S. (2005). Sperm-mediated gene transfer: Applications and implications. *BioEssays*, 27, 551-62.

Khripin, C. Y., Tu, X., Howarter, J., Fagan, J., & Zheng, M. (2012). Concentration Measurement of Length-Fractionated Colloidal Single-Wall Carbon Nanotubes. Analytical Chemistry, 84(20), 8733–8739.

Kim, S.Y., Yang, D., Myeong, J., Ha, K., Kim, S.H., Park, E.J., Kim, I.G., Cho, N.H., Lee, K.P., & Jeon, J.H. (2013). Regulation of calcium influx and signaling pathway in cancer cells via TRPV6-Numb1 interaction. *Cell Calcium. 53*(2):102-111.

Kohl, T., Heinze, K. G., Kuhlemann, R., Koltermann, A., & Schwille, P. (2002). A protease assay for two-photon crosscorrelation and FRET analysis based solely on fluorescent proteins. *Proceedings of the National Academy of Sciences*, *99*(19), 12161–12166.

Komatsu, N., Aoki, K., Yamada, M., Yukinaga, H., Fujita, Y., Kamioka, Y., & Matsuda, M. (2011). Development of an optimized backbone of FRET biosensors for kinases and GTPases. *Mol Biol* C*ell*, 3,4647-56.

Krusiński, T., Ożyhar, A., & Dobryszycki, P. (2010). Dual FRET assay for detecting receptor protein interaction with DNA. *Nucleic Acids Research*, *38*(9), e108–e108.

Kumar, N.; Kumbhat, S. Carbon-Based Nanomaterials. Essentials in Nanoscience and Nanotechnology. (2016). John Wiley & Sons, Inc.: Hoboken, NJ, U.S.A.; pp 189–236.

Kumoi, S. (1970). Spectrophotometric determination of water in organic solvents with solvatochromic dyes. *Talanta*, *17*(4), 319–327

Lai, C.M., Lai, Y.K., & Rakoczy, P.E. (2002). Adenovirus and adeno-associated virus vectors. *DNA Cell Biol*, 21, 895-913.

Lam, A.J., St-Pierre, F., Gong, Y., Marshall, J.D., Cranfill, P.J., Baird, M.A., McKeown, M.R., Wiedenmann, Lomzov, A. A., Vorobjev, Y. N., & Pyshnyi, D. V. (2015). Evaluation of the Gibbs Free Energy Changes and Melting Temperatures of DNA/DNA Duplexes Using Hybridization Enthalpy Calculated by Molecular Dynamics Simulation. *The*

Journal of Physical Chemistry B, 119(49), 15221–15234

Lundstrom, K., & Boulikas, T. (2003). Viral and non-viral vectors in gene therapy: technology development and clinical trials. *Technol Cancer Res Treat*, 2,471–86

Luque, I., Ochoa De Alda, J. A., Richaud, C., Zabulon, G., Thomas, J. C., & Houmard, J. (2003). The NblAI protein from the filamentous cyanobacterium Tolypothrix PCC 7601: regulation of its expression and interactions with phycobilisome components. *Molecular microbiology*, *50*(3), 1043–1054.

Ma, L., Yang, F., & Zheng, J. (2014). Application of fluorescence resonance energy transfer in protein studies. *Journal of molecular structure*, *1077*, 87–100.

Maffeo, C., & Aksimentiev, A. (2017). Molecular mechanism of DNA association with single-stranded DNA binding protein. *Nucleic Acids Research, 45*(21), 12125–12139.

Mahato RI, Smith LC, Rolland A. Pharmaceutical perspectives of nonviral gene therapy. *Adv Genet.* 1999; 41:95–156.

Mali, S. (2013). Delivery systems for gene therapy. *Indian Journal of Human Genetics*, 19(1), 3.

Mangham. & Destainville, N. (2016). Physics of base-pairing dynamics in DNA, *Physics Reports*, 631, 1-41.

Manning, G. S. (1969a). Limiting laws and counterion condensation in polyelectrolyte solutions. I. Colligative properties. *J. Chem. Phys*, 51, 924-933.

Manohar, S., Mantz, A.R., Bancroft, K. E, Hui, C.Y., Jagota, A.,& Vezenov, D.V. (2008). Peeling single-stranded DNA from graphite surface to determine oligonucleotide binding energy by force spectroscopy.*Nano Lett.* 8(12):4365-72.

Marini, A., Munoz-Losa. A., Biancardi.A., Mennucci. B. (2010). What is solvatochromism, *J. Phys. Chem. B,* 114, 17128–17135.

Mataga N., Kaifu Y., Koizumi M. (1956). Solvent effects upon fluorescence spectra and the dipole moments of excited molecules. *Bull. Chem. Soc. Jpn. 29* (1956) 465– 470.

McRae, E. G. (1957). Theory of Solvent Effects on Molecular Electronic Spectra. Frequency Shifts. *The Journal of Physical Chemistry*, *61*(5), 562–572.

Mingozzi, F. & High, K. A. (2011). Therapeutic in vivo gene transfer for genetic disease using AAV: progress and challenges. *Nature Rev. Genet*, 12, 341–355

Mitchell, D.M., Morgan, P.J., Prat, D.W., & Pull, P. (2008). Push-pull molecules in the gas phase: stark-effect measurements of the permanent dipole moments of p-aminobenzoic acid in its ground and electronically excited states. *J. Phys. Chem. A,* 112,12597–12601

Mittal, V. (2011). Surface Modification of Nanotube Fillers. *Wiley-VCH Verlag GmbH & Co. KGaA*

Miyawaki, A. (2011). Development of probes for cellular functions using fluorescent proteins and fluorescence resonance energy transfer. *Annu Rev Biochem,* 80,357-373.

Miyawaki, A., Llopis, J., Heim, R., McCaffery, J.M., Adams, J.A., Ikura, M., & Tsien, R.Y. (1997). Fluorescent indicators for Ca2+ based on green fluorescent proteins and calmodulin. *Nature,388(*6645),882-887.

Molling K. (1998). Vaccination and gene therapy with naked DNA. *Z Arztl Fortbild Qualitatssich,* 92: 681–83

Morley, J. O., Morley, R. M., & Fitton, A. L. (1998). Spectroscopic Studies on Brooker's

Merocyanine. *Journal of the American Chemical Society*, *120*(44), 11479–11488.

Nagarajan, A., Zhou, M., Nguyen, A. Y., Liberton, M., Kedia, K., Shi, T., Piehowski, P., Shukla, A., Fillmore, T. L., Nicora, C., Smith, R. D., Koppenaal, D. W., Jacobs, J. M., & Pakrasi, H. B. (2019). Proteomic Insights into Phycobilisome Degradation, A Selective and Tightly Controlled Process in The Fast-Growing Cyanobacterium Synechococcus elongatus UTEX 2973. *Biomolecules*, *9*(8), 374.

Naldini, L. (2011). Ex vivo gene transfer and correction for cell-based therapies. *Nature Reviews Genetics*, *1*(5), 301–315.

Navarro, J., Risco, R., Toschi, M., & Schattman, G. (2008). Gene therapy and intracytoplasmatic sperm injection (ICSI) - a review. *Placenta*, *29 Suppl B*, 193–199.

Nayerossadat, N., Ali, P., & Maedeh, T. (2012). Viral and nonviral delivery systems for gene delivery. *Advanced Biomedical Research*, 1(1), 27.

Nguyen, A. Y., Bricker, W. P., Zhang, H., Weisz, D. A., Gross, M. L., & Pakrasi, H. B. (2017). The proteolysis adaptor, NblA, binds to the N-terminus of β-phycocyanin: Implications for the mechanism of Phycobilisomes degradation. *Photosynthesis Research*, *132*(1), 95–106.

Nie, H., Yang, Z., Huang, S., Wu, Z., Wang, H., Yu, R., & Jiang, J. (2012). DNA-Wrapped Carbon Nanotubes as Sensitive Electrochemical Labels in Controlled-Assembly-Mediated Signal Transduction for the Detection of Sequence-Specific DNA. *Small*, *8*(9), 1407–1414.

Nigam, S., & Rutan, S. (2001). Principles and Applications of Solvatochromism. *Applied Spectroscopy*, *55(11)*, 362A–370A.

Nii, D., Hayashida, T., Yamaguchi, Y., Ikawa, S., Shibata, T., & Umemura, K. (2014). Selective

binding of single-stranded DNA-binding proteins onto DNA molecules adsorbed on single-walled carbon nanotubes. Colloids and Surfaces B: Biointerfaces, 121, 325–330

Nishitani, M., Sakai, T., Kanayama, H., Himeno, K., & Kagawa, S. (2000). Cytokine gene therapy for cancer with naked DNA. *Molecular urology*, *4*(2), 47–50.

O'Connell, M.J., Bachilo, S.M., Huffman, C.B., Moore, V.C., Strano, M.S., Haroz, E.H., Rialon, K.L., Boul, P.J., Noon, W.H., Kitrell, C., Ma, J., Hauge, R.H., Weisman, R.B., &Smalley, R.E. (2002). Band gap fluorescence from individual single-walled carbon nanotubes. *Science*. 297, 593–596.

Ojeda, I., Barrejón, M., Arellano, L.M., González-Cortés, A., Yáñez-Sedeño, P., Langa, F., & Pingarrón, J.M. (2015). Grafted-Double Walled Carbon Nanotubes as Electrochemical Platforms for Immobilization of Antibodies Using a Metallic-Complex Chelating Polymer: Application to the Determination of Adiponectin Cytokine in Serum. *Biosens. Bioelectron*, 74, 24–29.

Onsager L. (1936). Electric moments of molecules in liquids. *J. Am. Chem. Soc*, 58, 1482–1493.

Ortega, J., Rafols, C., Bosch, E. & Roses., M. (1996). Solute-solvent and solvent-solvent interactions in binary solvent mixtures. Part 3 A the Eτ (30) polarity of binary mixtures of hydroxylic solvents. *J Chem. Soc., Perkin Trans, 2* ,1497-1503.

Pemberton, J.M., Liu, Q., & Andrews, D.W. (2019). Measuring Small-molecule Inhibition of Protein Interactions in Live Cells Using FLIM-FRET. *Bio Protoc*,*9*(20), e3401.

Perebeinos, V., & Avouris, P. (2008). Phonon and Electronic Nonradiative Decay Mechanisms of Excitons in Carbon Nanotubes. Physical Review Letters, 101(5).

Pinheiro, J. M., & de Melo, C. P. (2011). Ab Initio Study of the Anomalous Solvatochromic Behavior of Large Betaines. *The Journal of Physical Chemistry A*, *115*(27), 7994–8002.

Pirbhai, M., Chandrasekar, S., Zheng, M., Ignatova, T., Rotkin, S.V., &Jedlicka, S.S. (2019). Augmentation of C17.2 Neural Stem Cell Differentiation via Uptake of Low Concentrations of ssDNA-Wrapped Single-Walled Carbon Nanotubes. *Adv. Biosys*, 3, 18003-21.

Prokop, A., & Davidson, J.M. (2007). In Lanza R, Langer R, Vacanti J (ed). Gene Delivery into Cells and Tissues. Princeples of Tissue Engineering. *Elsevier Academic Press*, ABD; pp: 493-515.

Punbusayakul, N., Talapatra, S., Ajayan, P.M., & Surareungchai, W. (2013). Label-Free As-Grown Double Wall Carbon Nanotubes Bundles for Salmonella Typhimurium Immunoassay. Chem. Cent. J., 7, 102.*Nanotechnol.* 2, 318–323.

Rance, G.A., Marsh, D.H., Nicholas, R.J., &Khlobystov, A.N. (2010). UV–vis absorption spectroscopy of carbon nanotubes: relationship between the p-electron plasmon and nanotube diameter. *Chem. Phys. Lett*. 493, 19–23

Raper, S.E., Chirmule, N., Lee, F.S., Wivel, N.A., Bagg, A., Gao, G.P., et al. (2003). Fatal s ystemic inflammatory response syndrome in a ornithine transcarbamylase deficient patient following adenoviral gene transfer. *Mol Genet Metab*, 80,148-58.

Record, M. T., Jr., C. F. Anderson, and T. M. Lohman. (1978). Thermodynamic analysis of ion effects on the binding and conformational equilibria of proteins and nucleic acids: the roles of ion association or release, screening, and ion effects on water activity. *Q. Rev. Biophys. 11*, 103-178.

Record, M. T., Jr., T. M. Lohman, and P. L. de Haseth. (1976). Ion effects on aligand-nucleic acid interactions. J. Mol. Biol. 107:145-158.

Reid, T., Warren, R., & Kirn, D. (2002) Intravascular adenoviral agents in cancer patients:

Lessons from clinical trials. *Cancer Gene Ther*,9, 979-86.

Roxbury, D., Jagota, A., & Mittal, J. (2011b). Sequence-Specific Self-Stitching Motif of Short Single-Stranded DNA on a Single-Walled Carbon Nanotube. *J. Am. Chem. Soc.*, 133, 13545–13550.

Roxbury, D., Tu, X., Zheng, M., & Jagota, A. (2011a). Recognition Ability of DNA for Carbon Nanotubes Correlates with Their Binding Affinity. *Langmuir*, *27* (13), 8282−8293.

Sadaoka, Y., Sakai, Y., & Murata, Y. (1992). Optical humidity and ammonia gas sensors using Reichardt's dye-polymer composites. *Talanta, 39*(12), 1675–1679S.

Saito, R., Dresselhaus, G., Dresselhaus, M. S. (1998). Physical Properties of Carbon Nanotubes; *Imperial College Press: London*.

Sasaki, T., Takeishi, H., & Yoshida, Z. (1999). Interpretation of solubility and solvation of phenol blue in supercritical carbon dioxide-based on solute–solvent interaction evaluated by solvatochromism, J. Supercrit. Fluids 15,23–31

Scherer, F., Anton, M., Schillinger, U., Henke, J., Bergemann, C., Krüger, A, et al. (2002) Magnetofection: Enhancing and targeting gene delivery by magnetic force in vitro and in vivo. *Gene Ther*, 9, 102-109.

Schmidt, C., & Storsberg, J. (2015). Nanomaterials—Tools, Technology and Methodology of Nanotechnology Based Biomedical Systems for Diagnostics and Therapy. *Biomedicines,3*(3), 203–223.

Shankar, A., Mittal, J., Jagota, A. (2014). Binding between DNA and Carbon Nanotubes Strongly Depends upon Sequence and Chirality. *Langmuir*, *30* (11), 3176−3183.

Smith K. R. (2004). Gene Therapy: The Potential Applicability of Gene Transfer Technology to the Human Germline. *International journal of medical sciences, 1*(2), 76–91.

Smith, D. A., Harris, S. A., & Stockley, P. G. (2008). Single-molecule fluorescence resonance energy transfer assays reveal heterogeneous folding ensembles in a simple RNA stem-loop. *Journal of Molecular Biology*, *384*(1), 264–278.

Stepanian, S. G., Karachevtsev, M. V., Glamazada, A. Y., Karachevtsev, V. A., &Adamowicz, L. (2008). Stacking Interaction of Cytosine with Carbon Nanotubes: MP2, DFT and Raman Spectroscopy Study. *Chem. Phys. Lett.,* 459:153-158.

Stryer, L. (1978). Fluorescence Energy Transfer as a Spectroscopic Ruler. *Annual Review of Biochemistry, 47(*1), 819–846.

Sullivan, S.M. (2003). In Sullivan SM, Rolland A (ed). Introduction to Gene Therapy and Guidelines to Pharmaceutical Development. Pharmaceutical Gene Delivery Systems. Eastern Hemisphere Distribution, USA; pp. 17-31.

Sustarsic, M., & Kapanidis, A. N. (2015). Taking the ruler to the jungle: single-molecule FRET for understanding biomolecular structure and dynamics in live cells. *Current Opinion in Structural Biology*, 34, 52–59.

Tabakman, S. M., Welsher, K., Hong, G., & Dai, H. (2010). Optical Properties of Single-Walled Carbon Nanotubes Separated in a Density Gradient: Length, Bundling, and Aromatic Stacking Effects. The Journal of Physical Chemistry C, 114(46), 19569–19575.

Takefumi, S., Akira, I., Shin, E., Shiro, B. (2005). *In Situ* Gene Therapy for Prostate Cancer. *Curr Gene Ther*,5,111–9.

Talone, C.J., Gao, J., Lynch, J.R., Tanu, R.M., & Deyrup, S.T. (2016). Determination of the ground- and excited-state dipole moments of bromocresol purple in protic and aprotic

solvents. *Spectrochim. Acta Part A,* 156, 138–142.

Thrasher, A. J., Gaspar, H. B., Baum, C., Modlich, U., Schambach, A., Candotti, F., & Fischer, A. (2006). X-SCID transgene leukemogenicity. *Nature*, *443*(7109), E5–E6.

Tu, X., Manohar, S., Jagota, A., & Zheng, M. (2009). DNA Sequence Motifs for Structure-Specific Recognition and Separation of Carbon Nanotubes. *Nature*, *460*(7252),250–253.

Tupin, E., Poirier, B., Bureau, M. F., Khallou-Laschet, J., Vranckx, R., Caligiuri, G., Gaston, A. T., Duong Van Huyen, J. P., Scherman, D., Bariéty, J., Michel, J. B., & Nicoletti, A. (2003). Non-viral gene transfer of murine spleen cells achieved by in vivo electroporation. *Gene therapy*, *10*(7), 569–579.

Vitha M.F & Carr, P.W (1998). Study of the Polarity and Hydrogen-Bond Ability of Dodecyltrimethylammonium Bromide Micelles by the Kamlet-Taft Solvatochromic comparison method. *J. Phys. Chem. B, 102*(11), 1888-1895

Vitha, M. F., Weckwerth, J. D., Odland, K., Dema, V., & Carr, P. W. (1997). An Adaptation of Kubista's Method for Spectral Curve Deconvolution. *Analytical Chemistry*, *69*(13), 2268–2274.

Vorburger, S.A., & Hunt, K.K. (2002). Adenoviral Gene Therapy. *Oncologist*, 7, 46-59.

Wang, C., Takei, K., Takahashi, T., Javey, A. (2013a) Carbon Nanotube Electronics–Moving Forward. *Chem Soc Rev.* 42:2592–2609.

Wang, S., Makhina, E.N., Masia, R., Hyrc, K.L., Formanack, M.L., & Nichols, C.G. (2013b). Domain organization of the ATP-sensitive potassium channel complex examined by fluorescence resonance energy transfer. *J Biol Chem. 288*(6):4378-88.

Wang, Z., Gao, D., Zhan, Y., & Xing, C. (2020). Enhancing the Light Coverage of Photosynthetic Bacteria to Augment Photosynthesis by Conjugated Polymer

Nanoparticles. *ACS applied biomaterials*, *3*(5), 3423–3429.

Watson, J.D. &Crick, F.H.C. (1953). Molecular structure of nucleic acid. *Nature*, 171 pp. 737-738.

Williams, D. A., & Orkin, S. H. (1986). Somatic gene therapy. Current status and future prospects. *The Journal of clinical investigation*, *77*(4), 1053–1056.

Wolf, D. P., Mitalipov, P. A., & Mitalipov, S. M. (2019). Principles of and strategies for germline gene therapy. *Nature medicine*, *25*(6), 890–897.

Wolf, E., Schernthaner, W., Zakhartchenko, V., Prelle, K., Stojkovic, M.,& Brem, G. (2000). Transgenic technology in farm animals-progress and perspectives. *Exp Physiol;* 85:615-25.

Wu, Y., Song, M., Xin, Z., Zhang, X., Zhang, Y., Wang, C., Li, S., & Gu, N. (2011). Ultra-small particles of iron oxide as peroxidase for immunohistochemical detection. *Nanotechnology*, *22*(22), 225703.

Wurm, C.A., Kolmakov, K., Gottfert, F., Ta, H., Bossi, M., Schill, H., Berning, S., Jakobs, S., Donnert, G., Belov, V.N., et al. (2012). Novel red fluorophores with superior performance in STED microscopy. *Opt Nanosc*, 1,7.

Yang, L., Zhou, Y., Zhu, S., Huang, T., Wu, L., & Yan, X. (2012). Detection and quantification of bacterial autofluorescence at the single-cell level by a laboratory-built high-sensitivity flow cytometer. *Anal Chem*, 84,1526-1532.

Yang, Y., Sharma, A., Noetinger, G., Zheng, M., & Jagota, A. (2020). Pathway-Dependent Structures of DNA-Wrapped Carbon Nanotubes: Direct Sonication vs Surfactant/DNA Exchange. The Journal of Physical Chemistry C.

You, C.C., Miranda, O.R., Gider, B., Ghosh, P.S., Kim, I.B., Erdogan, B., Krovi, S.A., Bunz,

U.H., Rotello, V.M. (2007). Detection and identification of proteins using nanoparticle-fluorescent polymer “chemical nose” sensors. *Nature Nanotech 2*, 318–323

Yu, A., Catherine, A., Darcie, T., Farrow, A., & Jonas, D.M. (2002). Solvatochromism and solvation dynamics of structurally related cyanine dyes. *J. Phys. Chem. A* 106, 9407–9419.

Zhang, H., Wang, C., Chen, B., & Wang, X. (2012). Daunorubicin-TiO2 nanocomposites as a "smart" pH-responsive drug delivery system. *International journal of nanomedicine*, 7, 235–242.

Zhang, Y., Liu, J.-Y., Ma, S., Zhang, Y.-J., Zhao, X., Zhang, X.-D., & Zhang, Z.-D. (2010). Synthesis of PVP-coated ultra-small Fe3O4 nanoparticles as an MRI contrast agent. *Journal of Materials Science: Materials in Medicine*, *21*(4), 1205–1210.

Zhao, C., Qu, K.G., Song, Y.J., Xu, C., Ren, J.S., Qu, X.G. (2010). A reusable DNA single-walled carbon-nanotube-based fluorescent sensor for highly sensitive and selective detection of Ag+ and cysteine in aqueous solutions. *Chemistry*, 16, 8147–8154.

Zheng, M. (2007). Redox Chemistry and Electrochemistry of DNA-Wrapped Carbon Nanotubes. *ECS Trans*., 6, 29-32.

Zheng, M. & Semke, E. D. (2007). Enrichment of Single Chirality Carbon Nanotubes *Journal of American Chemistry Soc*iety,*129*(19), 6084-6085.

Zheng, M., Jagota, A., Semke, E. D., Diner, B. A., Mclean, R. S., Lustig, S. R., Tassi, N. G. (2003b). DNA-assisted dispersion and separation of carbon nanotubes. *Nature Materials,2*(5), 338–342.

Zheng,M.,Jagota,A.,Strano,M.S.,Santos,A.P.,Barone,P., Chou,S.G., Diner, D., M.S.,

Mclean,R.S., Onoa,G.B., Samsonidze, G.G., Semke ,E. D., Usrey,M., &Walls,D.J. (2003a).Structure-Based Carbon Nanotube Sorting by Sequence-Dependent DNA Assembly. *Science*, *302*(5650), 1545-1548.

Zhu, L., Deng, C., Chen, P., Dong, X., Su, Y. H., Yuan, Y., et al. (2014). Glucose oxidase biosensors based on carbon nanotube non-woven fabrics. *Carbon* 67, 795–796.

APPENDIX A: EFFECT OF pH ADJUSTMENT ON FRET AT 488NM EXCITATION WAVELENGTH(BLACK) AND 570NM EXCITATION WAVELENGTH FOR SWCNT(RED). ABOUT 86% FLUORESCENCE QUENCHING WAS OBSERVED DURING THE pH DROP.

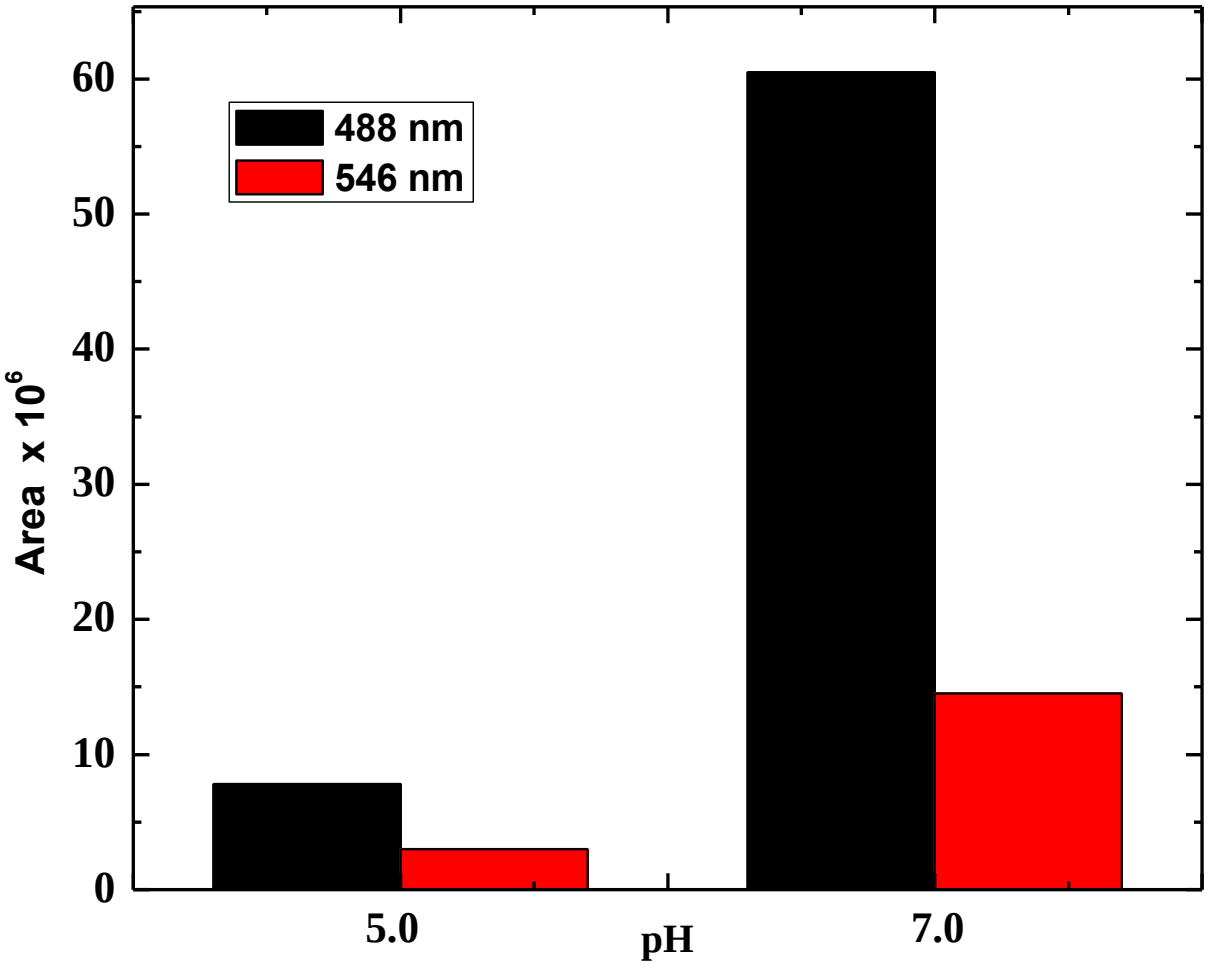

APPENDIX B: EFFECT OF MANNING OSSAWA COUNTER-ION CONDENSATION THEORY ON FLUORESCENCE INTENSITY USING ZINC CHLORIDE AT EXCITATION WAVELENGTH 488NM.

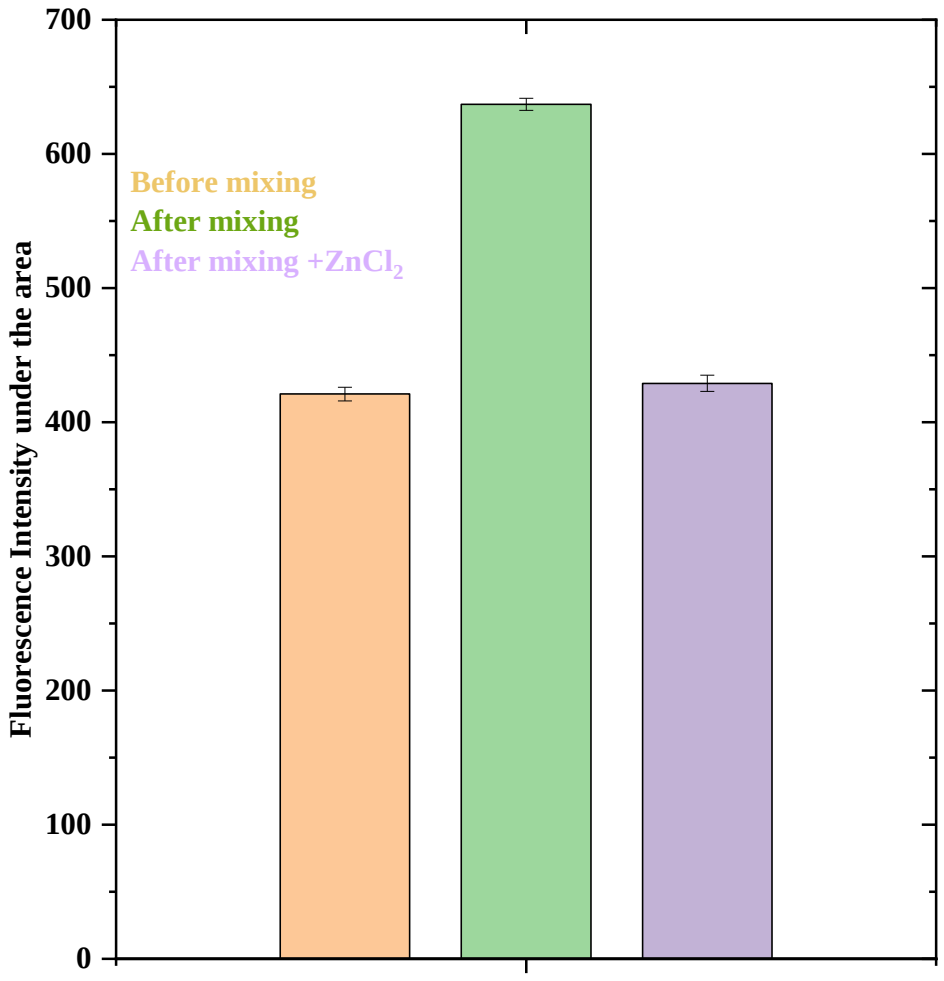

APPENDIX C: SOLVATOCHROMIC SHIFT OBSERVED IN SWCNT PHOTOLUMINESCENCE WITH $TBCl_3$ (BLUE) AND WITHOUT $TBCl_3$ (RED)

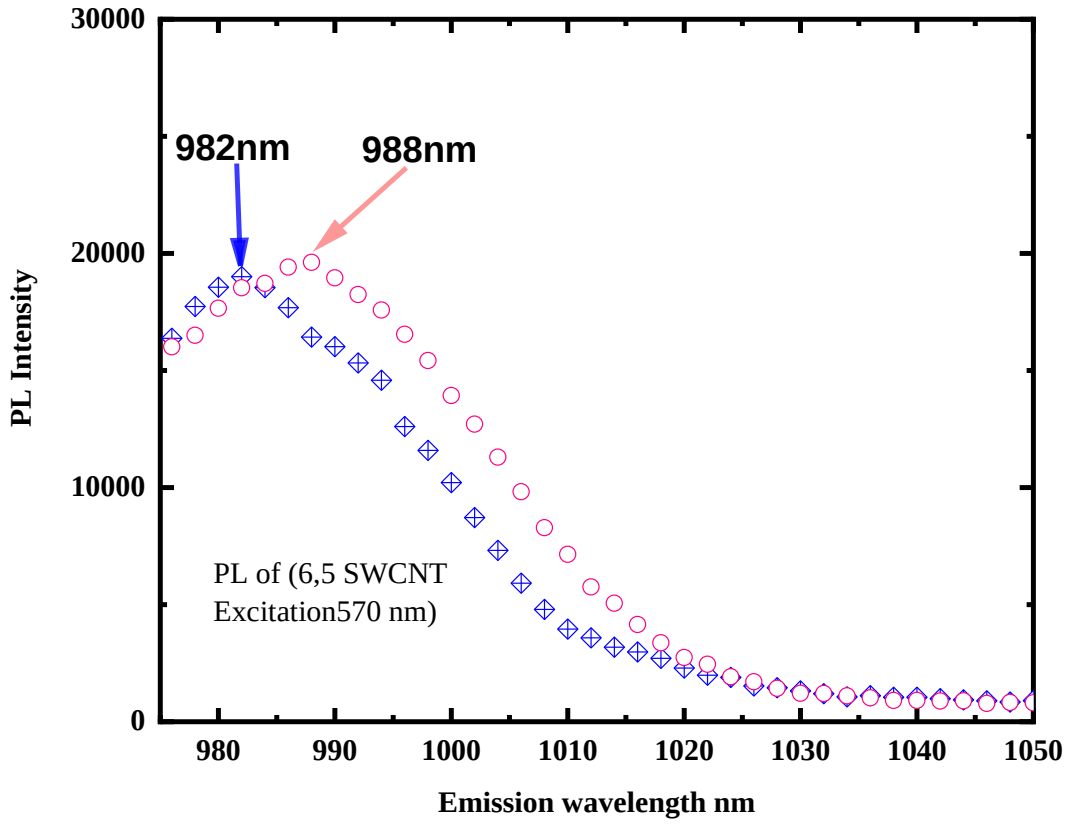

APPENDIX D: FLUORESCENCE SPECTRA OF PHYCOBILISOME EXCITED AT 548NM